Development of a physiologically complex model of the human intestine for the study of absorption and detoxification

A thesis submitted to the University of Manchester for the degree of Doctor of Philosophy in the Faculty of Science and Engineering

2021

Jessica R. Carter

Department of Physics and Astronomy, School of Natural Sciences

Table of Contents

Word count: 34994

List of Figures

List of Tables

Abbreviations

2D	Two Dimensional
3D	Three Dimensional
ABCB1	ATP Binding Cassette Subfamily B Member 1
ADME	Absorption, Distribution, Metabolism, Excretion
ALP	Alkaline Phosphatase
ATP	Adenosine Triphosphate
AUC	Area Under the Curve
BB	Brush Border
BCS	Biopharmaceutics Classification System
Bi	Bilayer
BM	Basement Membrane
BSA	Bovine Serum Albumin
Caco-2	Human Colorectal Adenocarcinoma Cell Line
CCD18co	Human Normal Colon Fibroblasts
cDNA	Copy DNA
C-M	Carrier-mediated
CM	Conditioned Media
Co	Co-culture
COL4	Collagen Type IV
CYP	Cytochrome P450
DAPI	Hoechst 33342
DDIs	Drug-drug Interactions
DNA	Deoxyribonucleic Acid
ECM	Extracellular Matrix
FDA	US Food and Drug Administration
FITC	Fluorescein Isothiocyanate
FN	Fibronectin
GFP	Green Fluorescence Protein
GI	Gastrointestinal
HGF	Hepatocyte Growth Factor
iPSC	Induced Pluripotent Stem Cells
KGF	Keratinocyte Growth Factor
LY	Lucifer Yellow
Mono	Monolayer
mRNA	Messenger RNA
MTT	3-(4,5-dimethylthiazol-2-yl)-2,5-diphenyltetrazolium bromide
NME	New Molecular Entities
PEPT1	Human Peptide Transporter 1
PET	Polyethylene Terephthalate

pFibres	Porous Fibres
PGA	Poly(glycolic acid)
PI	Propidium Iodide
PK	Pharmacokinetic
PLLA	Poly(L-lactic acid)
RNA	Ribonucleic acid
SEM	Scanning Electron Microscopy
sFibres	Smooth Fibres
TCPS	Tissue Culture Polystyrene
TEER	Transepithelial Electrical Resistance
TW	Transwell
UHQ	Ultra High Quality Water
UV	Ultraviolet
WCA	Water Contact Angle

Abstract

The attrition rates of pharmaceutical therapeutics are extremely high, with only 5% of drug candidates entering human trials eventually gaining approval. One of the main reasons attributed to such failures is a lack of suitable preclinical models that can accurately predict *in vivo* pharmacokinetics. As the primary site of absorption for oral therapeutics, the intestine is a dominant organ determining the final bioavailability of drug candidates. Yet the standard model, a monolayer of epithelial cells cultured on a semipermeable plastic membrane, lacks the physiologically relevant architecture, extracellular matrix (ECM) components and underlying stromal cells of intestinal tissue. Consequently, a number of limitations still persist in its utility to accurately predict *in vivo* compound permeability.

This thesis has evaluated electrospun poly(L-lactic acid) (PLLA) fibrous membranes as an alternative cell culture surface with which to develop a more physiologically relevant model of the human intestine. Characterisation of these fibrous membranes revealed a topographic architecture highly reminiscent of the fibrillous ECM structure of the intestinal basement membrane, which promoted the adhesion and growth of Caco-2 cells into contiguous monolayer. Immunofluorescence imaging, gene and protein expression techniques validated the PLLA fibre monolayer as equivalent in its differentiation and tight junction formation to the standard model, yet demonstrated notable morphological differences and improved barrier properties.

Following this, the physiological complexity of the PLLA fibre monolayer was further developed to include additional stromal elements, namely adjacent subepithelial fibroblast cells. A series of co-culture models with differing proximities of fibroblast cells revealed that intestinal permeability, enzyme and transporter protein activity had different sensitivities to fibroblast signalling. Comparison of fibroblasts co-cultures and monolayers in both standard and PLLA fibrous inserts, demonstrated that intestinal activity was most improved by both topographic cell culture surface and by fibroblasts incorporation. Taken together, the PLLA fibrous epithelial/fibroblast bilayer fabricated in this thesis provided a model of the intestine with the most physiological relevant function, and an improved preclinical tool for the study of absorption and detoxification.

Declaration

No portion of the work referred to in the thesis has been submitted in support of an application for another degree or qualification of this or any other university or other institute of learning.

Copyright Statement

Acknowledgements

Firstly, I would like to acknowledge the BBSRC DTP for funding this project, and for providing an opportunity to take on an industrial placement internship during the course of this PhD.

My biggest thanks go to my supervisor, Professor Jian Lu, for his endless patience, breadth of knowledge and time that he has commited to guide this project forward. I particularly thank you for your constant encouragement and positivity. Thanks also to my co-supervisor Dr Jeff Penny, for sharing your expertise in pharmacology and helpful advice and suggestions throughout the course of this project. I would also like to particularly thank Dr Jiashen Li for collaborating with us on this project and for providing the electrospun fibrous membranes and SEM images.

I am grateful to all my fellow researchers across the Lu and Penny groups who have dedicated their precious time and wisdom to assist me both technically and theoretically, but especially Dr Jing Zhang, Dr Yu Siong Ho, Dr Maryam Shubbar and Carl Carvalho, without whose help, this project would have taken much longer. I would like to also acknowledge Dr Steve Marsden and the Bioimaging Facility staff for all their assistance with confocal microscopy. Lastly, I am indebted to Dr Michael Smith for his generosity of ideas and helpful advice and assistance wherever he possibly could.

My life has been changed by this PhD, mostly by the people I have been fortunate to meet and call friends. To the entire Biological Physics group I extend my utmost gratitude, for all the laughter, cake, karaoke, and support. Most of all, to Vinay Kara and Jack Rowley Noble, whose unwavering support through the years will forever be appreciated.

Finally, to my family and friends who have shown me endless love and encouragement, kept me sane and renewed my strength when I needed it most. To my Mum and Dad I am ever grateful, for always motivating me to keep going and inspiring my love of science. And finally, my deepest thanks go to my ever-patient husband, Dan, for always wanting the best for me, your support and sacrifices made this possible.

1. General Introduction

The human intestine is the digestive organ of the body and functions to manage the uptake of important dietary nutrients and provide a physical barrier against harmful exogenous xenobiotics. With the development of modern medicine, the intestine now also functions as the major site of absorption for a multitude of therapeutic compounds.

The use of the gastrointestinal tract to deliver oral medications is frequently desired as a less invasive, cost effective protocol with a high level of patient compliance. Over half (51%) of the FDA approved new molecular entities (NMEs) over the past decade have been formulated for oral administration (Figure 1.1A). Moreover, 29% of the global therapeutics in the development pipeline are designed for oral routes [1]. However, the increasing costs of pharmaceutical research and development for new medicines (reported between $314M and $2.8B [2]), compounded by the extremely high attrition rates of drug candidates (Figure 1.1B) (an estimated 95% of drugs entering human trials failing to make approval [3]), highlights an immense need to close the gap between preclinical and clinical performance of NMEs both clinically and economically.

Preliminary drug discovery approaches such as high throughput screening and rational drug design are successful proven methodologies in developing lead candidates. However, both these approaches are biased towards identifying compounds with high target interaction and efficacy, and often overlook optimal absorption, distribution, metabolism and excretion (ADME) profiles and pharmacokinetics (PK), leading to compounds with poor solubility and permeability [4].

Understanding how therapeutics interact with the intestinal barrier is crucial in determining their final bioavailability profile. Therefore, the successful discovery of new drugs and improvement to existing therapies rely hugely on the development of rigorous and reliable methods of studying absorption and detoxification.

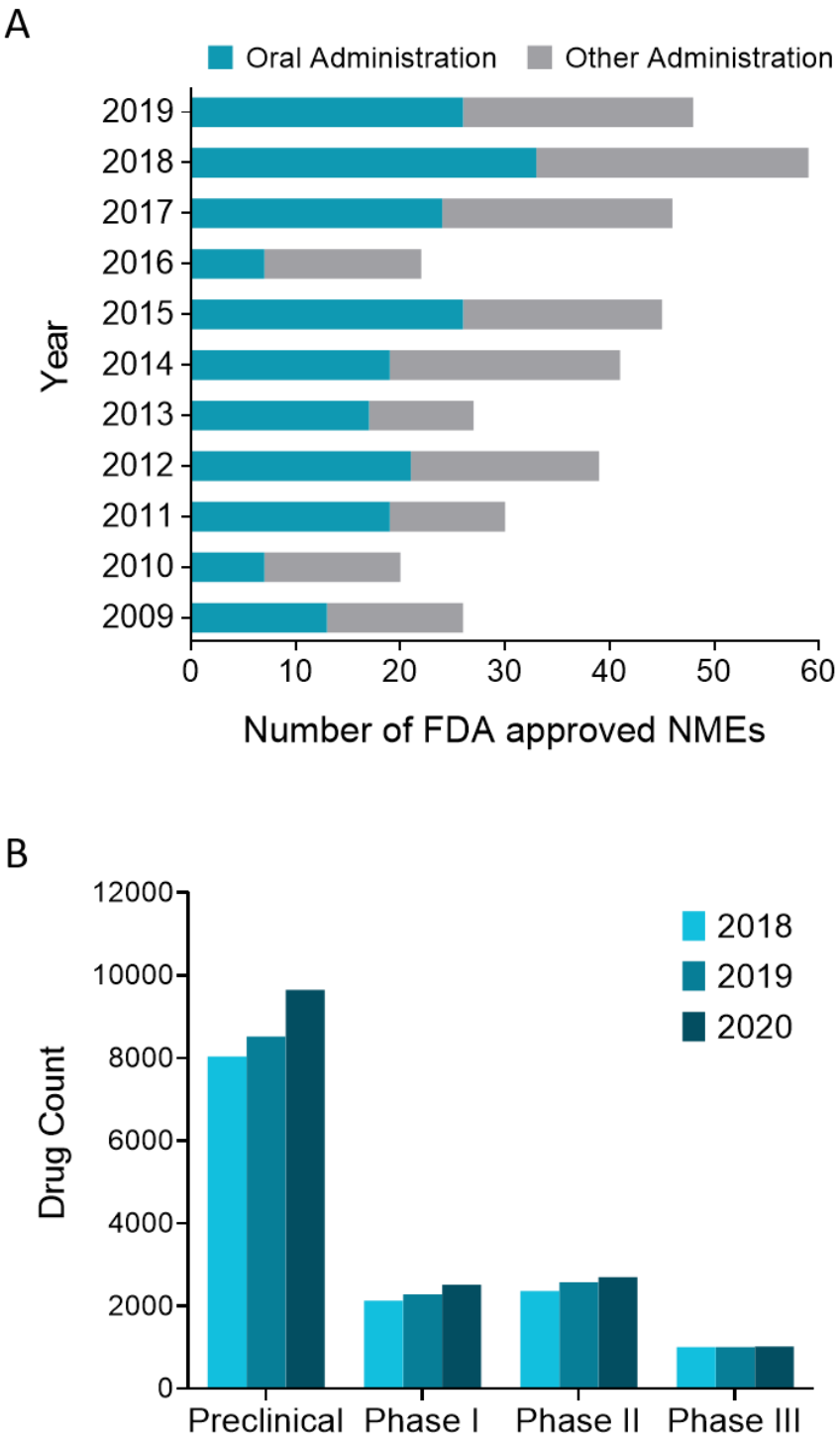

Figure 1.1 Oral Drugs in the Drug Discovery Process

(**A**) Number of FDA approved new molecular entities (NMEs) each year for the past decade, highlighting the number formulated for oral administration (in blue). Source US FDA Centre for Drug Evaluation and Research [5]. (**B**) Distribution of global pipeline drugs across the clinical phases for the past three years. Source Pharmaprojects Pharma R&D Review 2020 [1].

1.1 Intestinal Anatomy and Physiology

The small intestine is the longest part of the alimentary canal, measuring 3.05 m in a living adult; its name deriving from its "small" diameter of 2.5 cm relative to that of the large intestine (7.6 cm). Comprised of three structurally distinct regions; the duodenum, the jejunum and the ileum, it functions as the site of digestion, absorption and detoxification of chyme released from the stomach (Figure 1.2A).

Highly adapted for its absorptive function, the inner lumen circular folds (*plicae circulares*) created within the layers of intestinal tissue (Figure 1.2B) dramatically increase the luminal surface area, as well slowing the speed of movement of chyme through the intestine, maximising the interaction time for digestion [6]. Additionally, contributing further to its enormous surface area (approximately 200 m^2 [6]), are a vast number of finger-like protrusions called villi that cover the entirety of the intestinal lumen (Figure 1.2B). These villi are 0.5-1.6 mm in length [7] and contain arterial, venal and lymphatic capillary networks of the circulatory system, that deliver absorbed molecules, nutrients and compounds around the body, and are sheathed within each villus by an assortment of connective tissue, extracellular matrix (ECM) proteins and stromal and muscle cell types. The outer surface of the villi are covered in a single cell layer of specialised epithelial cells called enterocytes, which themselves have an outer brush border of microvilli. These polarised, columnar cells constitute the majority of the epithelial layer and are highly specialised for absorption and detoxification; expressing many enzyme and transporter proteins. It is the intrinsic barrier function of enterocyte cells that ultimately determines the capacity of an entity to pass from the intestinal lumen to the systemic blood supply, making them the critical gatekeepers in intestinal permeability [8,9].

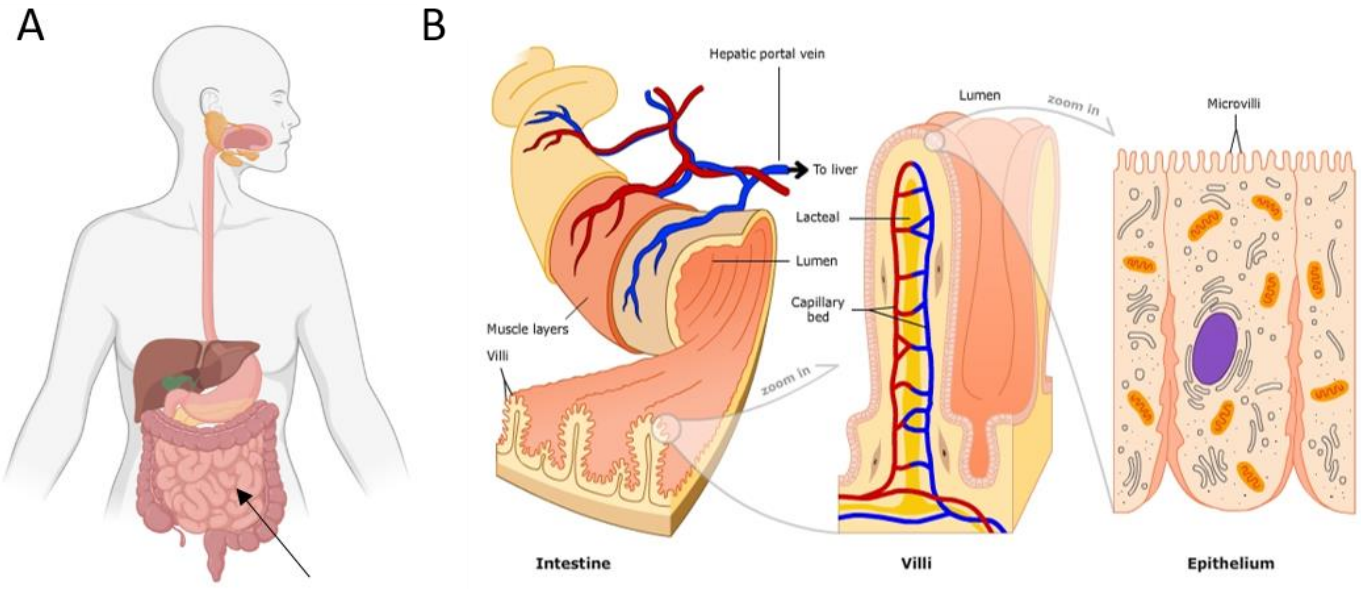

Figure 1.2 The Human Small Intestine

(**A**) The gastrointestinal system of the human body, with an arrow showing the location of the small intestine. Made with BioRender.com. (**B**) The cross-section of the small intestine lumen is ridged with circular folds within the mucosal and submucosal layers that are covered in vascularized protrusions called villi. Each villus is composed of an arterial, venal and lymphatic capillary bed connected to the body's circulatory system and is surrounded by an epithelial brush border made up of specialised enterocyte cells. Source The University of Waikato [10].

1.2 Intestinal Absorption and Detoxification

1.2.1 Routes of Absorption in the Intestine

Whether a product of diet, environment or therapeutic, moieties in the intestinal lumen must traverse the monolayer barrier of enterocytes lining the villi of the intestine in order to be delivered to their target site of action. Like other cell barriers throughout the body, the intestinal epithelium presents a multitude of mechanisms for absorption, including both active and passive transport routes. Endogenously organised to maximise the absorption of essential ions, peptides, sugars, lipids and vitamins from our diet, routes of absorption in the intestine are now carefully considered and exploited in the design of many drugs. Reaching the blood supply within a villus can be achieved either transcellularly, where molecules enter the enterocyte from the apical membrane, traverse the cell and exit the basolateral membrane; or paracellularly, moving though the small space between cells in order to cross the epithelial barrier (Figure 1.3).

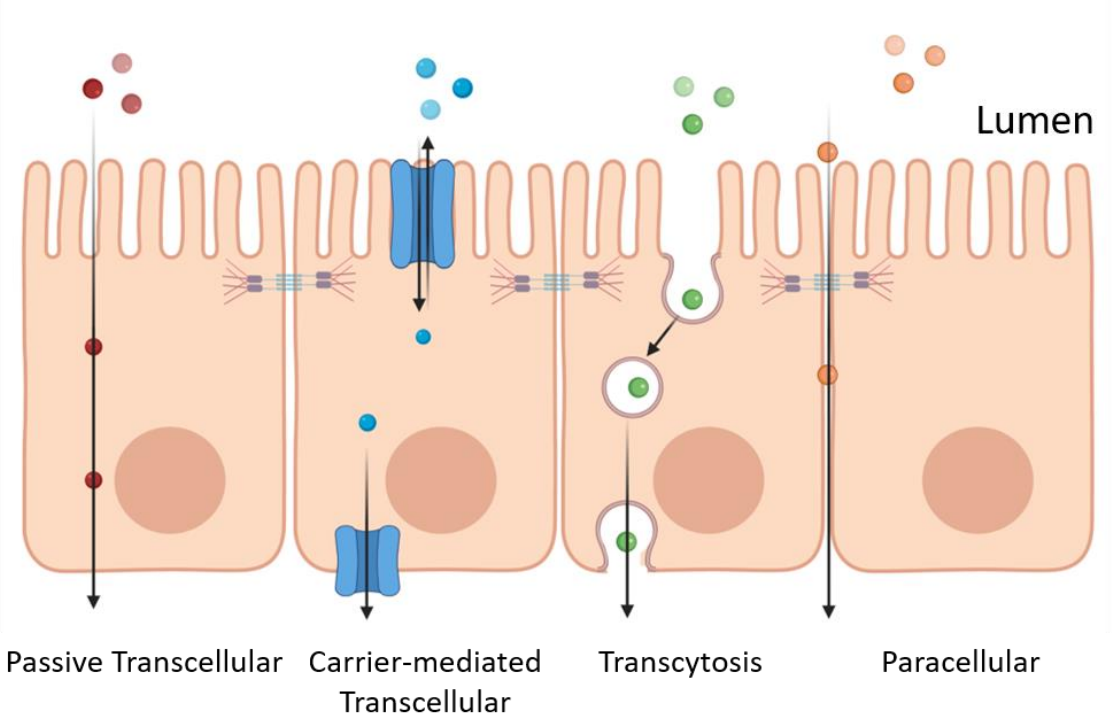

Figure 1.3 Routes of Absorption in the Intestine

Possible routes of absorption of a compound through the intestinal epithelia cells. These routes can be classified as *transcellular* (movement through enterocytes) or

paracellular (movement through intercellular junctions, between enterocytes). Made with BioRender.com.

1.2.1.1 Transcellular Transport

Arguably the simplest transport mechanism, and the most common for drug delivery, is transcellular passive diffusion (Figure 1.3). The phospholipids constituting the plasma cell membrane of enterocytes facilitate the diffusion of lipid-soluble nutrients or highly lipophilic compounds into enterocytes, down a concentration gradient [11]. The likelihood of a drug compound utilising passive transcellular diffusion mechanisms depends considerably on its physicochemical properties, which can be predicted using as set of guidelines known as the Lipinski's Rule of 5 [12]. This outlines the optimal parameters to consider for orally administered compounds, concerning size, hydrophobicity and lipophilicity; with small, hydrophobic, lipid-soluble compounds being most successful.

Alternatively, dietary compounds and xenobiotics can be transported transcellularly via specific protein transporters on the apical membrane of enterocytes (Figure 1.3). Carrier-mediated (C-M) transport of large hydrophilic molecules such as sugars, vitamins and small peptides, broken down by digestive enzymes from larger carbohydrates and proteins are naturally transported across intestinal wall using this mechanism; either by facilitated diffusion (down a concentration gradient) or by active transport (up a concentration gradient), with the expenditure of cellular energy in the form of Adenosine Triphosphate (ATP) [13]. Vast numbers of membrane carrier proteins have been identified in the intestine and classified into large families with similar genes; these include oligopeptide transporters (PEPTs), organic anion transporting polypeptides (OATPs), multidrug resistance proteins (MDRs) and multidrug resistance related proteins (MRPs) [14]. These transporters span an immense range of substrates, both endogenous and xenobiotic, including Angiotensin-converting enzyme (ACE) inhibitors, antibiotics and antivirals [15,16]. However, the relative contribution of C-M transport in pharmacokinetics has been an issue of contention over the last decade. Traditional beliefs of the co-existence of C-M and passive diffusion mechanisms [17] has been refuted, most notably by Dobson and Kell [18,19], who assert that transport is essentially C-M only; however, this was considered highly controversial by a number of

researchers who dispute the lack of evidence substantiating such a claim [20,21]. Nevertheless, the picture is still not clear due to the large number of transporters with as yet unidentified substrates, combined with the difficulty in empirically ascertaining the individual contribution of each mechanism to the overall permeability of a compound.

The final mechanism of transcellular transport is transcytosis (Figure 1.3); a unique form of endosome trafficking in polarised cells, which engulfs large solutes in vesicles for transport across the enterocyte [22]. Predominantly utilised by a range of pathogens including *Escherichia coli* Shiga toxins and Botulinum toxin [23,24], as well as endogenous substrates like Vitamin B12 and immunoglobulins [25,26], transcytosis is not commonly associated with drug delivery. However, emerging technologies of nanoparticle drug delivery systems have been designed to hijack glycosphingolipid trafficking for therapeutic peptides [27,28].

1.2.1.2 Paracellular Transport

Unlike hydrophobic molecules, which can partition through the phospholipid membrane to gain entry to enterocytes, hydrophilic or highly ionised molecules show relatively poor permeability. Dependent on their size, however, small hydrophilic molecules and ions can be absorbed between neighbouring enterocytes, via the paracellular route (Figure 1.3). Cells of the intestinal epithelia are connected by intercellular junctions; protein complexes that restrict the majority of trans-epithelial transport and regulate small molecule diffusion, these include tight junctions, adherens junctions and desmosomes [29]. For hydrophilic molecules with no likelihood of absorption through other mechanisms, some researchers have looked to modulating the paracellular pathway for drug delivery; disrupting these protein complexes at cell junctions to increase the permeability of otherwise poorly adsorbed drugs [30,31].

1.2.2 Oral Bioavailability

Bioavailability refers to the rate and extent to which the fraction of an initial dose of a drug successfully reaches the intended site of action, usually via the systemic

circulation, in an active and unaltered form. Understanding the bioavailability of a drug compound is a key parameter in determining its efficacy. For oral compounds this is more complex than intravenous drugs (which are considered to have 100% bioavailability), and more faceted than just the ability of a compound to be absorbed by the intestine. As discussed in the previous section, crossing the intestinal barrier is indeed one hurdle for drug compounds, however, its final bioavailability is determined by a number of compounding factors. If crossing transcellularly, a compound must be able to exit an enterocyte as well as enter it, passing across the basolateral cell membrane, unchanged, to reach the circulatory system. This can be hindered by the effect of efflux transporters, which pump compounds out of the cells and back into the intestinal lumen (see Section 1.2.4). Alternatively, compounds may be substrates for a number of enzymes which transform or metabolise the drug into other moieties (see Section 1.2.3). As capillaries in the intestine lead to the hepatic portal vein, and subsequently the liver, drugs must also survive first-pass metabolism in the liver, before making into the systemic circulatory system where it can access the rest of the body.

In pharmacokinetics, absolute bioavailability (*F*) is most commonly used to refer to the drug fraction and is summarised by the equation;

$$F=F_a F_g F_h \qquad (1.1)$$

where F_a denotes the fraction absorbed, F_g denotes the fraction escaping first-pass metabolism in the gut and F_h denotes the fraction escaping first-pass extraction in the liver[32]. Empirically, the most reliable measure of bioavailability is by determining the integrated plasma concentration-time profile, known as the area under the curve (AUC) as it is directly proportional to the fraction of the xenobiotic of interest reaching the systemic circulation [33].

Combined with the factors already mentioned, bioavailability can often be impacted by variables that are less predictable and are often of important consideration at the time of administration. Bioavailability of drugs can often be altered by chemical interactions in the gut; complexing with other ions or other drug compounds, hydrolysis from digestive enzymes or even by gut microflora. Moreover, patient specific factors such as age, sex, genetics and medical history can significantly alter the way drugs interact or are absorbed in the intestine [34]. Understanding of all these factors combined is critical

in designing, approving and administering drugs, as accurate oral bioavailability calculations of a compound affects both dosing and toxicity, impacting both clinical efficacy and safety.

1.2.3 Extra-hepatic metabolism

Intestinal cells contain both Phase I (modification) and Phase II (conjugation) metabolic enzymes which catalyse the biotransformation of endogenous and xenobiotic compounds (reviewed by Kaminsky & Zhang 2003 [35]). Before entering systemic circulation, the plethora of intestinal enzymes located within the epithelial monolayer (extensively reviewed by Xie et al. 2016 [36] and Peters et al. 2016 [37]) have the potential to eliminate a large proportion of xenobiotics, including therapeutic compounds. CYP3A is a highly abundant and broadly specific Phase I enzyme of the Cytochrome P450 (CYP) subfamily. It is most commonly implicated in intestinal metabolism and accounts for ~80% of total enteric CYP identified through immunoblotting [38]. The definitive contribution of the small intestine to first pass metabolism is difficult to determine empirically, as methods to decouple the influence of the liver and intestine are underdeveloped [39]; however, early clinical studies on patients undergoing liver transplant surgery showed a statistical difference between intraduodenally and intravenously metabolized Midazolam, indicating significant first-pass metabolic activity of mucosal enzyme CYP3A4 in the intestine [40]. Subsequent studies investigating the intestinal metabolic capacity, including comparison of intravenous and oral dosing [41], portal vein-cannulated preclinical animal models [42] and clinical grapefruit juice inhibitor interaction studies [43], all agree on the metabolic capabilities of the intestine, but also that its impact is variable based on the compound and patient.

Biotransformation can impact oral drug development, approval and administration on an immense magnitude. Of most concern is patient exposure to toxicity arising from increased doses of poorly bioavailable drugs, and the unpredictability of interindividual metabolic variability. The non-specific nature of the detoxification enzymes also lead to increased risk of drug-drug interactions (DDIs) [44,45] dependent on the rate of release of substrate fractions and inhibitors.

1.2.4 Efflux Transport

Additional pharmacokinetic complexity in intestinal absorption and disposition arises from the activity of efflux transporter proteins in the intestinal epithelia. These transporter proteins, located in the apical membrane of enterocytes, function to shunt molecules back across the epithelial membrane into the lumen of the small intestine to be excreted [46]. Numerous efflux proteins have been identified in the intestine as well as other tissues, and largely belong to a superfamily of ATP-dependent transporters known as the ATP-binding cassette (ABC) family. ABC drug transporters including P-glycoprotein (P-gp, also known as ABCB1 and MDR1 and will be referred to as ABCB1 from now on), Multidrug Resistance-associated Protein 1 (MRP1 also known as ABCC1) and Breast Cancer Resistance Protein (BCRP also known as ABCG2), were first discovered due to their efflux effects on chemotherapeutic drugs, but are now known to act on a large range of substrates absorbed by the intestine [47].

Despite knowledge of the existence of these transporters, navigating efflux transport is highly complex. The broad substrate specificity of each of the individual transporters is complicated further by the lack of observable structure-activity relationship of substrate compounds; making predictions as to which new compounds will be affected by efflux transport difficult. The substantial substrate spectrum overlap of CYP enzymes and efflux transporters [48] mean the fate of each absorbed molecule is independent; absorption may lead to direct entry into circulation, metabolism by CYP enzymes, efflux-mediated transport back to the lumen, or a combination of both [49] (Figure 1.4).

In particular, the interplay between both CYP enzymes and efflux transporters in preventing active compounds entering the bloodstream implies a synergistic mechanism that functions as an effective mechanism of defence from xenobiotics within the gut [50,51]. Indeed, many *in vitro* studies with epithelial monolayers have analysed the impact of the ABCB1 transporter on drug absorption and extraction ratios, using ABCB1 and CYP3A inhibitors [52,53], and demonstrate a considerable contribution of ABCB1 to drug disposition. However, limited transfection techniques have hindered the determination of the individual contribution of ABCB1 and CYP3A to their combined mechanism within the intestine *in vitro*. Most notably, *in vivo* studies

on combined CYP3A and ABCB1 knockout mice show significantly increased bioavailability yet dramatically increased lethal toxicity from anticancer drugs [54]. Thus, indicating the importance of their functional contribution to xenobiotic detoxification, and the necessity to be able to understand and predict their synergistic interactions for the design and administration of therapeutic drugs.

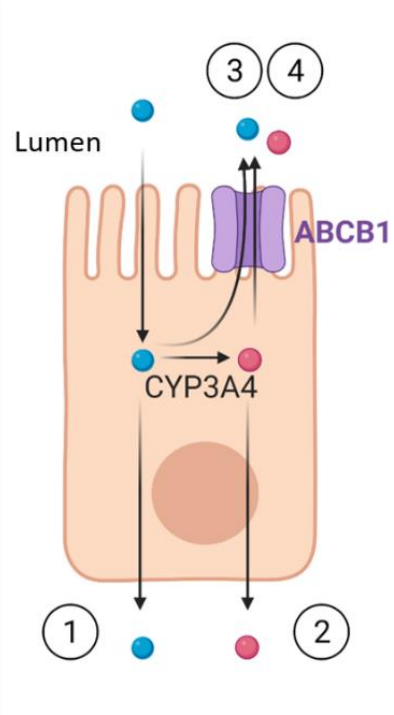

Figure 1.4 Efflux and Metabolism in Enterocytes

The interplay of efflux and metabolism in enterocyte can lead to different fates of a compound, when it is absorbed; (**1**) absorption leads to direct entry into circulation, (**2**) metabolism by CYP enzymes, in which the resulting metabolite enters circulation (**3**) efflux-mediated transport back to the lumen, (**4**) efflux of metabolite back to lumen. Made with BioRender.com.

1.3 Modelling Intestinal Pharmacokinetics

The expanse of interactions that occur between external compounds and the intestine and their implications on drug and compound delivery are not yet fully understood. Moreover, to develop new drugs and modalities of therapies, it is imperative to be able to predict and model what barriers they may face. Inevitably, no model can compete with the bioavailability and safety data accrued from human clinical trials, but in order to minimise clinical failure, drug discovery initiatives employ numerous preclinical models *in vivo* and *in vitro*, all varying in their relative complexities and the information they can contribute.

1.3.1 *In Vivo* Modelling

1.3.1.1 Animal Models

Although human studies can provide highly relevant results and overall correlation, the low throughput, high cost and ethical concerns weakens the justification for such studies preclinically. As such, *in vivo* animal studies are frequently used to translate predictions of human responses [55]. With the right selection, animal *in vivo* models can produce valuable multi-factorial results, accounting for a number of combined pharmacokinetic parameters including permeability, disposition, metabolism and excretion. Common absorption model species include dogs, rats and non-human primates, which are selected according to the compound of interest and the animal's physiological features such as gastrointestinal pH, intestinal length and transit time, transporter expression profiles and metabolic capacity. For example, dogs are best suited to study absorption profiles of pH-independent drugs, due to their elevated gastrointestinal (GI) pH, however, rat models are a more apt choice for pH-sensitive absorption [56].

The simplest method to determine the indirect *in vivo* contribution of the intestine to oral bioavailability and pharmacokinetics, is to compare the area under the curve (AUC) of plasma concentration against time for the same compound administered both intravenously and orally [57,58]. For many compounds, the experimental data achieved with comparable AUCs is sufficient to make suitable predictions of bioavailability. When assessing the specific contribution and interactions of the intestine however,

Kwan et al. 1997 [59] argues that the assumptions drawn from this model are over simplified. They suggest that a more applicable strategy would involve administration directly to the mesenteric artery, bypassing the intestinal permeability barrier, allowing the separate determination of intestinal absorption and later first-pass metabolism, as demonstrated in the study of Shin et al. 2014 [60]

As genetic manipulation techniques have developed, so too has the use of genetically modified animals as pharmacokinetic models; most frequently is the use of selectively engineered or specific gene knockout models to study the impact of intestinal metabolic CYP enzymes in a more direct and reliable approach. Humanised mice models with selective reinstatement of either liver or intestinal human CYP3A4, on complete CYP3A knockout background mice have proved a useful model in deciphering the independent contribution of hepatic and intestinal first-pass metabolism in oral bioavailability [61]. Moreover, the independent knockout of CYP3A and ABCB1 in genetically modified animal studies have elucidated key detoxification mechanisms and synergism [51,54]. Further to this, the organ-specific "knock in" has allowed drug-drug interactions (DDIs) to be investigated within a physiologically relevant yet controllable model for a more accurate understanding of *in vivo* drug dynamics [62]. Despite the success of these studies, the potential compensatory mechanisms, or alternative interactions from host (mouse) metabolising enzymes, cannot be overlooked and may affect data interpretation from these models.

1.3.1.2 *In Situ* Models

Whereas traditional *in vivo* animal models can demonstrate oral bioavailability on a whole animal scale, more detailed region-specific information can be accumulated from a range of *in situ* approaches including perfused gut loops [63] , portal vein sampling [42] and anhepatic models [64]. With correct preparation and experimental design, *in situ* models such as the perfused gut loop technique, can allow examination of intestine functionality from both the luminal and systemic sides in an anesthetised animal; allowing minimal disruption of normal intestinal function, a full complement of drug metabolising enzymes and transporters, as well as geometric and physical accuracies. Moreover, segregation of intestinal sections can allow for regional-specific

differences in drug absorbance to be compared; indeed, the regional impact of ABCB1 efflux on compound absorption from *in situ* models is well correlated with *in vitro* data [65,66]. However, the overarching utility of *in situ* models is limited by the extremely technical surgical procedures that are considerably more time and labour intensive and can incur significant costs. Additionally, the experimental parameters are limited to the tissue viability, which lasts only a matter of hours and requires intricate perfusion techniques, notwithstanding the tissue manipulation and effects of animal anaesthetics [37].

1.3.1.3 *Ex-Vivo* Models

Further augmentation of the traditional animal model comes in the form of intricate *ex-vivo* models; isolated organ and tissue samples derived from animal or human, maintained in experimentally controlled environments. Examples of such models include precision cut tissue slices (PCTS) [67], the Ussing Chamber [68], isolated tissue perfusion [69] and the everted sac model [70]. Not dissimilar to *in vitro* cell monolayer models, the Ussing chamber allows a section of intestinal tissue to be secured as a barrier between two separated artificial buffers representing the apical and basolateral sides of the intestine and can be observed for membrane transport, particularly of ions. The intestinal tissue represents all cell types present including enterocytes and goblet cells, and sustains their intact physiological interactions, alongside a full complement of drug metabolising enzymes at physiologically relevant expression levels. Various tissue perfusion models exist and work off a similar principle, maintaining fully intact cell structures for direct detection of permeability and metabolomics [71]. All *ex vivo* models permit the control and implementation of a range of external parameters including temperature, pH and blood flow enabling the study of a broad extent of intestinal conditions and their impact on xenobiotic compounds. Yet, the nature of *ex vivo* models means that their viability is extremely limited and necessitates extreme controls regarding oxygen and media flow, impeding the assessment of slow absorbing or metabolising xenobiotics [71].

1.3.1.4 Limitations of Non-Human *in vivo* Models

The largest problem facing pharmaceutical research and development is the extremely high attrition rates of potential therapeutics. Compounding this is the extent to which a new entity can survive the screening process until it is proved undesirable for human treatment; indeed, figures suggest that 80% of drugs deemed efficacious from preclinical animal studies fail in human clinical studies [72].

Historically one of the easiest animal models to work with experimentally, rodents are frequently used as an indicative model of xenobiotic therapeutic potential including toxicity and bioavailability. However, work comparing intestinal transporter expression profiles of both mice and rat compared to human shows considerable species diversity in the expressions of transporters for peptides, fatty acids, ions, and prominent efflux proteins [73] and therefore this work highlights considerable implications for xenobiotic absorbance and efflux in rodent models and humans, and may well contribute to differences arising from compound composition. The investigation of a variety of compounds of diverse absorption mechanisms in both rat and human in fact showed a moderate correlation between the transporter expression levels in both species, which correlated with similar absorption permeability [74]. However, they also concluded that due to no correlation in oral bioavailability values, that the rat is a poor model for drug studies, due to the marked differences in xenobiotic metabolism.

The differences in metabolism between a number of animal models has been extensively reviewed by Martignoni et al. 2006 [75] and highlights considerable dissimilarities regarding interspecies CYP3A expression and function, arguably the most important intestinal first-pass metabolising enzyme. Compared to rodents, dogs have been considered to have the most similar metabolic activity to that of humans [76], however, their absorption capacity relative to humans has been demonstrated to differ considerably [77] and may well stem from the diverse transcriptomic profiles of the two species [78]. A broad investigation comparing 184 compounds via linear regression methods reported no predictive correlation between compounds in any species; mouse, rat, dog and non-human primate [79]. Unsurprisingly, of all animal models, non-

human primates showed the highest correlation to human (R^2=0.7), yet the cost and ethical considerations make this an inefficacious model.

Although they are essential in simulating entire organism response to drugs and compounds, the utility of animal models in understanding the intestinal contribution to poor bioavailability are limited. Despite the additional physiology that animals can provide compared to *in vitro* models (whether as an entire organism, *in situ* or *ex vivo*), their intrinsic differences in absorption and metabolism of xenobiotics deem them an inefficient model for observing the intestinal contributions to bioavailability. Moreover, the expense, ethical issues and commitment to the 3R Principles of Replacement, Reduction and Refinement of animals in scientific research, call for alternative non-animal assays wherever possible. Development and improvement of *in vitro* preclinical models, which more accurately represent the human intestinal behaviour, would help bridge the gap between low throughput and variable animal models and high throughput, yet simple assays.

1.3.2 2D *In Vitro* Modelling

1.3.2.1 The Caco-2 Monolayer Model

The current "gold standard" *in vitro* predictive model for drug absorption and permeability accepted by the US Food and Drug Administration (FDA) is the Caco-2 Monolayer. The immortalised human colonic adenocarcinoma cell line Caco-2 was first pioneered as a polarised villus monolayer suitable for studying drug permeability in 1989 by Hidalgo and colleagues [80], and has since demonstrated remarkable accuracy in the prediction of transport and absorption of drug compounds [81–83].

Caco-2 cells grown on a permeable filter support are able to grow into a monolayer of epithelial enterocytes with an apical brush border and basolateral membrane (Figure 1.5). These permeable filters (also referred to as cell culture inserts or by the trade name Transwell®), are suspended in multi-well plates to create an upper and lower compartment, wherein test compounds can be added to the apical or basolateral side and compartment samples taken at subsequent time intervals for the determination of transcellular and paracellular absorption [84] (Figure 1.3).

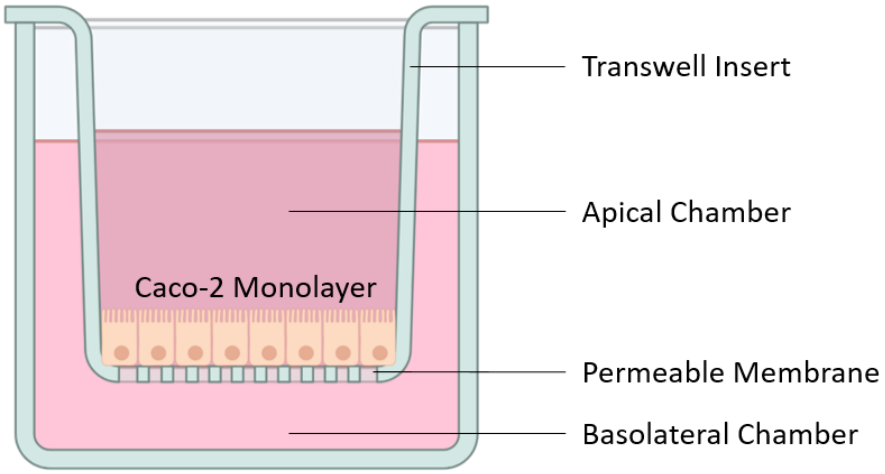

Figure 1.5 The Caco-2 Monolayer Model

Caco-2 epithelial cells grown on a permeable Transwell® insert suspended in a standard cell culture dish, to create apical and basolateral chambers representing the luminal and circulatory compartments respectively. Made with BioRender.com.

The popularity and success of the Caco-2 monolayer model derives from its remarkable morphological and functional accuracies; able to differentiate into a confluent monolayer culture resembling intestinal enterocytes. Caco-2 cells display microvilli, tight junctions and polarity in addition to expressing transporters, efflux proteins and Phase I and Phase II enzymes [85–88]. Such characteristics have facilitated the study of a vast range of major intestinal absorption mechanisms, including novel HIV treatments [89], oral antibiotics [90] and dietary iron bioavailability [91].

The efficacy of Caco-2 cells as a permeability and adsorption model unfortunately does not extend to determining extrahepatic first-pass metabolism due to the deficiency of CYP3A4 [92]. As the predominant Phase I metabolising enzyme in the small intestine [38], CYP3A4 contributes significantly to xenobiotic biotransformation of clinical relevance [49]. Amelioration of CYP3A4 expression and activity in Caco-2 cells has been undertaken, inducing expression with 1-α-2, 5-dihydroxyvitamin D3 [93] and transfection of human CYP3A4 copy DNA (cDNA) [53,94]; yet the resultant CYP3A4 expression levels remained substantially below that of the human intestine and, in the case of transfection methods, manifested a time-dependent decrease in expression attributed to DNA-methylation [95]. Protein expression profiles of Caco-2 display a number of functionally similar and overlapping enzymes of key biological significance to those found in scrapings of the human intestinal epithelium, however, there also exist a large proportion of proteins which display significant over- or under- expression compared to intestinal tissue [96]. Moreover, the similarities demonstrated in this study cannot be proven representative of the healthy human intestine, as the tissue scrapings utilised originate from colon cancer patients. Indeed, the Caco-2 cell line itself extends from cancer derived tissue and therefore resultant data must be interpreted with the knowledge that tumorigenic cells often demonstrate differential expression and altered metabolism [97]. Limitations of the Caco-2 monolayer model also derive from the cell's heterogeneous population, who's transient and mosaic gene expression can be modulated by both cell and culture-related factors [98]. Cell passage number has

demonstrated extensive impact not only on expression profiles and metabolic activities, but also differentiation and proliferation, causing many inter-lab inconsistencies [98]. Concordantly, the intrinsic simplicity of the Caco-2 monolayer model neglects numerous physiological factors which may impact on intestinal absorption and detoxification.

1.3.2.2 Alternative Monolayer Models

The Caco-2 monolayer as a simplistic and versatile model of intestinal absorption and permeability is unrivalled by any other *in vitro* methods. However, the limitations of the tumour-derived cell line to recapitulate key characteristics of the human intestinal epithelia have led to a call for more phenotypically relevant models.

One direct advance on the Caco-2 model has been established with the emergence of commercially available primary human intestinal epithelial cells (hInEpCs) (Lonza); a healthy epithelial tissue alternative characterised as suitably adapted to Transwell culture and expresses equivalent, if not more relevant intestinal biomarkers and barrier function than Caco-2 cells [99]. Moreover, somatic cells which can be re-programmed into embryonic-like pluripotent cells and then into a variety of cell lineages, named induced pluripotent stem cells (iPSCs) [100], provide a patient-specific source of human intestinal epithelial cells. Kauffman et al., 2013 [99] adapted the differentiation of iPSCs to intestinal epithelia to form a functional monolayer that showed extensive comparisons if not improvements on the Caco-2 model. Consistently, expression and functionality of membrane transporters [101], apparent permeability (P_{app}) values [102], barrier function [103] and metabolic activity [103,104] of iPSC-derived enterocytes showed significant promise as an improved *in vitro* monolayer model. However, the improved cellular similarities of both primary cells and iPSCs come at the cost of simplicity and time efficiency; both methods employing arduous cell culture techniques due to their sensitive viability, finite lifespans and expansion capacity. For iPSCs specifically, the long, sophisticated differentiation methods make the model considerably more complex than the original Caco-2 monolayer model.

As a homogenous cell population, the Caco-2 model is limited to the behaviour of its enterocytes only, whereas the absorptive surface of normal human intestinal villus

epithelia is studded with specialised intestinal cells, variably expressed and distributed amongst typical enterocytes (Figure 1.6). Modification to the standard Caco-2 monolayer by diversifying with multi-cellular and co-culture techniques has broadened the examination of cell type influence on intestinal behaviour. Of the specialised intestinal cells, goblet cells are the most studied in concurrence with Caco-2 cells; the cell line HT29-MTX mimics goblet cell function in producing mucus layers when co-cultured with Caco-2 cells [105]. Such models demonstrate increased paracellular permeability due to formation of fewer tight junctions than Caco-2 cells alone [105] and demonstrated a significant role in the absorption predictions of iron bioavailability [106]. Further advancement to the Caco-2/HT29-MTX model incorporates Raji B cells to create a triple co-culture model, including intestinal Microfold (M) cell phenotypes. These models have predominantly been used to dissect the transcytosis mechanism of intestinal transport, predominantly modulated by M cells, particularly in relevance to nanoparticle-type substrates [107–109].

Their amenability to a variety of assays make monolayer cultures an indispensable asset to intestinal research. However, their greatest drawback is the lack of diversity and tissue complexity that can be achieved in such a simplistic system. The absence of topological and structural features, in conjunction with underlying cell types and matrices of the epithelia have led to a call for more complex and developed models that recapitulate elements of the native tissue that cannot be achieved from monolayer culture alone.

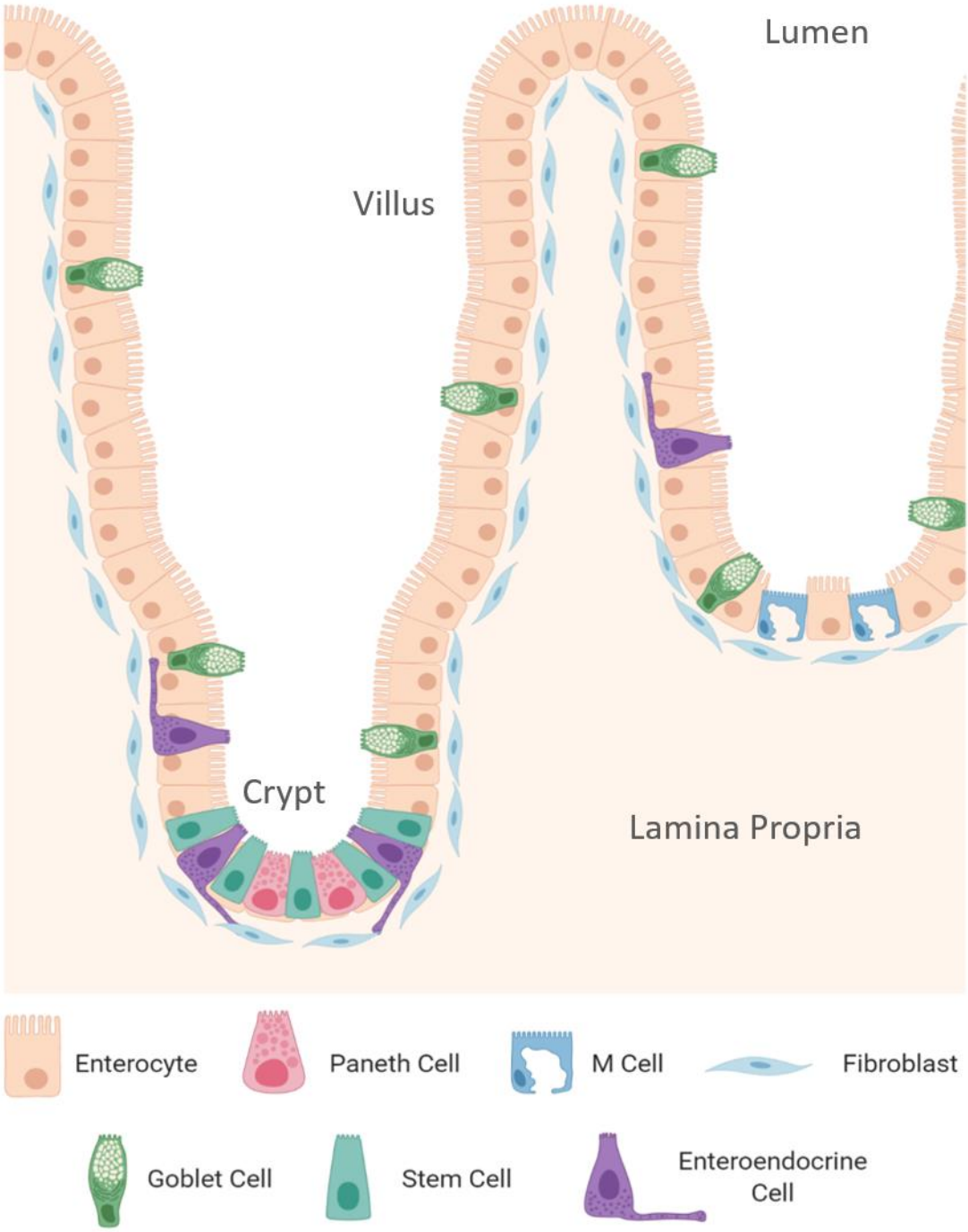

Figure 1.6 Cell Types of the Intestinal Epithelium

The absorptive enterocytes of the intestinal epithelia are supported by specialist cells with unique functions. Mucus producing goblet cells and enteroendocrine cells are widely distributed, whereas Paneth and intestinal stem cells are exclusively located in the intestinal crypts and M cells associated with inter-villi Peyer's Patches. Stromal fibroblasts line the basolateral side of the epithelia within the Lamina propria. Made with BioRender.com.

1.4 The Extracellular Matrix

In all organs and tissues, exists the non-cellular component known as the extracellular matrix (ECM), an intricate network of proteins, polysaccharides and growth factors, responsible for the mechanical and biochemical properties of tissues [110]. As a heterogenous and dynamic component of all tissues, the ECM functions as a mechanical framework expediting cell-cell interactions and organisation, as well as providing key chemical signals. These work together to control cell adhesion, migration, proliferation and differentiation on a cellular level [111] and morphogenesis, differentiation and homeostasis at a tissue level [110]. As such, the ECM maintains a crucial role in regulating numerous essential functions.

The ECM comprises of around 300 core proteins [112] that can be largely categorised into two classes of macromolecules; proteoglycans and fibrous proteins [110]. Proteoglycans assume the majority of the extracellular space as a hydrated gel, providing compression resistance and permitting the diffusion of small molecules [113]. The fibrous proteins of the ECM include elastin, fibronectin, laminin and most abundantly collagen. Collagen is predominantly a structural protein of the ECM, forming fibrils and networks that provide tensile strength to tissues, but also direct cell migration and adhesion [114]. Mesh networks of fibrils similar to collagen are produced by the ECM protein fibronectin, a key component in wound healing; its association with a range of integrins (a type of cell surface receptor) and the cellular cytoskeletal protein actin, make it a key regulator of cell adhesion and binding.

The ECM should not be thought of as merely a scaffold for cells however; its dynamic cross-talk between cells is multifaceted and reciprocal. Where mechanical and chemical cues of the ECM trigger cellular events, influencing cellular structure and differentiation, the cells themselves also alter the ECM. Stromal fibroblast cells that reside in the ECM, are the dominant cell type involved in ECM deposition and remodelling, having the ability to secrete and deposit ECM protein components, as well as the matrix metalloproteinases (MMPs) that degrade them. This ability to remodel the local proteomic environment and structure inevitably feeds back to impact cellular behaviour [115].

1.4.1 The Intestinal Extracellular Matrix

Like the majority of other epithelial and endothelial cells in the body, the intestinal epithelia sits on a bed of specialised ECM known as the basement membrane that resides above the bulk of the connective tissue of the villus, the *lamina propria* (Figure 1.7).

The intestinal basement membrane (BM) is comprised of two layers of ECM with distinct protein composition and topography; directly beneath the epithelial cells lies a thin layer of ECM proteins, the *basal lamina*, that sits above a highly fibrillous reticular sheet comprised of collagen fibres and subepithelial fibroblasts [116]. The most abundant ECM proteins of the basement membrane are collagen type IV, laminin, nidogen and fibronectin, along with the proteoglycan perlecan [113,117,118]. The proposed primary biological functions of the key ECM proteins are predominantly structural. Collagen type IV stabilises BM integrity and structure [119], fibronectin is a large, adhesive glycoprotein [120], whereas laminin is recognised in establishing epithelial cell polarity and maintaining villus architecture [117]. However as observed ubiquitously across all tissues, the ECM components have a unique interplay among themselves, and with stromal cells, to influence tissue behaviour and function.

Underneath the BM is a vast network of fibroblasts, immune cells and ECM proteins that form the dense sieve-like network of the lamina propria, which fills the space of the villus between the epithelium and the blood and lymphatic vessels (Figure 1.7). Compared to other tissues, the lamina propria of the intestine is incredibly cell-rich, containing a number of fibroblast and myofibroblasts cell types, expressing a variety of morphologies, surface markers and roles [116]. The function of fibroblast cells is broad, changeable and inconclusive; however, they are known to express and secrete a plethora of ECM proteins, particularly fibronectin [120,121], have mechanical contractility, as well as the ability to breakdown and remodel the ECM environment [116]. As a whole, the mesenchyme of the intestine (stromal cells and ECM) acts as a mechanical, biochemical and structural platform, supporting and modulating the specialist functions of the intestinal epithelium.

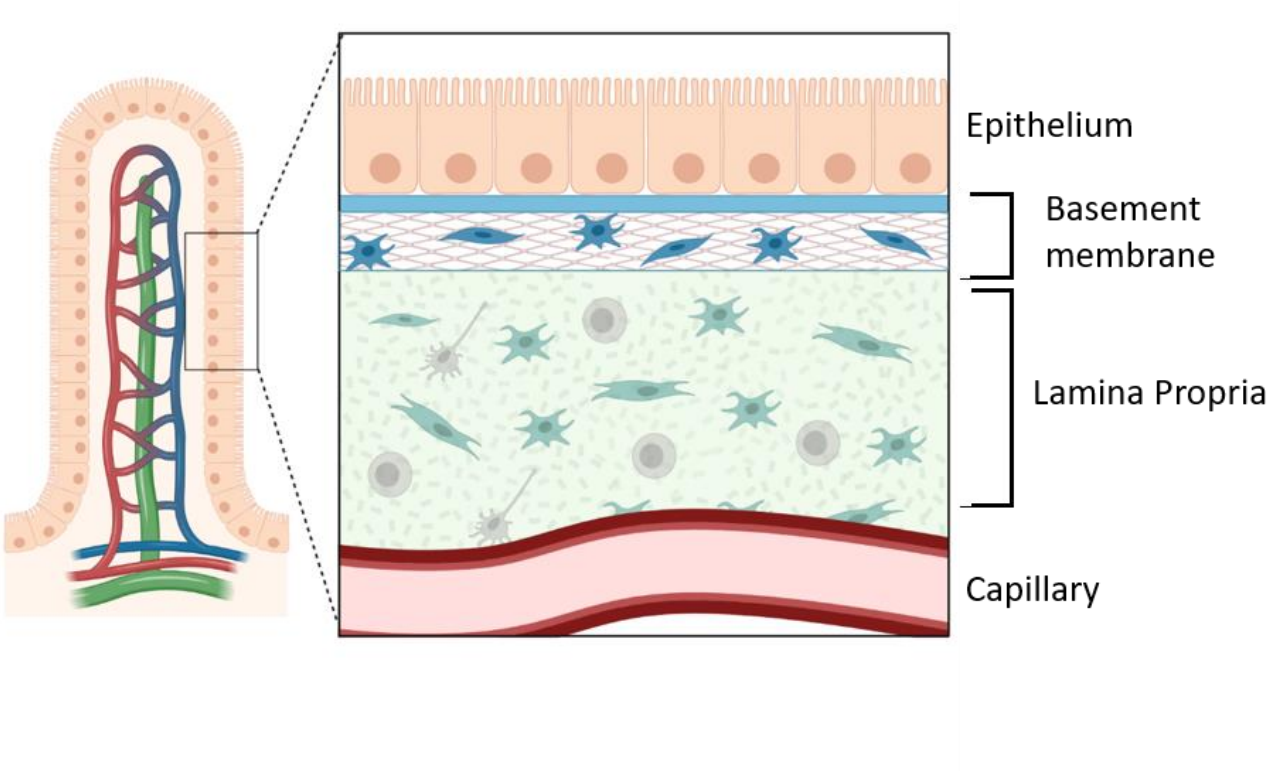

Figure 1.7 The Intestinal Extracellular Matrix

Beneath the epithelia of the intestinal villus resides the thin layer of ECM proteins known as the basal lamina that lies above a network of fibrous proteins and stromal fibroblasts that make up the subepithelial reticular sheet, together these are known as the basement membrane. The main bulk of the interstitial space between the basement membrane and the capillary bed is comprised of fibroblasts and immune cells within the connective ECM known as the Lamina propria. Adapted from Roulis et al. [116] Made with BioRender.com.

1.5 Three Dimensional Intestinal Modelling

Advances in biomedical approaches to tissue modelling for regenerative medicine, as well as the development of novel biomaterials and engineering processes, have led to opportunities to extrapolate from traditional two dimensional (2D) cellular assays, into more complex three dimensional (3D) models. The term 3D modelling covers a number of aspects which can be independently or collectively examined, and includes parameters such as 3D shape and geometry, cellular architecture and dimension, physiological composition and tissue complexity. Such models extend beyond flat monolayers, to generate tissue-like structures in a wholly *in vitro* experimental setting. The additional parameters incorporate key structural and cellular elements considered influential on intestinal functional behaviour, such as villus geometry [122–124], ECM proteins [125,126], or stromal cells [127–129], providing an opportunity to study a more representative depiction of tissues for both health and disease.

1.5.1 Multilayer Models

The role of the intestinal extracellular matrix (ECM) and underling stromal cells in potentiating mechanical and biochemical cues regulating intestinal function has encouraged the development of a variety of increasingly complex multilayer intestinal models. Not dissimilar to their monolayer counterparts, multicellular models incorporating cells of the stroma, such as ECM producing fibroblasts or immune cells, in cell culture inserts with the traditional Caco-2 epithelial cells (Figure 1.8A), have enabled an examination of the function of the intestine in a more physiological tissue environment. A handful of studies using fibroblast/epithelia bilayers have demonstrated more physiologically relevant intestinal permeability and tight junctions [127,130] as well as morphological characteristics [128] upon incorporation of these stromal elements. In these studies, the Transwell system was used, as in monolayer cultures, but with fibroblast cells embedded in collagen gels or commercially available sponge-like scaffolds beneath the epithelial cell layer. Additionally, studies have even integrated immune cells and goblet cells into their intestinal milieu, for a truly multicellular tissue model [131]. Furthermore, advancements and awareness of 3D printing technologies have allowed the 3D bioprinting of myofibroblasts and human

intestinal epithelial cells in a bilayer culture that demonstrated the recapitulation of a number of major intestinal features and biological function in permeability, metabolism and toxicity studies [129]. By rooting their models in the same assay format of the Transwell insert as the successful monolayer cultures, multilayer models are able to extrapolate well-characterised transport and permeability studies and easily apply them to more physiologically complex epithelia. However, despite having overcome the monolayer limitations of cellular complexity, these models still do not address any of the structural or mechanical elements of the native intestinal villi.

1.5.2 Scaffolds

The protruding invaginations of the intestinal villus structure, is a distinct structural feature which maximises the absorptive surface area of the intestinal lumen. Further to this, the structure-activity relationship of the crypt-villus axis is crucial in intestinal cell differentiation, gene expression, and cell maturation. To this end, incorporation of villi microstructures into 3D models of the intestine have been explored using a range of scaffold materials and fabrication methods [132] (Figure 1.8B).

Early published work initially demonstrated that Caco-2 cells cultured on polydimethylsiloxane (PDMS) villi microstructures had a wider variety of cyto-structural protrusions and less morphological uniformity [133]. This is in agreement with more recent work that showed enhanced cell polarisation when culturing Caco-2 cells on a bioprinted, fibronectin enriched synthetic hydrogel villi [122]. Studies exploring the intestinal activity detailed lower trans-epithelial electrical resistance (TEER) values, higher permeability and elevated enzymatic activity, of epithelial cells cultured on villi-shaped inserts made of collagen hydrogels [123,134] or synthetic poly(lactic-co-glycolic acid) (PLGA) [125]. It was noted in these studies, however, that the scaffold itself posed a physical barrier to rapidly transported drug compounds, limiting its use in determining accurate permeability and transport data.

Contrasting previous indirect methods of creating villi structure, W. J. Kim & Kim, 2018 [135] used 3D bioprinting to directly fabricate a villus from cells suspended in a collagen bioink, to form a multicellular model villi with surprisingly physiologically accurate

dimensions. Taking an altogether different approach, porous silk scaffolds have been used to create a multicellular tubular intestinal model, capturing the overarching luminal architecture of the intestine [136]. Further work by the group enabled the investigation of gut microbe interactions [137], but the structure of the model is limited in its utility to luminal interactions only, due to the physical inhibition of the scaffold structure to apical-basolateral transport experiments.

1.5.3 Organoids

Organoid is a broadly overarching term commonly used to describe three dimensional cellular models with structure, compositions and functions similar to that of the native tissues. These models developed from the observation that, upon stimulation with external growth factors and chemical signals, stem cells can differentiate into specific well-defined cell types of a particular tissue. Given the intestines natural differentiation gradient along the crypt-villus axis, stem cells can therefore be programmed to form intestinal tissues with a full complement of cell types in its epithelia.

With regards to intestinal organoid models, these can be further distinguished into organoids and enteroids depending on the initial source of stem cells; “organoids” being the term associated with induced pluripotent stem cell (iPSC) derived cellular structures, and “enteroids” with models derived from intestinal stem cells isolated from the crypts of human tissues [138,139] (Figure 1.7C). Intestinal organoids are unique spheroids with an almost full complement of epithelial cells and the underlying mesenchyme including fibroblasts [140]. The superior tissue complexity of these models make them invaluable for the study of developmental biology and show promise for evaluating different intestinal disease states. However, the phenotype of the cells in these models more closely represent that of the foetal intestine. Enteroids on the other hand show more mature intestinal differentiation, yet only comprise of the intestinal epithelia, lacking the underlying stromal elements. These were first developed after the discovery and understanding of stem cells specific to the intestinal crypts [141] and their ability to form crypt-villus spheroid structures *in vitro* [142]. The remarkable capacity of these highly physiologically comparable models to be maintained and propagated for years, has revolutionised intestinal tissue modelling.

The biggest limitation of both organoids and enteroids, however, is their spherical nature, which negates the majority of conventional *in vitro* assays useful for drug screening, absorption and metabolism [143].

1.5.4 Gut-on-Chip Models

Gut-on-chip models are a novel platform that stemmed from the establishment of microfluidic technology. The integration of a microscale, multi-chamber permeable cell surface, with microfluidic dynamics enabled the establishment of an intestinal model that addressed the previously unconsidered aspects of flow and mechanics of the intestinal lumen.

The first and most simple intestinal chips established by Imura et al. 2009 [144] demonstrated the incorporation of a Caco-2 monolayer into a microfluidic chip and its utility in observing the transport of compounds under simulated luminal and vascular flow. Further to this, studies have shown that the addition of mechanical elements of cyclical strain in later microfluidic devices led to the unstimulated morphological differentiation of Caco-2 cells into villus structures [145]. Other research groups have incorporated additional elements from other 3D models such as 3D villus structure [146] or enteroid-differentiated human primary cells [147]. Remarkably, recent work incorporated both fibroblast enriched collagen hydrogels with villus structures and enteroid derived murine epithelial cells, in the first reported study to allow the co-culture of both epithelial and stromal cells in a gut-on-chip device [148].

Despite their ingenuity and additional dynamic elements, gut-on-chip models do have their drawbacks. The design of these chips is often PDMS based, which is known to adsorb small hydrophobic molecules, making them unsuitable for drug screening. Moreover, where their microscale is often quoted as beneficial, utilizing fewer cells and media reagents, there are questions as the extent to which the data acquired on such a small scale can represent native intestinal behaviour. As discussed, the basic models that include the most mechanical and fluid dynamics do not incorporate any elements of the intestinal ECM, stromal cells or villus microstructure, however, when these elements are added, the same physical barriers to conventional absorption and permeability are encountered as in organoid or scaffold models.

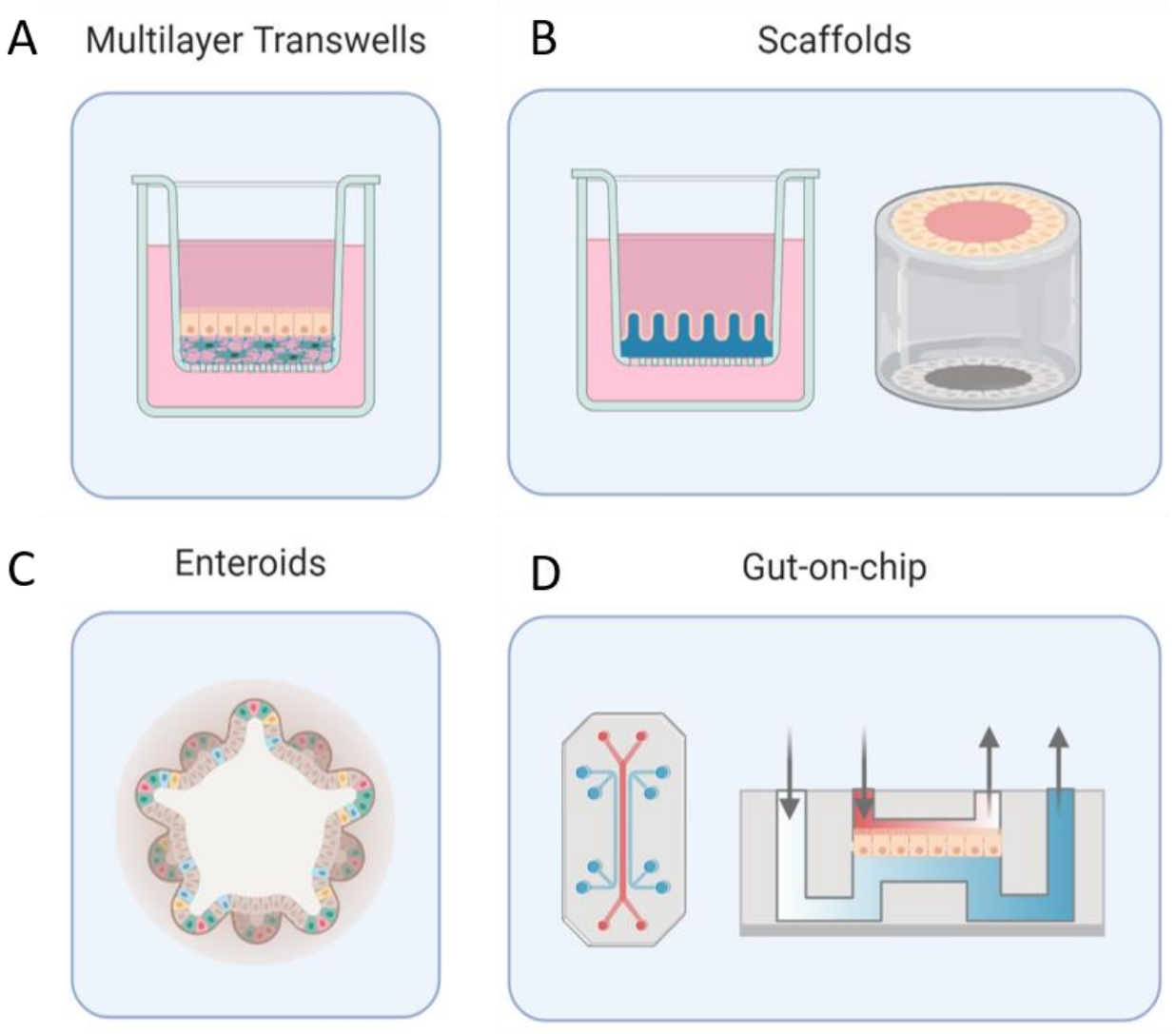

Figure 1.8 Summary of 3D Models

Incorporating 3D elements of cellular and tissue complexity, architecture and dynamics has been achieved through a number of different modalities and modelling techniques. (**A**) *Multilayer Transwell* models demonstrating fibroblast and epithelial co-culture within the established Transwell cell culture insert. (**B**) Epithelial cells grown on fabricated *scaffolds* mimicking villus structure or larger luminal architecture. (**C**) Intestinal stem cell derived spherical *enteroids* producing a full complement of epithelial cell types. (**D**) Epithelial cells grown on a permeable membrane in a microfluidic *Gut-on-chip* device are subjected to apical and basolateral flow, mimicking luminal and circulatory fluid dynamics. Not to scale. Made with BioRender.com.

1.5.5 2D vs 3D Models

Direct comparisons of the cellular behaviour and responses of the intestinal cell line Caco-2 in 2D and 3D monolayer culture have been defined across a range of 3D models. These studies have shown that Caco-2 cells grown in 3D culture show differences in morphology, proliferation, differentiation, lifetime, as well as TEER values, genetic markers and protein secretion [136,149–153]. When grown in 2D monolayers, cells are spread out, flat, on inert plastic surfaces and do not represent a realistic *in vivo* microenvironment. The gene expression differences observed from the 2D and 3D cultures may therefore arise from stress induced by unnatural cellular growth and/or the absence of environmental signalling cues. Furthermore, the ability of 3D structures to create an environment of hierarchical heterogeneous cell structures may alter not only the gene expression profiles of cells, but also their capacity for proliferation and differentiation, dependent on their spatial and temporal exposure to signalling cues. Nevertheless, it cannot be assumed that the differences observed in 3D cultured cells as opposed to traditional monolayers are necessarily more physiologically relevant. In fact, it is known that both the composition [154] and stiffness [155] of 3D scaffolds can modulate the behaviour and functionality of cells. Indeed, even basic cellular functions of proliferation and differentiation can be altered by the stiffness of a scaffold [156]. Therefore some differences observed and attributed to the microenvironment of cells may in fact be a product of the scaffold itself.

3D modelling methods have enabled the inclusion of aspects of ECM and stromal cells, structure, tissue complexity and maturity as well as fluid dynamics. However, the majority of these advancements in tissue engineering are not compatible in observing trans-epithelial transport, absorption and detoxification, as more often than not, their novel structural elements are physically inhibitive (Table 1.1). Therefore despite significant available modelling techniques, there is not yet a 3D model suitable in advancing the identification of successful oral small molecules. Moreover, the intrinsic limitations of the current 2D Transwell culture still persist. As such, there is still a need to develop accurate and reliable models suitable for high-throughput and cost effective screening for new oral therapeutics.

Table 1.1 Summary of the Features Captured by 3D Models

3D Feature	Model Type			
	Multicellular	Scaffolds	Enteroids	Gut-on-chip
Stromal Cells	●	●	●	●
Villi Structure	●	●	●	●
Fluid Dynamics	●	●	●	●
Drug screening	●	●	●	●

● YES ● In some cases YES ● NO

1.6 Thesis Outline

The aim of this thesis was to develop a physiological complex model of the human intestine, using porous PLLA fibrous membranes, as an improved preclinical tool for the study of absorption and detoxification *in vitro*.

Chapter 2. Materials and Methods

This Chapter details the experimental methods used throughout this thesis.

Chapter 3. Characterisation of Porous PLLA Fibres as a Cell Culture Surface

This first results chapter describes the characterisation of the morphological and topographical properties of electrospun poly(L-lactic acid) fibrous membranes and their relevance to *in vivo* tissue architecture. The fibres are also examined for their surface properties and how these affect their biocompatibility and use as a cell culture surface.

Chapter 4. Fabrication and Evaluation of a Fibre Membrane-Based Intestinal Monolayer Model

The PLLA fibrous membranes are used to fabricate a novel fibrous cell culture insert, upon which a Caco-2 intestinal monolayer model is developed. This fibre-based monolayer is then evaluated for its differentiation, morphology and ECM expression, and ultimately its barrier function, compared to the standard Transwell Caco-2 model.

Chapter 5. Intestinal Bilayer Models and the Role of Subepithelial Fibroblasts

This final results chapter describes the creation of a series of models, centred on the development of a bilayer model which incorporates both PLLA fibrous architecture and subepithelial fibroblasts cells. Tissue models with differing spatial arrangements of fibroblasts, are compared to the monolayer model on both Transwell and PLLA fibre surfaces, to allow the dissection of the role of fibroblasts on intestinal function, as compared to the impact of culture surface.

Chapter 6. General Discussion and Future Work

This chapter discusses the impact and limitations of the major findings of each chapter and highlights potential future work opportunities.

2. Materials and Methods

2.1 Electrospun PLLA Fibre Characterisation

2.1.1 Electrospinning of Fibrous Membranes

The porous poly(L-Lactic acid) (PLLA) fibres used throughout this study were kindly gifted from Dr Jiashen Li, Department of Materials, University of Manchester. The electrospinning methods can be found previously published by Lu et al., 2020 [157]. Briefly, PLLA (1.6 wt%) was heated until dissolved in a 95:5 ratio Dichloromethane: Dimethylformamide. After electrospinning at high voltage, the collected neat PLLA fibrous membranes were completely dried before immersion in acetone for 5 min at room temperature. When air dried, the acetone treatment induces PLLA recrystallization that produces the porous structure of the fibres.

2.1.2 Analysis of SEM Images

Scanning electron microscopy images collected by Dr Jiashen Li, were analysed using Image J software. Inter-fibre pore diameters were classed as membrane pores and were measured using the Feret's Diameter feature on thresholded images with noise from surface pores removed using the despeckle tool. Fibre diameters themselves were calculated using the Image J plugin Diameter J with M8 segmentation. Fibre surface pits and pores were measured manually.

2.1.3 Contact Angle Measurements

Surface wettability of cell culture surfaces were analysed using the sessile drop method to measure the contact angle of 4 µl UHQ water on dry, untreated PET membranes excised from Transwell® plates, porous PLLA fibre membranes, smooth PLLA fibres (no acetone treatment) and glass cover slips. Contact angles were recorded using CAM2008 software over ten frames and the mean calculated from left and right contact angles.

The contact angle (θ) is calculated by Young's equation

$$\gamma_{lv}\cos\theta = \gamma_{sv} - \gamma_{sl}\,, \tag{2.1}$$

where γ_{lv}, γ_{sv} and γ_{sl} denote the surface tensions of the three interfaces; liquid-vapour, solid-vapour and solid-liquid, respectively, as seen in Figure 2.1.

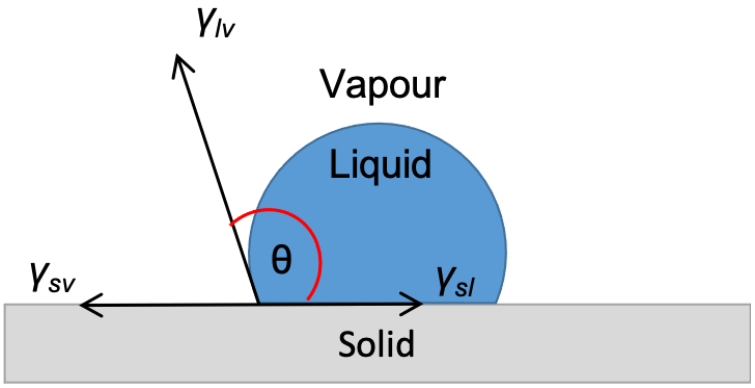

Figure 2.1 Water Contact Angle Measurement

Water contact angle (θ) as explained by Young's equation surface tension between three interfaces.

2.1.4 Protein Adsorption

2.1.4.1 Immunofluorescence of Protein Adsorption

Adsorption of protein onto PLLA fibres was determined using immunofluorescence staining for Fibronectin and Collagen Type I. 5 mm^2 squares of porous and non-porous PLLA fibre membranes as well as Transwell PET membranes were soaked for 30 min in 70% ethanol before soaking for 30 min in PBS (Control), DMEM media supplemented with 10% FBS (for fibronectin staining) or 0.5mg/ml Rat Tail collagen I solution (for collagen I staining). Membranes were then washed twice in PBS and once in UHQ. Membranes were then probed with anti–fibronectin or anti-collagen I antibody (1:100) for 2 hr, before washing 3x with PBS and incubating for 1 hr with FITC-conjugated secondary antibody (1:100). After antibody staining cell surfaces were imaged using Nikon Eclipse TE2000-U fluorescence microscope.

Quantification of protein adsorption on membranes was calculated in Image J using the mean gray value of images, after background subtraction with a rolling ball radius of 50.0 pixels. The mean gray value of serum and collagen soaked membranes was

calculated by subtracting the mean gray value of PBS-soaked fibres, to negate differences in membrane autofluorescence.

2.1.4.2 Bovine Serum Albumin Adsorption Quantification

Protein adsorption of BSA to fibres and Transwell membrane was assessed using the solution depletion method. 5 mm^2 squares of porous and non-porous PLLA fibre membranes as well as Transwell PET membranes were soaked for 30 min in 70% ethanol before soaking for 30 min in 1 ml of 0.5 mg/ml BSA: PBS solution in a 24-well cell culture plate at room temperature. As a control, the same BSA solution was also added to an empty well to account for any BSA adsorption to the well plate. After 30 min the BSA protein concentration of the solution was assessed using a UV-Vis Spectrophotometer (ThermoSpectronic Genesys6) and the concentration determined using a standard curve of known BSA concentration. The percentage adsorption of BSA was calculated by determining the reduction in solution concentration from time 0 min, minus the percentage adsorption of the control.

2.1.5 Fabrication and Preparation of PLLA Fibre Inserts

PET membrane films were removed from Transwell cell culture inserts with a scalpel to leave the polystyrene cell insert. Clear acetoxy silicone (King British Aquarium Sealant) was applied to the perimeter of the insert base and adhered to the PLLA fibrous membrane with a firm but gentle application. This was left to cure overnight on the bench at room temperature. Excess PLLA membrane was cut away and the resultant PLLA insert moved to a 24-well plate. Newly fabricated PLLA inserts were sterilised with UV light on both sides, before soaking for 30 min in 70% ethanol, followed by 30 min in complete medium.

2.2 Cell Culture Techniques

2.2.1 Cell Lines, Cell Media and Culture Components

Human colon adenocarcinoma Caco-2 cells at passage number P50-60 and NIH3T3 mouse fibroblasts were kindly donated by Dr Jing Zhang, Biological Physics Group, University of Manchester. Caco-2 cells expression green fluorescence protein GFP-Caco-2 cells were kindly gifted from the Hurlstone lab, University of Manchester. Normal human intestinal fibroblast cell line CCD-18co (CRL-1459) were acquired from the American Type Culture Collection and used at passage number P2-10.

Dulbecco's Modified Eagles Medium (DMEM) - high glucose (D6429), Foetal bovine serum (FBS) (F9665), Penicillin-Streptomycin (P4333), Dulbecco's Phosphate Buffered Saline (DPBS) (D8537) and Trypsin-EDTA solution (T3924) were all purchased from Sigma, UK.

2.2.2 Plasticware

All routine cell culture was carried out in tissue culture treated, vented cap, T75 flasks or 6,12, 24, 96-well plates from Corning Life Sciences. For experimental cell culture Transwell® inserts (12-well) (Corning S3460) and TC inserts (24-well) (Sarstedt 83.3932.041) both PET, 0.4 µM pore size were used with the relevant the aforementioned well plates.

2.2.3 Routine Cell Culture

All cells were routinely cultured in T75 flasks with Dulbecco's Modified Eagles Medium supplemented with 10% Foetal bovine serum (FBS) and 100 UmL^{-1} Penicillin/ 100 µg mL^{-1} streptomycin (this was excluded for the culture of CCD-18co cells) and incubated at 37 °C and 5% CO_2. Cell media was replaced every two days.

Cell passaging or harvesting prior to experiment seeding was carried out using the following the protocol. When cells were observed to be 80-90% confluent, they were washed twice with 2 ml dPBS before detachment with 1ml Trypsin-EDTA at 37°C (typically incubated for 5 min before checking under light microscope for level of detachment). When cells were considered detached the Trypsin enzyme was

neutralised using a minimum of 5 ml pre-warmed complete medium in which cells were resuspended. A 100 µl sample of the detached resuspended cell solution was then counted by diluting 1:1 (v/v) with Trypan Blue solution and using a Haemocytometer. Cells were then diluted in pre-warmed cell media to a seeding density according to the relevant protocol.

2.2.4 Creation of Intestinal Models

All cell models used in this thesis were cultivated on either PET Transwell cell culture inserts, or PLLA fibrous membrane inserts. Unless otherwise stated, all cell models were seeded with cells at the following densities; Caco-2 intestinal epithelial cells at $1x10^5$ cells/cm^2, NIH3T3 Mouse fibroblast cells at $0.5x10^5$ cells/cm^2, CCD18co intestinal subepithelial fibroblasts at $0.5x10^5$ cells/cm^2. Cells were cultured for 21 days in an incubator at 37°C and 5% CO_2, with high glucose DMEM media supplemented with FBS changed every two days.

2.2.4.1 Monolayer Models

Monolayers on both Transwell and PLLA fibre inserts were seeded as above with Caco-2 epithelial cells.

For ECM coated monolayers, sterile PLLA fibre monolayers were soaked in 0.5 mg/ml Rat Tail Collagen type I solution in PBS for 1 hr, air dried in the biological safety cabinet and then washed with PBS. Fibres were soaked for 30 min in cell culture media before seeding.

2.2.4.2 Bilayer Models

For Bilayer models, Transwell and PLLA fibre inserts were first seeded with fibroblasts cells, either non-specific NIH3T3, or intestinal-specific CCD18co, and left to attach and cultivate for 24 hours before seeding on top with Caco-2 cells.

2.2.4.3 Co-culture Models

For Co-culture models in both Transwell and PLLA fibres, CCD18co fibroblasts were seeded into the bottom of the well of a 12-well culture plate. On the same day, Caco-2 cells were seeded into cell culture inserts, residing in a different well plate, to prevent cross contamination of cells whilst they were still suspended. After 24 hr of attachment and growth, the inserts were moved to hang in the same wells as the CCD18co fibroblasts.

2.2.4.4 Conditioned Media Models

For conditioned media models, CCD18co cells cultured in T75 flasks were incubated with fresh cell culture medium. After 24 hr, the media was harvested and filtered through a 0.2 µm filter to remove any cells and debris. It was then mixed at a 1:1 ratio with fresh media before adding both apically and basolaterally to a Caco-2 monolayer. Excess media was stored at -20°C to prevent protein degradation.

2.3 Cell Viability and Proliferation Analysis

2.3.1 MTT Cell Viability Assay

In Chapter 3, Caco-2 cells were seeded onto 5 mm^2 squares of Transwell membrane, PLLA fibrous membrane or TCPS of a 96-well plate at a density of $1x10^5$ cells/cm^2 and cultured over 21 days. At each time point, before the assay solution was added, both membranes were gently transferred to a fresh well so as to only include cells attached to the membrane and not to the bottom of the plate.

In Chapter 4 Caco-2 epithelial cells and NIH3T3 fibroblast cells were seeded at a density of $1x10^5$ cells/cm^2 in a 96-well TCPS plate with a dot of acetoxy silicone glue, or Super Glue (cyanoacrylate) to determine the most suitable cell safe adhesive. After 3 days of growth, cell viability was assessed.

Cultures were replaced with 100 µl fresh media and 10 µl of 5 mg/ml MTT solution (Thiazolyl Blue Tetrazolium Bromide, Sigma) was added to each sample and incubated at 37 °C and 5% CO_2 for 2 hr. 200 µl DMSO was then added to dissolve the generated

formazan crystals and samples were incubated for a further 1 hr. 200 µl samples were then transferred to a new 96-well microplate and the was absorbance read at 570 nm on a microplate reader (Tecan Sunrise). Results are given as raw absorbance values or as a percentage of the control.

2.3.2 Live/Dead Viability Imaging

Caco-2 cells seeded at a density of $1x10^5$ cells/cm^2 cultured on regular tissue culture polystyrene (TCPS), Transwell PET membrane and PLLA fibrous membranes were assessed after 21 days of culture. Cells were washed twice with PBS before incubating for 30 min at room temperature with Hoechst 33342 (DAPI) (excitation/emission wavelengths 350/470 nm), staining the cell nuclei of all cells. Cells were gently washed with PBS to remove excess stain, before incubating for a further 30 min with Propidium Iodide (PI) (excitation/emission wavelengths 493/636 nm), staining all dead cells. Images of the same area of cells was taken using the Nikon Eclipse TE2000-U for both DAPI and PI. Percentage dead cells was calculated using the mean gray value of PI image, obtained in Image J, divided by that of the DAPI image.

2.3.3 Cell Proliferation

GFP-Caco-2 cells were seeded at a density of $1x10^5$ cells/cm^2 on both Transwell membranes and PLLA fibrous membrane. Cultures were imaged using fluorescence imaging on the Nikon Eclipse TE2000-U, 1, 2, 3, 4, 7 days after seeding to monitor the proliferation of cells grown on each culture surface. Images were analysed in Image J using rolling ball background subtraction of 50 pixels, followed by thresholding to make a binary image, and using the number of white pixels (representing areas of fluorescent cells) as an indirect measure of cell confluence. Proliferation rate was calculated by dividing the cell confluence over time. As an additional measure of cell confluence, the total protein content lysed from each culture surface was calculated as described in methods Section 2.7.4.

2.4 Trans-epithelial Electrical Resistance (TEER) Measurements

TEER measurements assessing the epithelial barrier integrity were taken for Caco-2 cells cultured on cell culture inserts. The Evom2 Voltohmmeter with STX2 chopstick electrodes were sterilised with ethanol for two minutes before equilibrating with cell media for two minutes prior to resistance measurements. Each cell culture insert was measured twice using different electrode placement locations. Reported resistance measurements are inversely proportional to the tissue area measured, therefore to compare results between different sized culture inserts and published values, the final TEER measurements were calculated using the following equation;

$$\text{TEER} = (R_{Exp} - R_{Bl})A \,, \tag{2.2}$$

where R_{Exp} is the experimental resistance value, R_{Bl} is the resistance value of a blank culture insert and A is the surface area of the cell culture insert.

2.5 Immunofluorescence Imaging Analysis

2.5.1 Immunofluorescence Staining

All immunofluorescence imaging and fluorescent confocal microscopy samples were prepared using the same staining protocol, with the variation of antibodies used based on experimental design. A detailed list of antibodies used throughout this work can be seen in Table 2.1. All antibodies were used as a 1:500 dilution in Phosphate Buffered Saline (PBS) unless otherwise stated.

Cultured cells on glass coverslips or culture inserts were washed twice with PBS and fixed with 4% paraformaldehyde at room temperature for 10 min. Permeabilisation was with 0.2% Triton–X100 for 15 min at room temperature, followed by blocking to prevent non-specific protein interactions, for 20 min with 1.5% BSA/PBS solution. Primary antibodies were incubated at room temperature for 2 hr in a humid environment, before washing twice with PBS and incubating with the corresponding fluorescently-conjugated secondary antibody at room temperature for 1 hr protected from light, to prevent photo-bleaching. Cell nuclei and actin protein were then

counterstained with 1:1000 Hoechst 33342 and Phalloidin respectively, for 30 min before gently washing three times with PBS.

For cells cultured on cell culture inserts, the culture surface was then carefully removed using a scalpel and mounted on glass slide with VETORSHIELD® mounting medium and sealed with a glass coverslip and nail varnish.

Table 2.2 List of Antibodies

Antibody Name	Supplier (product code)
Anti-Human ZO-1 (Mouse)	BD Bioscience (610966)
Anti-Human Fibronectin (Rabbit)	Sigma (F3648)
Anti- Human Collagen Type IV (Rabbit)	Abcam (ab6586)
Anti-Mouse IgG FITC (Goat)	Dakocytomation (F0479)
Anti-Rabbit IgG Alexa Fluor® 488 (Donkey)	Invitrogen (A21206)
Anti-Rabbit IgG Alexa Fluor® 594 (Goat)	Invitrogen (A11037)
Anti-Collagen I (Mouse)	Sigma (C2456)

2.5.2 Confocal Laser Scanning Microscopy Imaging

Confocal laser microscopy images were obtained with the inverted Leica SP8 with LASX software in the Bioimaging Centre, University of Manchester. Z-stack images were typically acquired using 63X magnification with the suggested step depth of 0.3 µM unless otherwise stated in figure caption. Magnification is demonstrated on all samples using scale bars. All image analysis was undertaken in Image J software

2.5.2.1 GFP-Caco-2 Monolayer Z-stacks

Green fluorescent protein (GFP) expressing Caco-2 cells seeded at a density of $1x10^5$ cells/cm^2 were cultured on PLLA fibre inserts for 21 days before fixing with 4% PFA and permeabilisation with Triton-X 100 and counterstaining with DAPI. Mounted samples were imaged with 20x and 63x oil lenses on the Leica SP8 inverted confocal laser scanning microscope and images presented using ImageJ software.

2.5.2.2 ECM Protein and Actin Expression Z-stack Analysis

Caco-2 cells seeded at a density of $1x10^5$ cells/cm^2 were cultured on PLLA fibre inserts for 21 days before following the immunostaining protocol. Confocal images obtained were curated and analysed in Image J software. For quantification of protein expression, the mean gray value of the Sum Z-project image of each protein was recorded. For analysis of the distribution of the fluorescently bound proteins, the plot Z profile feature in Image J was used to plot the gray value as a function of depth for both the protein of interest and of DAPI. Nuclei elongation and cell height measurements were conducted manually using Image J measure tools.

2.5.2.3 ZO-1 Tight Junction Expression Z-stack Analysis

Caco-2 cells seeded at a density of $1x10^5$ cells/cm^2 were cultured on PLLA fibre inserts for 21 days before following the immunostaining protocol. Confocal images obtained were curated and analysed in Image J software. ZO-1 expression quantification followed previously published methods [158]. Briefly, Sum Z-project images of Z-stacks were generated for ZO-1 and the background was subtracted (Rolling ball 50 pixels). Enhanced contrast images were used to create a binary image by auto-threshold, which were used to assess expression. Four horizontal and vertical lines across the image were used to derive a plot profile, of which the number of peaks exceeding the pixel intensity threshold (twice the mean of the background noise) was calculated and used to quantify the relative ZO-1 expression.

2.6 Quantitative real time Polymerase Chain Reaction (RT-qPCR)

Caco-2 cells seeded at a density of $1x10^5$ cells/cm^2 were cultured on PLLA fibre inserts for 2, 7, 14, 21 days before following the RT-qPCR protocol.

2.6.1 RNA Extraction

RNA from Caco-2 cells was isolated by adding 1 ml TRIZOL® to cell cultures followed by vigorous pipetting. After transfer of the homogenate to a separate tube, it was allowed to sit for 5 min at room temperature (RT) before chloroform phase separation. 200 µl Chloroform was added to each sample tube and immediately agitated quickly by hand for 15 sec. After 3 min incubation at RT, samples were centrifuged at 10,000 rpm at 4°C and the upper aqueous phase of the solution was transferred to a new Eppendorf tube. RNA precipitation was with 500 µl isopropanol incubated at RT for 10 min before centrifugation for 10 min at 10,000 at 4°C. Afterwards the supernatant was removed and the RNA pellet was washed with 1 ml 70% ethanol (in DEPC-treated water). Ethanol was removed and evaporated by air drying for 5 min on the lab bench. The RNA pellet was dissolved in 100 µl DEPC water and the concentration measured using the NanoDrop Nucleotide Reading Programme.

2.6.2 cDNA Synthesis

2 µg RNA was DNase treated using RNase-Free DNase Set (Qiagen) and incubated at RT for 15 min. 5µl of 50mM EDTA solution was then added to each sample and heated at 65°C for 10 min. 1 µg of DNase treated RNA was then taken for cDNA synthesis using the Protoscript II first strand cDNA synthesis kit as per the manufacturer's protocol.

2.6.3 RT-qPCR Reactions

Selected genes were amplified by quantitative real time PCR (RT-qPCR) in 20 µl reactions using Sygreen (PCR Biosystems). Relative expression was calculated using the delta-delta CT methodology [159] and beta-actin was used as the reference housekeeping gene. The cycling conditions were as follows: enzyme activation at 95 °C for 10 min

followed by 40 cycles; 95 °C for 30 s and at 60 °C for 30 s and 72°C for 30s. Specific transcripts were detected with primers following evaluation for their amplification efficiency. qPCR primers were designed using Primer 3 or Primer-BLAST based on reference gene sequences from the NCBI RefSeq database. A detailed list of Primer supplier and sequences can be found in Table 2.2.

Table 3.2 List of qPCR Primers

Target Name	Gene Name	Forward Primer Sequence	Reverse Primer Sequence	Supplier
Aminopeptidase N	ANPEP	TCAACTACACCCTCAGCCAG	TCTGACATTGCCCTCCATGT	Invitrogen
ATP Binding Cassette Subfamily B Member 1	ABCB1	TCAGCTGTTGTCTTTGGTGC	GGTCGGGTGGGATAGTTGAA	Eurofins
Claudin 1	CLDN1	TGCTTGGAAGACGATGAGGT	CAGTGAAGAGAGCCTGACCA	Eurofins
Collagen type I	COL1A1	GCTACTACCGGGCTGATGAT	ACCAGTCTCCATGTTGCAGA	Eurofins
Collagen type IV	COL4A1	CAGGTGGAGGCAAATCTTCG	AGTTGTTGCAAGCCGAAGAG	Invitrogen
Fibronectin 1	FN1	GTATACGAGGGCCAGCTCAT	CCCAGGAGACCACAAAGCTA	Eurofins
Intestinal Alkaline Phosphatase	ALPI	GATTCTTCCTCCCAACCCCA	CCTGATCCACCCAAGTCCTT	Eurofins
Laminin alpha 3	LAMA3	CATCAGAGCGCCAGTTTACC	AGTGAGCCAAGACGACATGA	Invitrogen
Laminin alpha 5	LAMA5	CTGTGCAAACCCAACTTCCA	CTGGCAGAGAGGGAAGTGAA	Eurofins
Nidogen	NID1	GACTGACCTTCGATGCGTTC	CAAGATCGAGAGCAACCACG	Invitrogen
Occludin	OCLN	GGGCATTGCTCATCCTGAAG	GAGTAGGCTGGCTGAGAGAG	Eurofins
Peptide transporter 1	SLC15A1	TGTGTCGCTCTCCATTGTCT	GATTCCTCCAGTCCCGAGAG	Invitrogen
Perlecan	HSPG2	CACCTGATCTCCACCCACTT	GTCTCCCTGGTATGTCTCCG	Invitrogen
Villin 1	VIL1	TTGGGAAACATGCCAACGAG	CCAGTCCCTAGAGTTGCCAA	Invitrogen
Zona Occludens 1 (isoform v1)	TJP1	CCAGCATCATCAACCTCTGC	CATGCGACGACAATGATGGT	Invitrogen

2.7 Intestinal Function Assays

2.7.1 Paracellular Permeability Assays

In all cases, the paracellular permeability coefficient P_{app} was calculated using the following equation,

$$P_{app} = \frac{1}{c_0}\frac{dQ}{dt}, \tag{2.3}$$

where *dQ/dt* denotes the rate of change in basolateral compound concentration over time, C_0 denotes the initial concentration of compound in the apical chamber, and *A* denotes the surface area of the culture insert.

2.7.1.1 Lucifer Yellow

Cells were first gently washed 3x with Hank's Buffered Saline solution (HBSS) and moved to a fresh receiver plate. 1 ml of HBSS was added to the basolateral side, and 500 µl of 100 µM Lucifer Yellow (LY) added to the apical compartment of the insert and the plate was incubated at 37°C for 2 hours. 50 µl samples from both apical and basolateral compartments were transferred to a 96-well sample plate and the fluorescence measured using the excitation/emission wavelengths 485/530 nm. Sample concentrations were calculated by comparing fluorescence to a standard curve of known concentrations of LY.

2.7.1.2 FITC-Dextrans

Cells were first gently washed 3x with Hank's Buffered Saline solution (HBSS) and moved to a fresh receiver plate. 1 ml of HBSS was added to the basolateral side, and 500 µl of FITC-Dextran at 0.4mg/ml either molecular weight 4 kDa (FD4) or 70 kDa (FD70) added to the apical compartment of the insert and the plate was incubated at 37°C for 4 hr. At 30, 60, 90, 120, 180, 240 min after addition, the entirety of the 1ml basolateral chamber solution was replaced for fresh HBSS, to maintain sink conditions. These 1 ml samples were transferred to a 24-well plate and the fluorescence measured using the excitation/emission wavelengths 490/520 nm. Sample concentrations were

calculated by comparing fluorescence to a standard curve of known concentrations of FD4 and FD70.

2.7.2 Enzyme Activity Assays

2.7.2.1 Alkaline Phosphatase Assay

ALP enzymatic activity was assayed on day 21 using previously published methods [160]. Firstly, cells were washed gently 3x with Hank's Buffered Saline solution (HBSS) and moved to a fresh receiver plate. 1 ml of HBSS was added to the basolateral side, and 500 µl of ALP solution (*p*NPP) added to the apical compartment of the insert. 50 µl samples were transferred at the time points 2, 6, 10, 14, and 18 min after addition of the ALP solution, to a 96-well sample plate containing 50 µl of 0.5M NaOH to quench any further enzyme activity. These samples were then read using the absorbance function of the Tecan Sunrise plate reader at 405nm and compared to a standard curve of ALP product (*p*-NP). Using this data, rates of reaction were then calculated.

2.7.2.2 CYP3A4 Metabolic Activity Assay

Cells were first gently washed with HBSS 3x before adding 1 ml HSS to the basolateral compartment and 250 µl of 10 µM BOMCC substrate to the apical compartment and incubated for 30 min at 37°C. 50 µl samples from the apical compartment were then transferred to a 96-well plate and fluorescence read at 415/460nm.

2.7.3 Transporter Activity Assays

2.7.2.1 PEPT1 Influx Activity

Cells were first gently washed with HBSS 3x before adding 1 ml HSS to the basolateral compartment and 250 µl of 25 µM D-Ala-Leu-Lys-7-amido-4-methylcoumarin (AMCA) substrate to the apical compartment and incubated for 4 hr at 37°C. Cells were then washed with HBSS to remove non-transported AMCA and lysed in RIPA buffer. 50 µl lysate samples were then transferred to a 96-well plate and fluorescence read at 350/430nm.

2.7.2.2 ABCB1 Efflux Activity

Before assaying, cell culture media was removed from cells, gently washed 2x with HBSS, before incubation at 37°C for 30 min in HBSS to prevent interference from serum. For ABCB1 inhibited cells 250 µl of 10 µM Verapamil was added to the apical compartment and incubated for 30 min. For cells not inhibited, 250 µl HBSS was added. 250 µl of 1 µM Calcein AM was then added apically (for a final concentration of 0.5 µM) and incubated for a further 30 min. Cells were then gently washed with ice cold PBS to remove extracellular Calcein. 50 µl lysate samples were then transferred to a 96-well plate and fluorescence read at 485/530 nm.

2.7.4 Protein Quantification

Total protein quantification was used as a normalisation method for fluorometric cellular assays and as an indirect measure of cell number using the DC Protein Assay. Cells were lysed using 250 µl (12-well plates) or 50 µl (24-well plates) of RIPA Lysis Buffer; 150 mM NaCl, 1% (v/v) Triton X-100, 0.5% (w/v) Sodium Deoxycholate, 0.1% (w/v) SDS, 50 mM TRIS, pH 8.0, for 10 min at 4°C. After agitation with a pipette to mechanically lyse and mix the cell solution, 5 µl samples were pipetted into a 96-well microplate in triplicate. To each sample well, 25 µl of Solution A' (20 µl Solution S per 1 ml Solution A) and 200 µl of Solution B were added and left for 15 min at room temperature before reading the absorbance on a microplate reader at 750 nm. Absorbance values of samples were converted to a concentration in mg/ml by comparing to a standard curve prepared with a serial dilution of Bovine Serum Albumin (BSA) in PBS.

2.8 Statistical Analysis

All statistics were carried out using GraphPad Prism 8.0 software. Specific statistical analysis is stated in the figure captions, alongside the n numbers; total number of technical replicates from a number of experimental replicates, which where possible was always carried out in triplicate. Any deviation from this is stated in figure captions.

P values ≤ 0.05 were considered significant and are denoted using the following format; * p≤0.05, ** p≤0.01, ***p ≤ 0.001, ****p≤0.0001.

2.9 Chemicals

All other chemicals and reagents used in this thesis are as follows. Dimethyl sulfoxide (DMSO) (D8418), Hank's Buffered Salt Solution (HBSS) (55037C), Thiazolyl Blue Tetrazolium Bromide (MTT Solution) (M2128), *P*-Nitrophenol (*p*-NP) (241326), Alkaline phosphatase Yellow Liquid Substrate (*p*NPP) (P7998), D-Ala-Leu-Lys-7-amido-4-methylcoumarin (AMCA) (A8171), Vivid™ BOMCC Substrate (P2975), Verapamil Hydrochloride (V0100000), DAPI/Hoechst 33342 (B2261), FITC-Dextran 4 kDa (46944), FITC-Dextran 70 kDa (46945), Lucifer Yellow solution (LY) (L0144) and Propidium Iodide Solution (P4864) was purchased from Sigma. DC Protein Assay Reagent (5000116) was purchased from Bio-Rad. Alexa Fluor™ 647 Phalloidin (A22287), Alexa Fluor™ 594 Phalloidin (A12381) Invitrogen™, Alexa Fluor™ 647 Phalloidin (A22287) and TRIZOL® was from Invitrogen™. VECTASHIELD® Antifade Mounting Medium (H-1200) was from Vector Laboratories. Calcein AM (C3100MP) was purchased from Life Technologies. ProtoScript® II First Strand cDNA Synthesis Kit (E6560S) was purchased from New England Biolabs Inc. Rat Tail Collagen type I (60-30-807) was purchased from First Link.

3. Characterisation of Porous PLLA Fibres as a Cell Culture Surface

3.1 Introduction

The extracellular matrix (ECM) is an assortment of proteins and proteoglycans occupying the interstitial space in all tissues. The intrinsic connection of cells to this protein rich matrix is responsible for a large proportion of cell function, behaviour and homeostasis. External cues, mediated by the ECM can initiate a myriad of behaviours including cell proliferation, migration, and differentiation as well as determining cell phenotype [110]. In addition to the underlying composition and structure of the ECM providing chemical and mechanical signalling, the topography, roughness and elasticity of the matrix also contribute to cell function [161]. The topographic landscape of native ECM is a mixture of fibres, pores and ridges, unique to each individual tissue according to its constituent composition and ratios of fibrous collagen, laminin, fibronectin as well as proteoglycans, hyaluronan and water. ECM proteins provide individual nanoscale topography, nanometre wide fibrils forming fibres tens of microns in length, but can combine together (as in a basement membrane) to bend or fold to create secondary microscale topography [162]. Larger structural differences (submillimetre) occur in specialist tissues, which usually connote specific tissue function, such as intestinal villi folds creating large absorptive surface area.

The phenomenon of contact guidance, in which cell geometries and orientations are influenced by surface patterning is probably the most perceptible impact that topography has on cell behaviour. Numerous cell types, including fibroblasts, neurites and osteoblasts, have shown to align and elongate their morphology according to micro and nanogrooves in culture surfaces as compared to smooth surfaces [163–165]. However, the culture of cells on nanopits or nanoposts (nanoscale, conical cavities or protrusions) generally have more subtle impacts on cell morphology, showing reduced cell spreading, yet increased cell attachment [166]. The secretion of ECM components has also been shown to be regulated at the mRNA level by surface topography, with

increased fibronectin expression, secretion and assembly observed in human fibroblasts cultured on grooved surfaces [167]. Most remarkably, Cukierman et al. 2001 [168] demonstrated the influence of ECM topography on cell behaviours, when comparing human fibroblasts cultured on 3D ECM deposited from NIH3T3 fibroblasts, to the exact same ECM matrix composition mechanically flattened to a 2D matrix surface. Interestingly, fibroblasts cultured on the 3D ECM showed 10-fold higher adhesion than the 2D matrix, as well as earlier spindle morphology and slower migration times. The impact of topographical cues compared to biochemical ones was also eloquently revealed in a study wherein cells cultured on surfaces striped with fibronectin proteins, perpendicular to topographic grooves, demonstrated preferentially alignment with the underlying physical geometry, as opposed to the ECM protein [169].

Topography is therefore highly relevant when investigating cell behaviours *in vitro*, yet large proportions of cell culture materials and models fail to represent this. When considering the intestinal ECM, many models (as discussed in section 1.5) focus on recapitulating the macro-structural elements of the tissues, such a villi, rather than the incorporation of the fibrous reticulum structure of the basement membrane (Figure 3.1). The exception to this, is the use of decellularised tissues as 3D matrix scaffold for intestinal models. Decellularised tissues derive from extracted animal or human intestines which have undergone enzymatic treatment to remove all elements of cellular tissue except its extracellular structural proteins. The resultant decellularised matrix can then be repopulated with immortalised cell lines and kept in extended culture. Using decellularised porcine intestines, multiple cell types have been able to recapitulate intestinal transport and permeability, showing reliable immunohistochemical staining of key efflux proteins [149,150]. Yet, the nature of the enzymatic clearance of original tissue has a high probability of damaging the extracellular proteins and affecting the ability of new cells to proliferate and correctly differentiate[170]. Furthermore, it relies on a source of native tissue, is species independent, and is not amenable for high throughput scale-up.

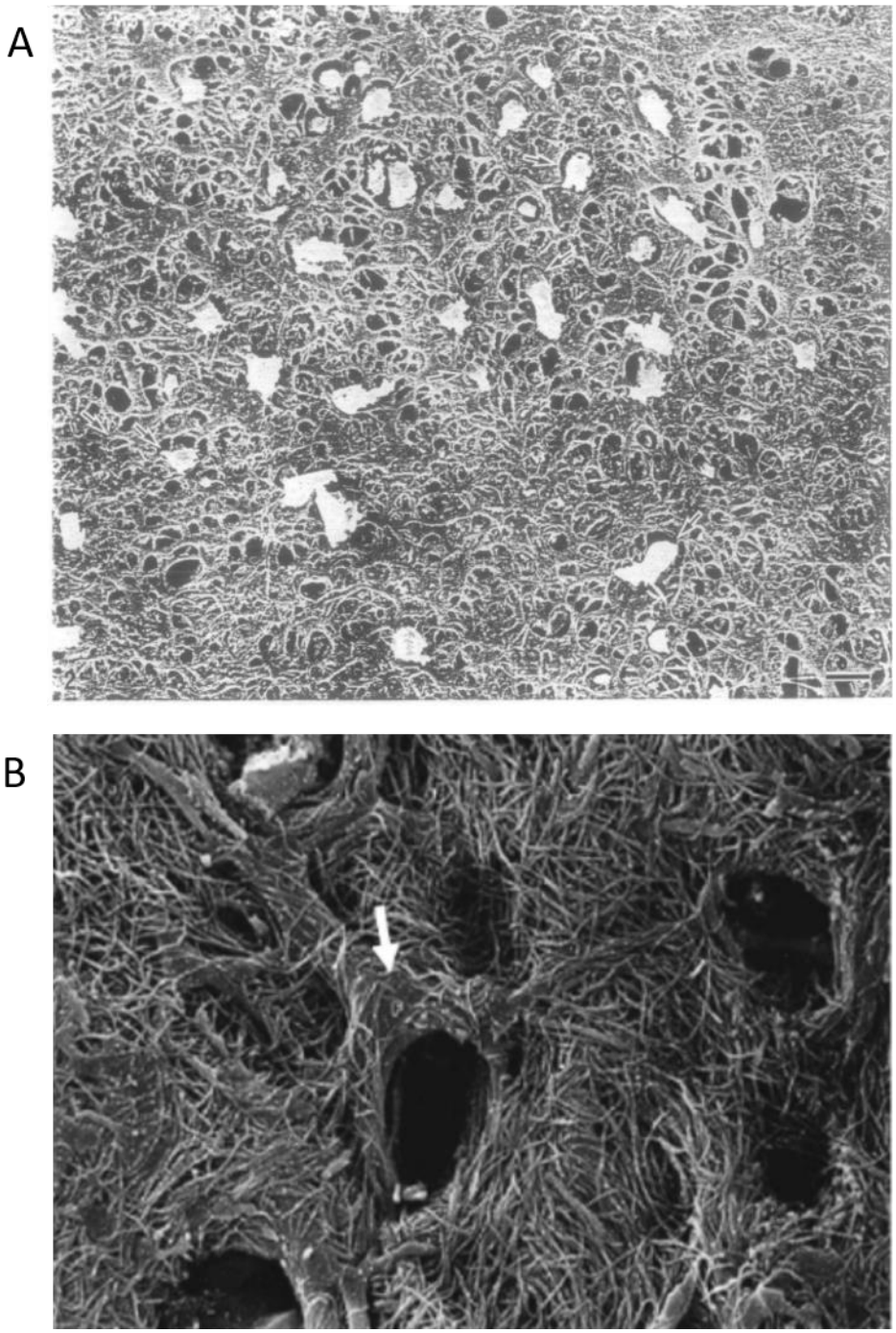

Figure 3.1 Topography of the Intestinal Basement Membrane

(**A**) Basement membrane of the rat small intestine after removal of the epithelial cells and basal lamina. Stellate fibroblasts are labelled with asterisks and arrows denote the basal processes of the epithelial cells cut during sample preparation. Magnification =1900x, scale bar =5 μm.[171]. (**B**) The reticular sheet of the rat intestine showing the underlying fibrous topography. Arrows show sub-epithelial fibroblasts. Magnification =8800x. [172].

Native ECM biopolymers such as elastin and collagen would be natural candidates for replicating the ECM nanotopography *in vitro*, however, maintaining quality and bioactivity of these proteins remains difficult, in addition to concerns about the use of animal products [173]. As such, synthetic alternatives, in the form of polymers, modifiable in composition, shape and scale have emerged. Most notably, the application of electrospinning, used for decades in the textile and materials industry, has come to the fore in the development of nanofibrous scaffolds. Electrospinning allows the production of continuous, highly porous non-woven fibrous matrices, by using electric force to draw polymer solutions into defined fibres [174]. The resultant 3D fibrous membranes mimic ECM topography, with porous, ridged micro and nanoscale structures that provide a large surface-to-volume ratio for cell adhesion and contact [173].

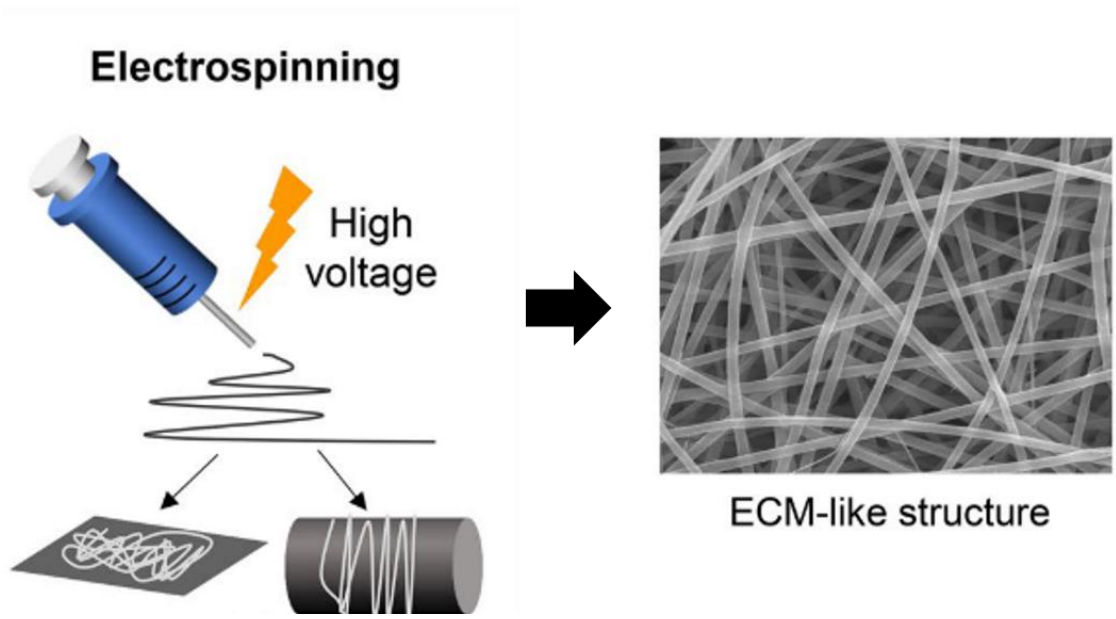

Figure 3.2 Electrospinning of Synthetic Fibrous Membranes

The use of electrospinning techniques has become prevalent in creating synthetic fibrous membranes that mimic ECM structure. Adapted from [175].

A variety of synthetic polymer materials are amenable to the electrospinning process including poly(lactic acid) (PLA) and poly(glycolic acid) (PGA), both biocompatible and biodegradable polymers approved by the FDA for medical devices and drug delivery systems [176]. The ease of modification of electrospun material properties including fibre orientation, diameter, porosity, combined with more recent advancements in creating copolymers blends and post-spinning treatment with functional biomolecules, has opened up a broad range of tissue applications [175]. Regenerative medicine approaches have employed electrospun fibrous membranes as ECM mimetic scaffolds for bone, cartilage and ligaments; highly porous scaffolds allowing cell infiltration, yet resistant to mechanical stress [177]. Others have utilised the porosity and highly networked structure of poly(ε-caprolactone) (PCL) and PLA fibrous membranes, to create vascular models, recreating the tubular arterial wall with the ECM mimetic membrane [178,179].

The importance of the ECM in dictating the functional behaviour of cells is well established, yet incorporation of its features, particularly topography, remains exclusive to tissue regenerative medicine and is yet to be fully embraced by tissue engineering models. Electrospun fibrous membranes provide a simple and cost effective method of producing biomimetic ECM cell surfaces for 3D models. Together, this suggests that electrospun fibrous membranes may be a promising material for incorporating 3D ECM structures into intestinal permeability models.

3.2 Aims

The aims of this thesis chapter were to investigate the suitability of novel porous poly(L-lactic acid) electrospun fibrous membranes as a potential biomaterial for the development of intestinal models, by investigating and characterising the physical surface properties of this material. Specific aims included:

- Characterisation of the morphology and topography of PLLA fibrous membranes
- Investigation the surface properties of PLLA fibrous membranes
- Examination of the biocompatibility of PLLA fibrous membranes

3.3 Results

3.3.1 Surface Topography of Porous PLLA Fibres

Post-electrospinning treatment of PLLA fibres with acetone produces fibre membranes with a porous surface morphology as a result of crystallisation. This induces a nanotopography upon the fibres themselves, as well as the microtopography generated by the mesh-like fibrous membrane. In order to identify the overall morphology of these fibre membranes for use in this thesis, SEM images of the fibres at increasing magnifications were analysed using Image J to quantify the fibre dimensions (**Figure 3.3A, B, C**). The electrospun fibres were determined to have a mean fibre diameter of 3±1 µm (±SD) (**Figure 3.3D**) and to be covered in randomly orientated surface pores with a mean diameter of 0.5 ±0.2 µm (±SD) (**Figure 3.3E**). This surface topography of the fibres shows a high degree of roughness, and a mixture of submicron ridges and pores, with non-specific geometries, covering the entire surface of all fibres. These fibre dimensions provide high surface interaction area, with additional nanotopography, whilst maintaining the typical fibrous landscape of the ECM environment. Importantly, the fibrous membrane showed overall porosity with average pore sizes 6±4 µm (**Figure 3.3F**), much larger than commercial Transwell inserts (0.4 µm), and within the size range of pores in the *in vivo* intestinal basement membrane reticular network (3-7 µm) [116]. Moreover, these pores (inter-fibre distances) have a greater size distribution, making them more physiologically relevant than the uniformly distributed pores seen in classic cell permeable membranes.

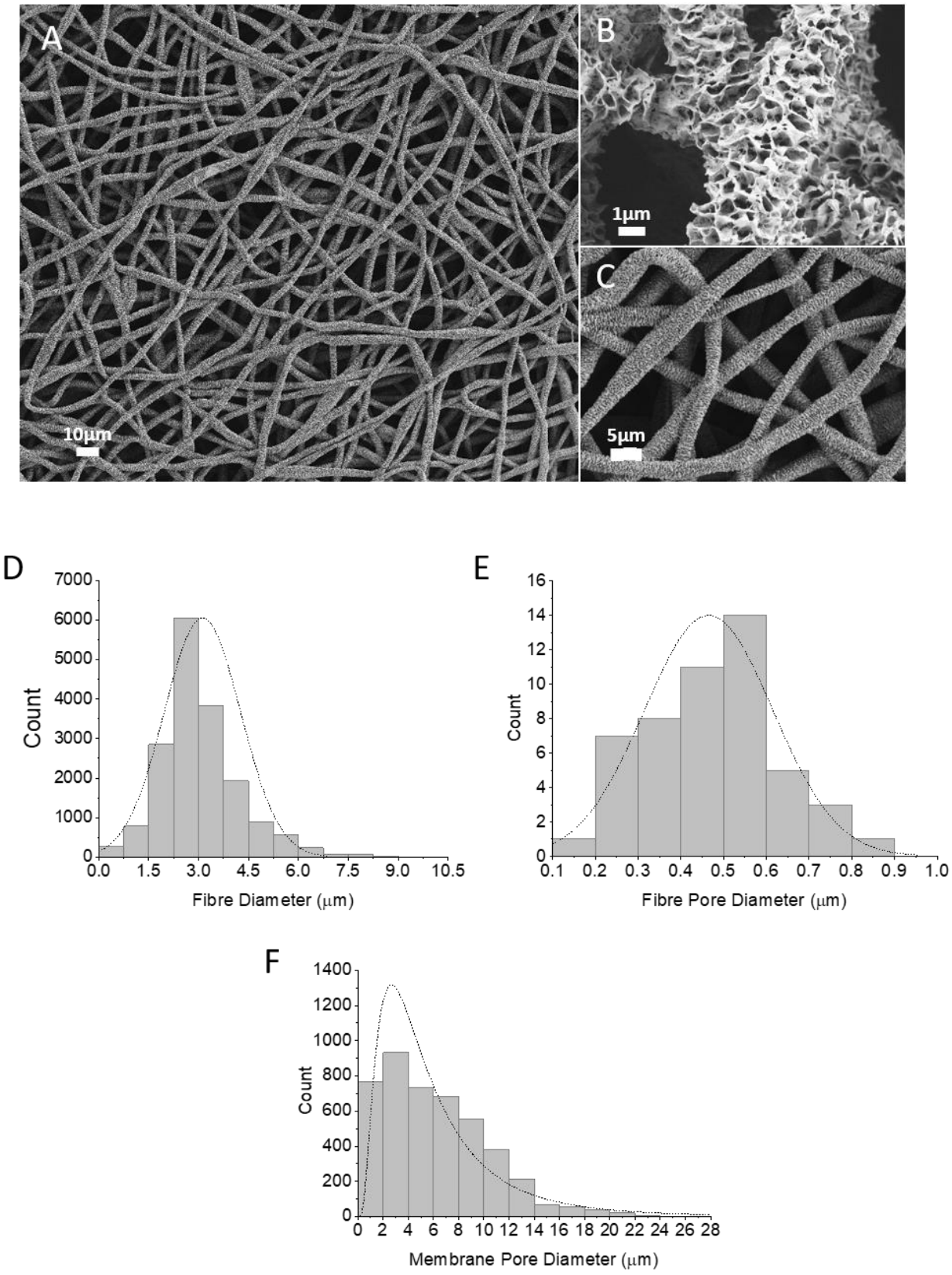

Figure 3.3 Morphology and Dimensions of Porous PLLA Fibres

SEM image of porous PLLA fibres at magnification 1KX (**A**), 20KX (**B**) 5KX (**C**) and the distribution of (**D**) fibre diameters, n=17642, normal distribution curve (**E**) fibre pore diameters n=50, normal distribution curve, and (**F**) membrane pore diameters, n=4453, log normal distribution curve.

3.3.2 Surface Properties of Porous PLLA Fibres

The surface properties of biomaterials are hugely influential to the way in which they interact with cells: particularly materials for adherent cell culture surfaces, as cell adhesion, spreading and proliferation are critical for cell survival. Moreover, material surface properties are a multifaceted set of chemical and physical aspects that can individually and collectively alter cell behaviour. The degree of wetting (wettability) of a material surface is the balance of surface energy at the interface between air, liquid and solid materials, as measured by the contact angle, which can determine how it interacts with solutions of proteins or cells [180]. To this end, the surface wettability of the porous PLLA fibres were assessed using water contact angle measurements alongside a number of standard cell culture surfaces, as well as smooth, untreated PLLA fibres (**Figure 3.4**). Glass coverslips and Transwell membranes showed significantly higher ($P>0.0001$) surface wettability (29.2° and 57.8°) than both smooth and porous fibres, which had an average contact angle of 117.1° and 122.9° respectively. Fibres therefore demonstrate contact angles within the range considered hydrophobic, whereas traditional glass, and Transwell surfaces both lie in the hydrophilic region [181]. By comparing porous fibre membranes to smooth fibre membranes, any differences in surface wettability, independent of material chemistry could be identified. In this instance, the difference in contact angles between smooth and porous fibres was not considered statistically significant, although porous fibres did demonstrate an increased contact angle.

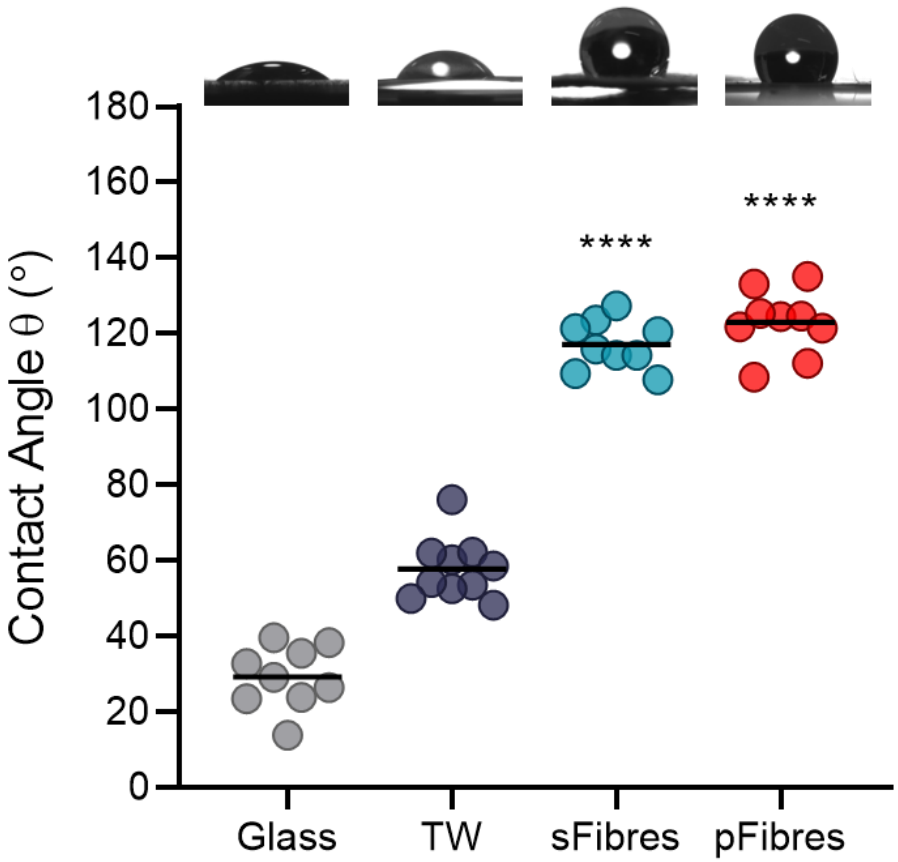

Figure 3.4 Surface Wettability of PLLA Fibres

Advancing contact angles of Transwell (TW), smooth (s) and porous (p) fibres shown next to that of a glass coverslip control. Bars show the mean. Significance determined using one-way ANOVA with Tukey's post-hoc comparisons, asterisks show significance compared to TW, $P<0.0001$. Representative images of water contact angle on each of the cell surfaces are shown above the graph.

Wettability is a surface tension related interfacial process that can modulate protein conformation, and subsequently the affinity of a protein to material surfaces [182]. Protein adsorption is a crucial element for cell-surface interactions, as cell adhesion occurs via interactions between cell surface receptors and key adhesion proteins; thus, without an adsorbed protein layer, material surfaces are unlikely to promote cell attachment [183]. Given that any cell culture surface *in vitro* is continuously immersed in cell culture medium, containing a vast variety of proteins that both promote and inhibit cell adhesion, the capacity of the fibres to adsorb components found in cell media serum, was assessed. Using the solution depletion method [184], the quantity of Bovine serum albumin (BSA) (a cell adhesion inhibitive protein) adsorbed to both Transwell and fibre membranes was analysed as a percentage of the initial protein solution using UV-Vis spectroscopy. Although both smooth and porous fibres adsorbed a higher percentage of BSA from solution than the TW membrane, it was not calculated to be statistically significantly different and remained below 3% (**Figure 3.5A**). In a more direct assessment of cell media protein adsorption, membranes were soaked in 10% FBS serum-supplemented media and probed for fibronectin protein using immunostaining (**Figure 3.5D**). Quantification of protein staining, compared to PBS controls, revealed fibre membranes to adsorb significantly more fibronectin than the Transwell membrane (P=0.0036 and 0.0002 respectively, for smooth and porous), and of the two, porous fibres showed a significantly increased capacity for fibronectin binding than smooth fibres (P=0.0367) (**Figure 3.5B**). Finally, the same immunostaining technique was employed to observe the adsorption of collagen type I, a highly abundant ECM protein (**Figure 3.5C**). Herein, similar trends of adsorption, as seen with both BSA and fibronectin, were observed, with porous fibres showing significantly more adsorption than both Transwell (P=0.0019) and smooth fibres (P=0.0414).

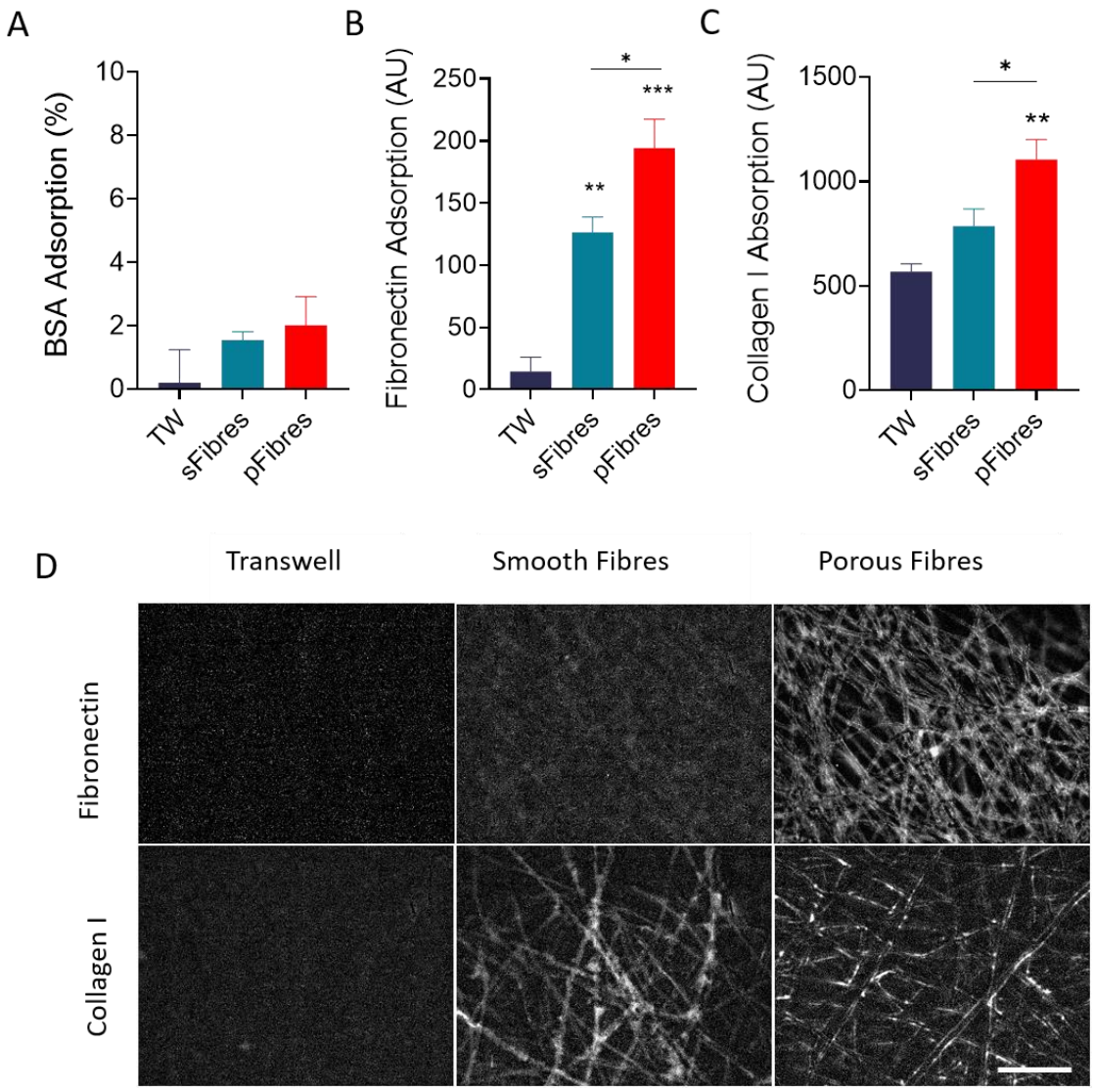

Figure 3.5 Protein Adsorption on PLLA Fibres

Protein adsorption was observed on Transwell membranes (TW), smooth (s) and porous (p) fibres. (**A**) Percentage of BSA adsorption calculated using the solution depletion method and UV VIS quantification. Protein adsorption quantified from fluorescence microscopy image analysis following immunostaining for (**B**) Fibronectin and (**C**) Collagen I. Mean ± SEM, n≥3 for all. Significance calculated using one-way ANOVA and Tukey's multiple comparisons test. (**D**) Representative fluorescence microscopy images of cell surfaces soaked in media supplemented with FBS and probed for Fibronectin, and cell surfaces soaked in Rat Tail Collagen I solution and probed for Collagen I using immunofluorescence staining. Scale bar = 50 µm.

3.3.3 Biocompatibility of porous PLLA fibres

When considering materials for biological uses, especially cell culture, it is vital that the material not simply be non-cytotoxic, but also able to promote further cell growth. The MTT assay is a widely used colorimetric evaluation of biocompatibility, based on the metabolic activity of viable, actively growing cells to reduce the MTT assay reagent to purple formazan crystals [185]. As such, Caco-2 intestinal epithelial cells were seeded onto both Transwell and porous fibre membranes as well as the most common cell culture substrate tissue culture polystyrene (TCPS). The MTT assay was run every other day for a week and then once a week for the following two weeks, in order to observe the viability of cells over the normal differentiation period required for culturing intestinal epithelial cells (21 days). All cell culture surfaces showed highly comparable activity over the period of 21 days; displaying an overall increase in metabolic activity of cells, that can be associated with the maintenance of cell health, alongside an increase in cell number due to cell proliferation over time (**Figure 3.6A**). Furthermore, the similarity of the absorbance value magnitudes over time for all three surfaces demonstrate that porous PLLA fibres have no cytotoxic or detrimental effects on normal and expected cell viability and growth. Further confirmation of equivalent cell viability was presented using fluorescent imaging of cells cultured on different surfaces, incubated with Propidium iodide (PI) stain, which fluoresces in dead cells. Caco-2 cells cultured on PLLA fibres, had a similar distribution and percentage of cell death (22%), indicated by PI staining, as cells grown under standard culture conditions on Transwell and TCPS (18% and 16% respectively) (**Figure 3.6B, C**).

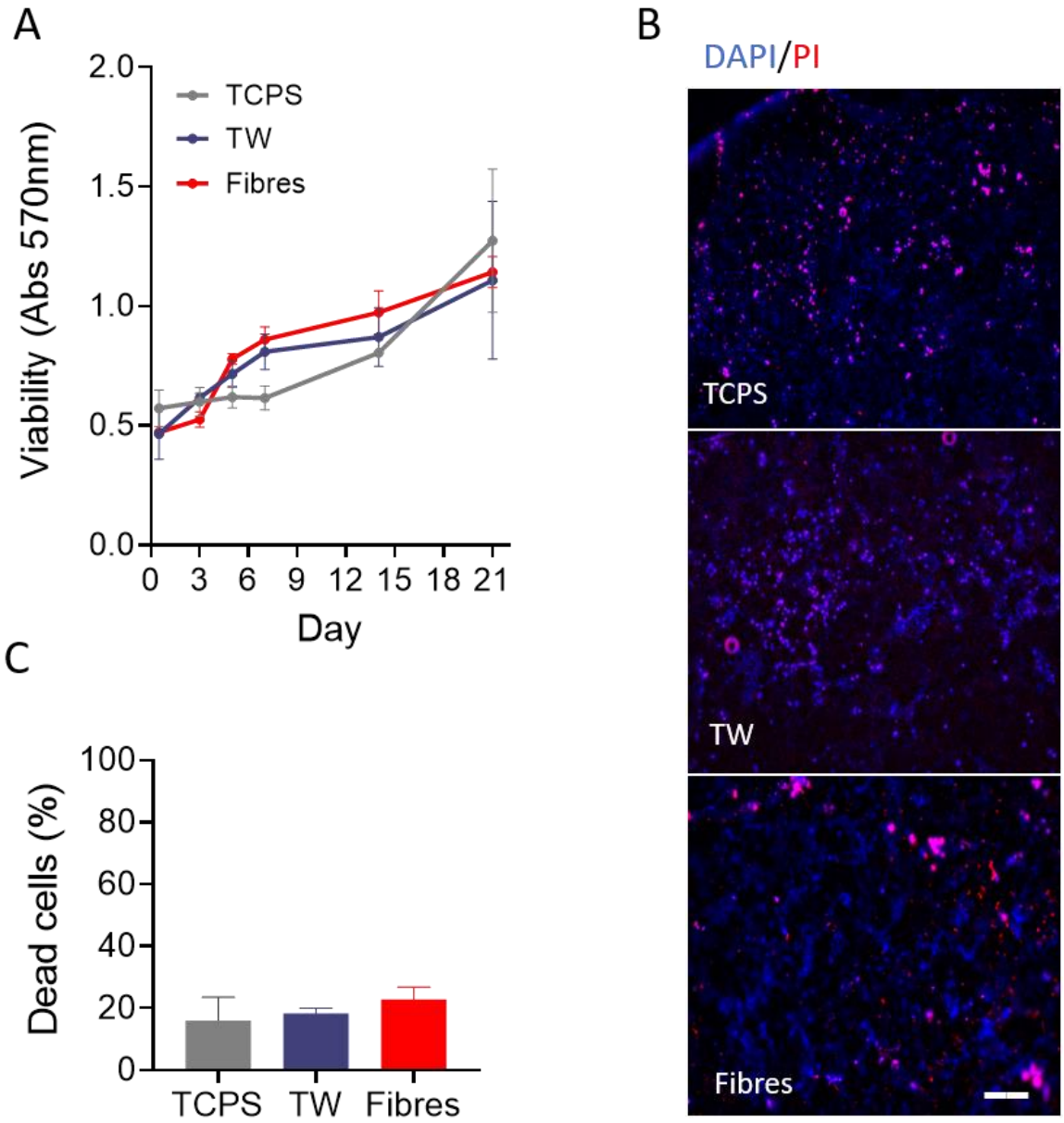

Figure 3.6 Cell Viability of Cell Culture Surfaces

Caco-2 cells grown on cell culture surfaces; Tissue culture polystyrene (TCPS), Transwell membrane (TW) and porous fibres. (**A**) Cell viability determined by MTT assay, mean ± SEM, n=3. (**B**) Representative images of cells stained using the nuclear stain DAPI (blue) to indicate total number of cells and with Propidium Iodide (PI)(red), an indicator of dead cells, scale bar = 200 µm. (**B**) Percentage of dead cells (PI/DAPI) quantified from images, mean ± SEM, n=3.

To further quantify the impact of PLLA fibres, specifically on the proliferation of intestinal cells compared to the standard Transwell membrane insert, the growth of Caco-2 cells constitutively expressing green fluorescence protein (GFP) was captured using fluorescence microscopy over the initial week of growth (**Figure 3.7A**). The use of GFP-expressing cells allowed for the direct visualisation of cells growing on fibre membranes; as these fibres are not an optically transparent material, rendering it inaccessible for phase contrast microscopy. Proliferation was qualified as an increase in cell confluence, which is commonly defined as the surface area coverage of cells in 2D culture, and was quantified using binary thresholded images (**Figure 3.7B**). Quantification of GFP-Caco-2 cells showed that by day 7 cell confluence was higher on PLLA fibres (78%) compared to Transwell (55%). Additionally, when calculated as a proliferation rate over the seven days, Caco-2 cells proliferated faster when cultured on PLLA fibres (11%/Day), than on Transwell membranes (8%/Day) (**Figure 3.7C**), confirming not only that PLLA fibres are compatible for cell attachment and growth, but that they actively promote cellular proliferation. This was supported up to 21 days by total protein quantification of cell lysates cultured on fibre membranes and Transwells, which produced 0.49 mg protein and 0.38 mg protein, respectively (**Figure 3.7D**). Together, these data support that from **Figure 3.6**, in confirming that PLLA fibres are a suitable biocompatible material for use as a cell culture surface.

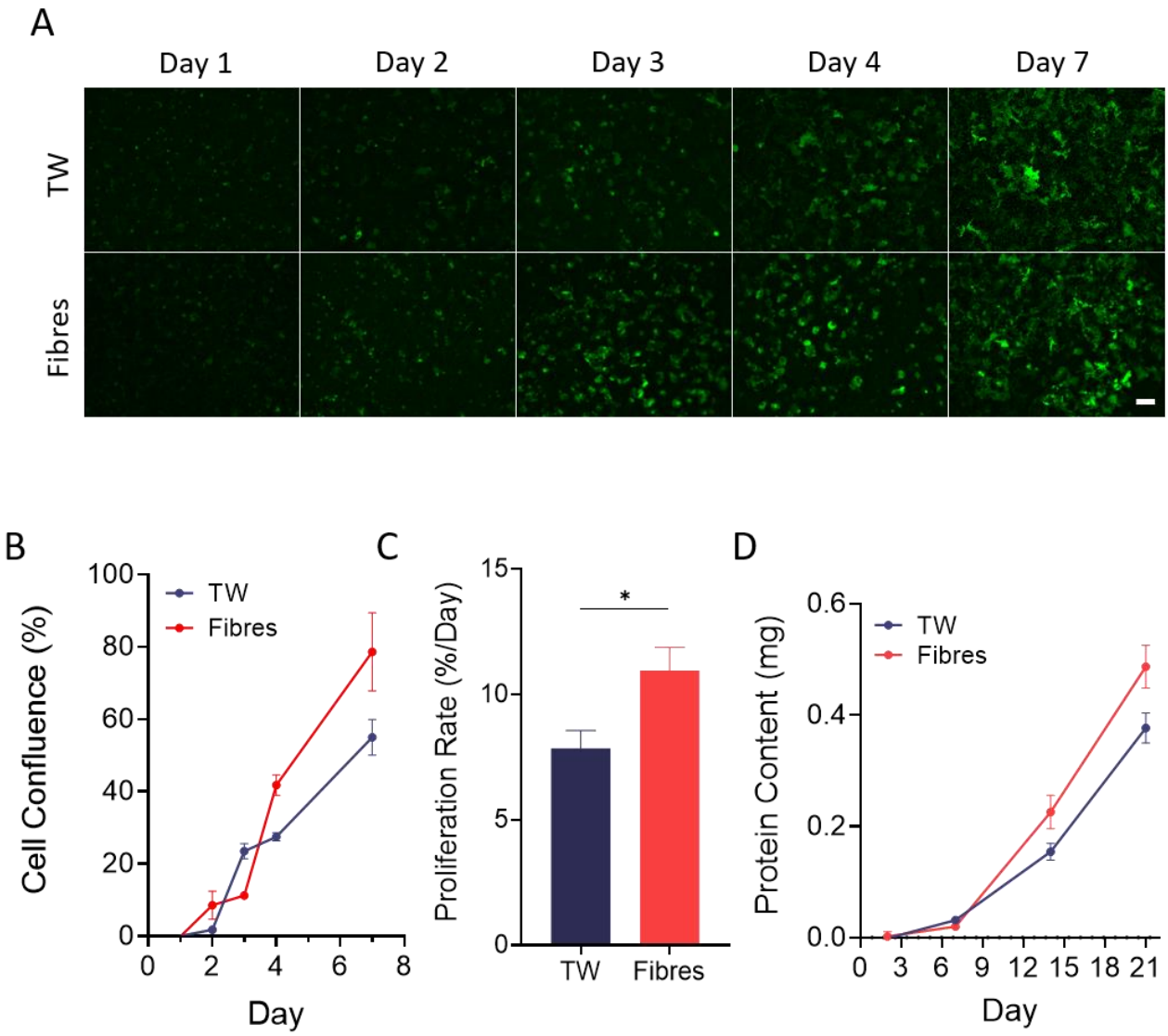

Figure 3.7 Cell Proliferation on Cell Culture Surfaces

(**A**) Representative images of GFP-Caco-2 cell confluence over 7 days on TW and Fibre surfaces, scale bar = 200 µm. (**B**) Confluency of GFP-Caco-2 cells on Transwell (TW) and porous fibre membranes over 7 days, quantified from mean GFP fluorescence. (**C**) Rate of proliferation of Caco-2 cells. Significance calculated from unpaired t-test, P value= 0.0371. (**D**) Total protein content of Caco-2 cells determined from DC protein assay. Mean ± SEM, n≥3 for all.

3.4 Discussion

Electrospun fibres are a low cost, reproducible and simple technique that produces polymer materials with a variety of surface textures and porosity. The versatility of nano and microscale topographies and porosity of these membranes has given rise to their increased popularity across a vast number of bioengineering fields and a number of different tissues. Due to its architectural similarity to native ECM in its most basic form, fibres can be adapted, functionalised and applicable to a range of *in vitro* cell models for both hard and soft tissues.

3.4.1 PLLA Fibrous Membranes Recapitulate Topography of the Intestinal Basement Membrane

Herein, the structure and architecture of acetone treated PLLA fibres were analysed using SEM image analysis to determine their similarity to the intestinal basement membrane (BM). As shown in **Figure 3.1**, the BM is a myriad of fibrous proteins interwoven to a porous mesh; a fibrous landscape seen replicated to high degree of similarity in these PLLA fibres. Analysis of the exact dimensions of these fibrous membranes established that the PLLA fibres were just wider than 1 µm, therefore designating them microfibres; which although larger than native ECM fibrous proteins [162], was considered a reasonable biomimetic due to the additional nanotopography of the rough fibres themselves. Moreover, with inter-fibre spaces creating membrane pores with a mean diameter within the range observed *in vivo* [172] the dimensions of the fibres were considered well matched for intestinal permeability modelling. Additionally, the intrinsic porosity of the fibres themselves post-acetone treatment, displayed pores with a variety of submicron diameters, randomly distributed across the entirety of the fibres, creating a nanotopographic landscape of ridges and pits, typical of the BM ECM [186]. The analysis of porous PLLA fibres was carried out on images obtained from SEM, the most common method in providing detailed information about the surface topography of materials. However, SEM images represent the dehydrated state of the material, and is not necessarily representative of the hydrated state of the fibres when used in cell culture. As hydration is known to influence the mechanical properties of PCL fibres [187], examination of these PLLA fibrous membranes

with environmental SEM or AFM would be advantageous to confirm its hydrated topography and morphology.

3.4.2 Adhesion Promoting Proteins Adsorb To PLLA Fibres, Despite Surface Hydrophobicity

The study of materials for biological purposes has defined the importance of surface physical properties on their behaviour *in vitro* and *in vivo*; surface chemistry, topography and wettability are all features that can dramatically alter the way in which biomaterials interact with cells [181]. Given the promising morphology and topography of the PLLA porous fibres in mimicking the ECM environment, we next endeavoured to examine their surface properties suitability for intestinal epithelia cell culture. The results of water contact angle (WCA) measurements on the PLLA fibres were as expected, demonstrating significantly higher WCA compared to Transwell membranes and glass, correlating with a lower surface wettability. Despite both Transwell PET and fibre PLLA being intrinsically hydrophobic polymers, the Transwell PET membranes are tissue culture treated, commonly with gamma radiation, to increase the surface hydrophilicity and induce surface charge. Moreover, Transwell membranes have an overwhelmingly a smooth surface, despite their porosity, compared to the rougher surface of both smooth and porous PLLA membranes, induced by the fibrous microtopography of electrospinning. This roughness is also a likely contributing factor to the decreased wettability of PLLA fibres, as increased roughness of a surface correlates with increased hydrophobicity [188,189], due to air entrapment, as in the Cassie-Baxter model [180]. Interestingly, the difference in hydrophobicity between smooth and porous fibres was not pronounced, indicating that micro-roughness has larger impact on hydrophobicity than nano-roughness.

A long held theory in the literature suggests that hydrophobic, poorly wettable surfaces are undesirable characteristics for cell culture as they do not promote cell adhesion. Instead, moderately wettable surfaces with WCA between 40° and 80° are cited as the most optimal [190,191]. One reason attributed to the preferential cell adhesion to hydrophilic surfaces, is its propensity to adsorb the cell adhesion promoting serum protein fibronectin (FN), rather than the cell adhesion inhibitive

protein BSA [192,193]. A similar phenomenon of preferential adsorption on hydrophilic surfaces was also seen in a solution of BSA and Collagen I [194], together suggesting that hydrophobic surfaces are cell adhesion inhibitive due to the formation of a inhibitive layer of BSA. Given the high WCA observed with the PLLA fibres, the protein adsorption capacity of these hydrophobic fibres was therefore examined, to determine whether their intrinsic hydrophobicity was indeed inhibitive to cell adhesion protein adsorption and consequently cell adhesion.

Encouragingly, we observed no significant increase in the percentage of BSA protein (adhesion inhibiting) adsorbed to fibres than to the Transwell membranes. Although the porous fibre membranes showed the highest BSA adsorption, correlating with being the most hydrophobic surface, the mean percentage of BSA adsorbed remained less than 3%. These results were obtained using the solution depletion method of quantifying protein adsorption, which although commonplace, is an indirect method of quantification. Additionally, it is a technique known to show improved accuracy for materials with large surface areas [184], indicating confidence in our results could be obtained from larger membrane samples, or further protein adsorption techniques such as Fourier transform infrared spectroscopy. Observations of FN and Collagen I adsorption showed significantly increased protein on fibres than Transwell, with the porous fibres adsorbing the most protein in both cases. Here, the method of antibody staining allowed an insight into the distribution of the proteins and a visual comparison across all three materials. A limitation of this method is the possibility of non-specific antibody binding overestimating the quantity of adsorbed protein, however, multiple washing steps were introduced to minimise artefacts of this kind. Together, this data indicates that despite their highly hydrophobic surface, fibres did not promote a substantial increase in binding of inhibitive BSA. Moreover, it appears that fibres improve the adsorption of cell adhesion promoting FN from serum relative to the Transwell membrane, as well as the ECM protein Collagen I.

Although contrary to the general belief that WCA directly determines the adhesion of the protein layer, and therefore cell adhesion, our data suggests that hydrophobicity is neither the only, nor the strongest physical surface parameter dictating protein interactions. Akin to our observations, other work has shown that on materials with

surface chemical modification, WCA does not predict the same protein adhesion trends aforementioned. In a study with a *N*-isopropylacrylamide-based co-polymer surfaces, composition-induced increases in hydrophobicity promoted the highest FN binding compared to more hydrophilic blends [195]. In addition, unmodified PLLA surfaces with higher WCA were shown to promote increased concentration and rate of FN binding compared to PLLA surfaces modified to be more hydrophilic [196]. More relevant to this work, is the impact of surface topography and roughness on protein adsorption and cell adhesion. In agreement with our observations, was the demonstration that rough PLLA surfaces with higher WCA showed less BSA adsorption than their chemically identical but topographically smooth counterparts [197]. Moreover, significant increase in overall serum protein adsorption was observed on porous electrospun poly(D,L-lactide) fibre surfaces, than on smooth fibres or films of the same polymer [198]. Most prominently, work on porous and non-porous PLLA also correlated improved protein adsorption with rougher porous surfaces, but more specifically saw higher FN adsorption than BSA on such surfaces, whereas the non-porous surface showed equivalent FN and BSA binding [199]. Adsorption of a cell adhesion promoting protein layer upon biomaterials is the most critical factor for cell adhesion. Our results combined with that of previous published work suggests that wettability is not a direct predictor for protein binding, and is in fact a multifactorial process between numerous surface properties. In this study, despite being highly hydrophobic, PLLA fibrous membranes showed a high degree of FN and Collagen I adsorption, combined with no significant increase in BSA adsorption. These results therefore indicate that pro-adhesion protein adsorption is more greatly influenced by the topography of the electrospun fibres and the nano-roughness of the porous fibres themselves.

3.4.3 PLLA Fibres Show Improved Cell Adhesion and Proliferation

Most importantly however, was to confirm that the observed protein adsorption on PLLA fibres was indicative of favourable cell interaction with these biomaterials and their suitability for intestinal epithelial models. Using a number of methods, we were able to demonstrate that intestinal epithelial Caco-2 cells showed no difference in their distribution, rate of death or viable metabolic capacity when cultured on porous fibres compared with Transwell membranes or the traditional TCPS surfaces. Further to this,

PLLA fibre grown Caco-2 cells showed improved proliferation rates than on Transwell membranes, in both colorimetric confluence analysis and total protein content assays. The rationale for the use of textured, topographic fibres in this study, is that cells in vivo do not natively grow on smooth, flat, planar surfaces. The results herein establish that, whether attributable to larger surface area, number of cell-surface contact points, pro-adhesion protein adsorption or specific topographical cues, increased cell proliferation is induced by porous PLLA fibre membranes. The amenability of electrospun fibres with a porous nanotopography to support cell growth for soft tissue is supported by recent literature [200–202], in addition to direct evidence of Caco-2 cell growth on non-porous electrospun PET scaffolds [203].

The demonstration that Caco-2 cells can adhere and proliferate on porous PLLA fibres across a number of different assays establishes a high level of confidence that they provide a marginally enhanced surface for Caco-2 cell culture over a 21 day period. As the most important aspect in evaluating porous PLLA fibres as a cell culture surface, it was important to this study that this be confirmed over a number of direct and indirect methods. Moreover, this data has established that unlike a large majority of other similar synthetic polymer biomaterials, the addition of pro-adhesion coatings is unnecessary for successful adhesion and growth. This is of great advantage for the ongoing work of this thesis in developing an intestinal model, as we can evaluate cell behaviour and function, unhindered or altered physically or chemically by fabricated protein deposition.

3.5 Conclusions

This chapter has confirmed porous PLLA fibre membranes as a biocompatible culture surface that demonstrates a highly similar topographic surface to the intestinal basement membrane ECM. Additionally, the surface roughness of these fibres have been shown to induce pro-adhesion protein binding, correlating with improved Caco-2 intestinal epithelial cell proliferation. Overall, these findings confirm porous PLLA fibrous membranes to be a suitable surface for the development of an intestinal model.

4. Fabrication and Evaluation of a Fibre Membrane-based Intestinal Monolayer Model

4.1 Introduction

The inception of the Caco-2 monolayer model for the study of intestinal permeability and adsorption, in the late 1980s and early '90s, was catalysed by the discovery that the immortalized adenocarcinoma cell line Caco-2 could spontaneously differentiate to display highly similar morphological and functional characteristics of human intestinal enterocytes [204]. Despite its colonic, cancerous origin, when cultured to confluency, Caco-2 cells exhibit polarised cells with apical microvilli, cell-cell tight junctions, and a plethora of protein transporters and enzymes [205]. Following these observations, Hidalgo et al. [80] developed the first monolayer model, by culturing Caco-2 cells on a porous polycarbonate membrane, akin to the modern Transwell membrane insert. This was swiftly followed by a numerous seminal publications by Per Artursson and colleagues [81,82,206] that were foundational in the development of the Caco-2 Transwell monolayer model into the functional biopharmaceutical tool established today [84]. The functional resemblance of the Caco-2 monolayer model to *in vivo* absorption and permeability characteristics [207–209] led to its mainstay usage in both academic and industrial pharmaceutical research [203]. The ability of the Caco-2 monolayer model to accurately predict highly permeable compounds, in particular, those transported via passive transcellular and paracellular routes, has led to its dubbing a "gold standard" model in preclinical pharmacokinetic studies [84]. Such is its perceived accuracy, that for the US FDA, Biopharmaceutics Classification System (BCS) Class I drugs showing >90% intestinal epithelial permeability in the Caco-2 monolayer model, there is a "biowaiver" precluding any further bioequivalence clinical studies [210].

The existence of relevant transporters, enzymes and nuclear receptors in Caco-2 cells have contributed to their wide utility in not only determining the permeability and

absorption of drug compounds, but also as a useful research tool in probing the mechanisms of intestinal absorption. However, it has become apparent that the function of the Transwell Caco-2 monolayer consistently presents limitations in its capacity to recapitulate certain aspects of the *in vivo* human intestinal epithelia.

The function of the Caco-2 epithelium as a selective barrier monolayer is modulated by its intercellular tight junctions; which in turn can regulate the passive absorption and permeability of molecular entities. One way of determining this characteristic in *in vitro* systems is to measure the ionic conductance of the paracellular pathway through the non-invasive Transepithelial electrical resistance (TEER) measurements. In this method, the electrical resistance is measured according to Ohm's Law using electrodes placed either side of the cell monolayer to apply an alternating current voltage signal [211]. TEER values of a Caco-2 monolayer can vary hugely, from 150-2500 Ωcm^2, and is highly influenced by culture conditions such as the surface area and material of the permeable membrane, the passage number of the cells, the origin of the cell line, as well as media composition [212]. The general consensus however, is that all of these values are higher than the human intestine values [101,129]. These higher TEER values indicate that the Caco-2 Transwell monolayer has heightened tightness between enterocytes that gives rise to alterations in permeability.

Indeed, correlating with higher TEER values in these models, is an observed decrease in the permeability of certain compounds. Although an accurate predictor of rapid, passively transported compounds, the Caco-2 Transwell monolayer does not correlate well with *in vivo* data for slowly, passively transported molecules [213], particularly small hydrophilic molecules [81,214,215]. Furthermore, due to differences in the expression of a range of protein transporters compared to native intestine, absorption in the Caco-2 monolayer may falsely represent true *in vivo* bioavailability. For example, the over expression of efflux proteins, including ABCB1 [216,217], results in underestimates of absorption potential.

An additional, recurring limitation of the Caco-2 monolayer model has been its variability and inter-lab inconsistencies in key permeability parameters [98], largely attributed to discrepancies in culture conditions [84,218]. This feature of the Caco-2

monolayer unveils an interesting parameter of the model; notably how variations in culture conditions influence function. The success of the Caco-2 monolayer model can largely be attributed to its simplicity, yet the smooth, flat nature of its culture surface, is far removed from its native basement membrane both structurally and molecularly. As discussed in Chapter 3, it is well established how influential the topography and material surface can be in directing and cell growth and morphology, however evidence suggests that these physical characteristics may have further impacts on Caco-2 intestinal function.

Besides the rudimentary aspects of cell adhesion and growth, Caco-2 cells have demonstrated considerable alterations in their intrinsic epithelial barrier function when cultured on different materials; showing that polyethylene terephthalate (PET) membranes cultivate epithelial monolayers with higher TEER values, lower apparent permeability coefficients (P_{app}) and even reduced PEPT1 transporter expression, compared to those grown on polymer and nitrocellulose membranes [219,220]. In addition to the monolayer support material, incorporation of ECM proteins into the Caco-2 monolayer affect cellular differentiation and growth [221], as well as differentially increasing brush border enzyme activities [222]. Large variations in TEER values are observed in Caco-2 monolayers cultured on Transwells coated with different ECM proteins collagen, fibronectin and laminin [223]. Moreover, the thickness of the collagen ECM layers have been shown to lower TEER values, and remarkably increase expression of BCRP and MDR2 efflux transporter expression [224]. A recent review by Snyder et al., [225] has comprehensively summarised the effect of 3D ECM-based scaffolds on Caco-2 function, including lower TEER values and more physiologically relevant permeability on Collagen I villi structures [146,226]. Additionally, Caco-2 Transwell monolayers cultured on a decellularised ECM basement membrane, produced by Calu-3 airway epithelial cells, demonstrated altered Caco-2 morphology, however, concluded that the ECM matrix itself hindered the transport of molecules and therefore the determination of accurate permeability values [227].

The Transwell Caco-2 monolayer is unrivalled in modelling the intestinal epithelial permeability and absorption of certain classes of pharmaceutical drugs, as a result of its simplicity, scalability and versatility. However, its recurrent limitation in producing a

tighter epithelium, with low permeabilities and variable transporter expression are due to the lack of native tissue complexities. However, it is clear that the Caco-2 cell line demonstrates a considerable plasticity in its phenotypic expression and function as a result of cell culture surface properties and culture factors. It is therefore hypothesised that by incorporating topographic elements of the underlying basement membrane into the simplistic nature of the monolayer model, the function of the Caco-2 cells can be improved to represent more physiological results.

4.2 Aims

Following on from the results of Chapter 3, in which PLLA fibrous membranes were characterised as a basement membrane-like ECM mimic, compatible for cell culture, this chapter aims to utilise these as an alternative cell culture surface for an intestinal epithelial monolayer model. As a more physiologically relevant culture surface, we aimed to compare this to the standard Transwell based Caco-2 monolayer.

- Fabrication of a PLLA membrane based cell culture insert
- Evaluation of Caco-2 differentiation on PLLA fibrous inserts
- Analysis of ECM expression and deposition on PLLA fibres compared to Transwell inserts
- Comparison of barrier function in both monolayer models

4.3 Results

4.3.1 Fabrication of PLLA Fibrous Cell Culture Inserts for Intestinal Monolayers

Having established the biocompatibility of PLLA fibres in the previous chapter, fibrous cell culture inserts were fabricated as a culture surface suitable for intestinal modelling. The design of the Transwell culture insert (**Figure 4.1A**) creates a cell culture well divided into two chambers on either side of the cultured intestinal epithelia. This design makes it amenable to interrogate the function and behaviour of the epithelia from both apical and basolateral sides, and easily monitor transport across the epithelia itself. Given its versatility and simplicity, this element of a cell culture insert was taken forward and developed for the PLLA fibrous inserts. Before fabricating an insert from PLLA fibres, it was necessary to determine a suitable adhesive with which to attach the PLLA fibres to the polystyrene insert that would produce a reliable and reproducible seal without altering or changing the PLLA surface, but that was also biocompatible. Therefore, the viability of cells grown on TCPS with a small dot of cyanoacrylate or a silicone based glue was assessed using the MTT assay (**Figure 4.1B**). For both NIH3T3 fibroblast cells and Caco-2 intestinal epithelial cells, silicone glue showed significantly ($P<0.0001$) higher viability (53.3 % and 44.8%, for NIH3T3 and Caco-2 respectively), than the cyanoacrylate glue (16.4% and 14.4%) and was therefore selected for the fabrication of PLLA fibre inserts. Polyethylene terephthalate (PET) membranes were removed from the polystyrene Transwell inserts with a scalpel and replaced with PLLA fibrous membranes adhered with a silicone adhesive to produce the PLLA fibre inserts (**Figure 4.1C, D**) that were comparable to Transwell in all aspects of culture surface area, diameter and well volume ratios.

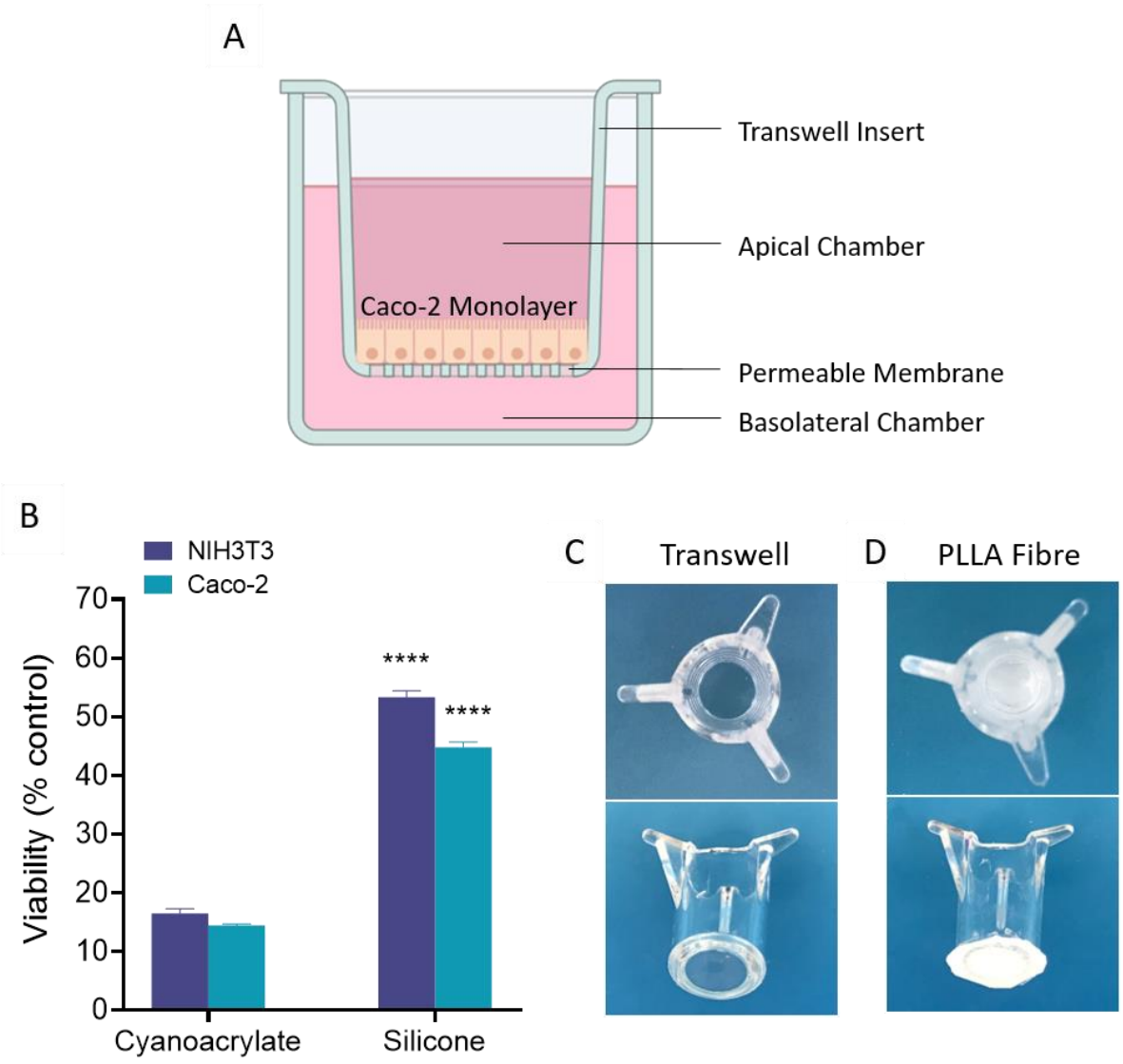

Figure 4.1 Fabrication of PLLA Fibrous Cell Culture Insert

(**A**) Diagram of a cell monolayer cultured on a porous insert. (**B**) Cell viability as determined by MTT assay for epithelial Caco-2 cells and NIH3T3 fibroblast cells when cultured with different adhesives (Mean ± SD, n=3) Significance calculated from a two-way ANOVA with Sidak's multiple comparisons test P <0.0001. (**C**, **D**) Photographs of a Transwell insert and a fabricated PLLA fibre insert.

The subsequent culture of a Caco-2 intestinal epithelial monolayer on the fabricated PLLA fibre cell culture inserts was observed using confocal microscopy (**Figure 4.2A &B**). Green fluorescent protein (GFP)-expressing Caco-2 cells were grown for 21 days and counter stained with nuclear dye DAPI in order to visualise the morphology and distribution of the enterocytes on the PLLA fibres. At both low and high magnifications, GFP-Caco-2 cells display a fully confluent planar monolayer atop of the PLLA fibres representative of the native epithelial monolayer. There was no indication of multilayer growth or cell infiltration into the PLLA fibres, and displays a homogenous layer of cell growth and proliferation with equivalent distribution across the fibre surface. These images confirm that Caco-2 cells cultured on PLLA fibres can develop epithelial monolayers suitable for intestinal modelling.

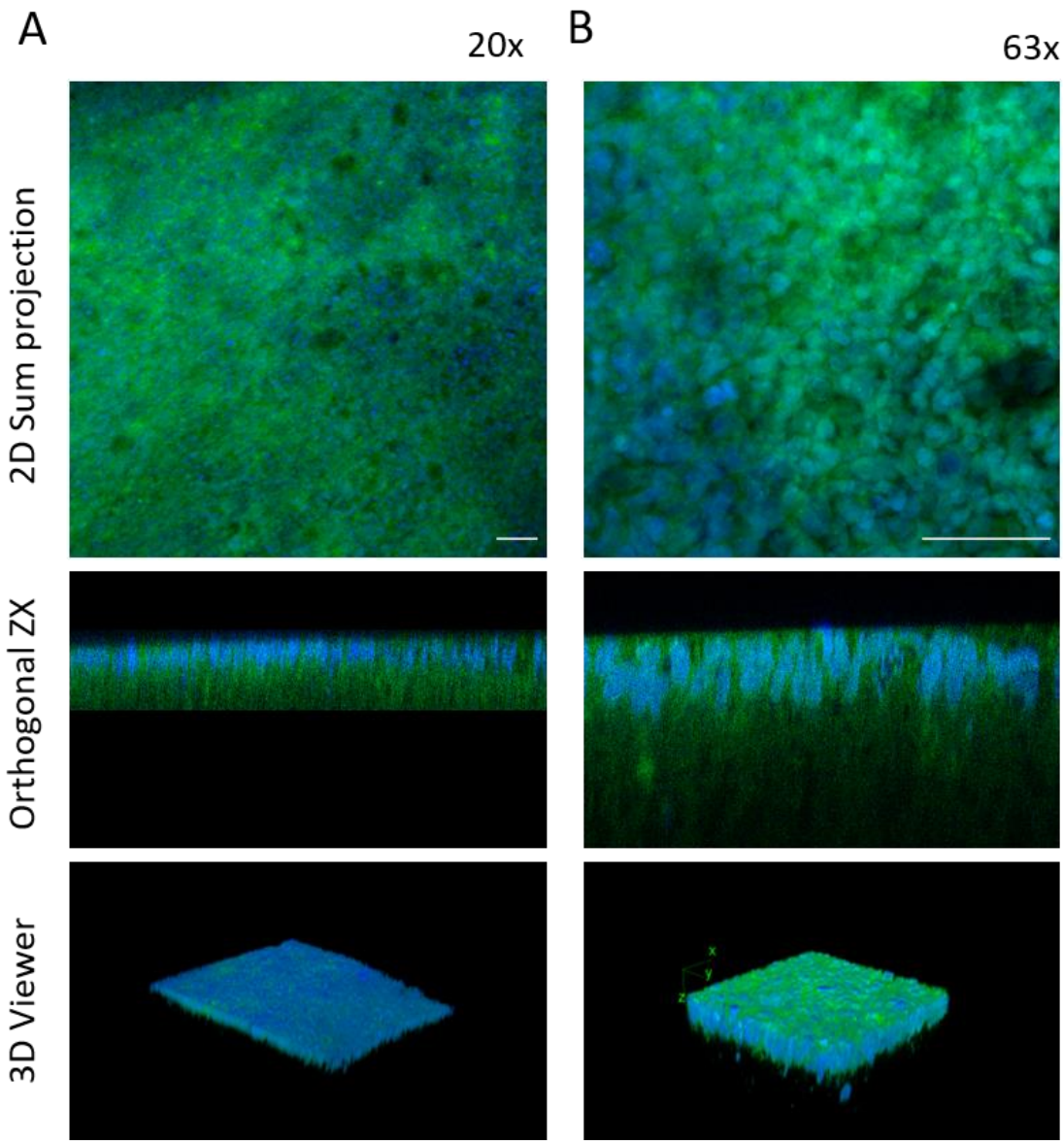

Figure 4.2 Caco-2 Monolayer Cultured on PLLA Fibre Insert

Confocal Z-stack images of a GFP-Caco-2 monolayer cultured on PLLA porous fibres at magnification 20x (**A**) and 63x (**B**) Images show 2D Sum projection view, orthogonal ZX view and 3D rendered view. Scale bar = 50 µm.

4.3.2 Assessment of Differentiation in Intestinal Monolayers

Despite its colonic origin, Caco-2 cells can remarkably emulate native human enterocytes when grown in culture for 21 days, and still represent the most reproducible *in vitro* model cell type for absorptive enterocytes [228]. The ability of Caco-2 cells to differentiate spontaneously when cultured on permeable supports gives rise to a mature monolayer that demonstrates morphological and functional features representative of the small intestine. It was therefore necessary to confirm that Caco-2 cells cultured on PLLA fibres for 21 days also displayed this differentiation. Therefore, cells grown on both classic Transwell and PLLA fibres for 21 days were assessed for the relative gene expression of typical markers of intestinal differentiation (**Figure 4.3**). The protein Villin 1 (VIL1) and the two enzymes, alkaline phosphatase (ALP) and aminopeptidase (ANPEP), are markers of a developed microvilli brush border typical of mature intestinal enterocytes. Additionally, protein transporter proteins ABCB1 and PEPT1 (gene name SLC15A1) are also indicative of differentiated Caco-2 cells. The heat map shows that for all intestinal differentiation markers, relative gene expression increases considerably over the period of 21 days in both models. Moreover, both models show comparable magnitudes of expression; for example both exhibiting very high levels of Villin 1 expression even at day 2, and both showing particularly low expression levels of ANPEP and SLC15A1, that increases rapidly over the 21 days.

To further assess the differentiation of Caco-2 cells in both models, the functional activity of the alkaline phosphatase (ALP) brush border enzyme was measured over the period of 21 days (**Figure 4.4**). ALP catalyses the hydrolysis of *p*-Nitrophenyl phosphate (*p*-NPP) to a soluble, yellow product *p*-Nitrophenol (*p*-NP) that can be quantified using absorbance spectroscopy. As demonstrated by both models, there was a significant increase in the enzyme activity over the course of 21 days, reflecting the increase in gene expression observed in the previous figure (**Figure 4.3**). The ALP activity of the PLLA fibres appears to be slightly delayed compared to the Transwell model, but rapidly increases up to day 14 to eventually show marginally higher activity (28.4 $\pm$2.4 $\mu Mmin^{-1}$) on day 21 than the Transwell monolayer (23.6 $\pm$2.8 $\mu Mmin^{-1}$). The data shown in these figures therefore confirm that the Caco-2 monolayer developed on PLLA fibres shows equivalent expression and activity of essential markers of

differentiation, suggesting its similarity to the native human intestinal function is comparable, if not augmented, compared to the standard Transwell monolayer model.

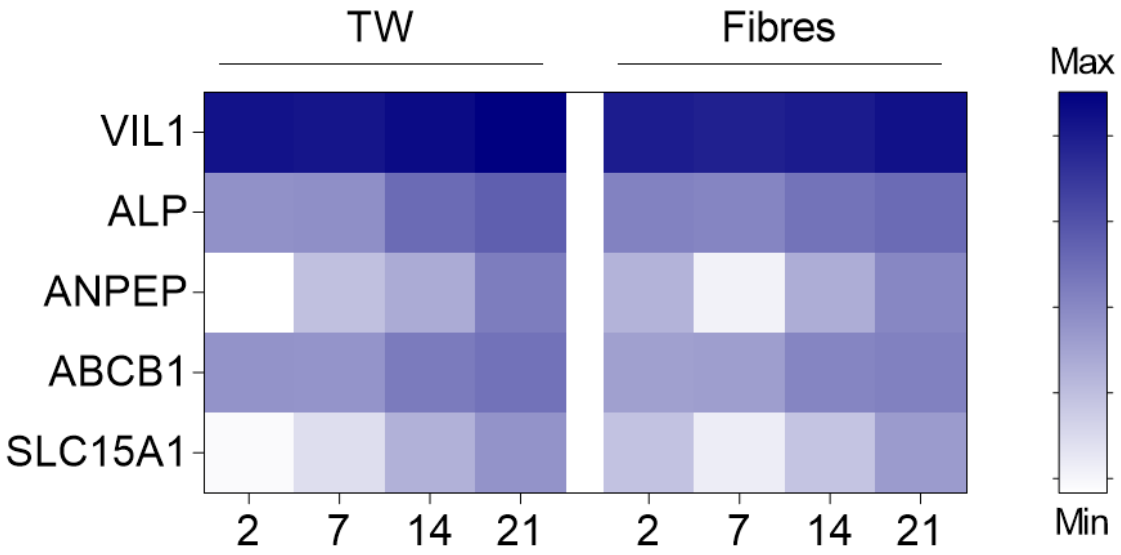

Figure 4.3 Gene Expression of Intestinal Markers of Differentiation

Heat map of the relative mRNA expression of key intestinal proteins at day 2, 7, 14 and 21 in Caco-2 monolayers grown on Transwell (TW) and PLLA fibre inserts (Mean, n=3). Relative expression plotted as $-\log(2^{\Delta Ct})$ compared to housekeeping gene β-actin, Min = -5.17, Max = -0.49.

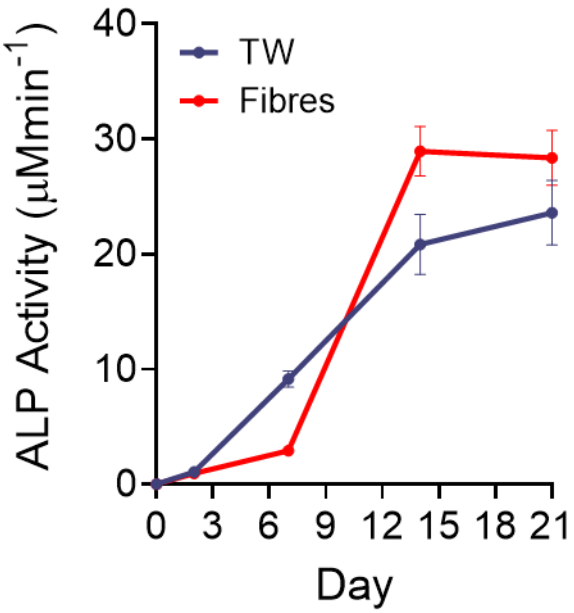

Figure 4.4 Alkaline Phosphatase Activity

ALP brush border enzyme activity of TW and PLLA Caco-2 monolayers over 21 days, measured as a rate of product concentration (Mean ± SEM, n≥3).

4.3.3 Expression of Basement Membrane ECM in Intestinal Models

The development of an intestinal monolayer model using biomimetic, topographical PLLA fibres as a culture insert is driven by the hypothesis that the intestinal behaviour and function of this model will more accurately represent that of *in vivo* intestines, as a result of its underlying ECM-like scaffold structure, compared to the flat, smooth Transwell inserts. In order that the behaviour of cells cultured on PLLA fibre models was unaltered by the artificial addition of ECM protein components, PLLA fibres were used neat and uncoated, unlike previous studies in which fibres were coated with collagen I [203]. As a result, we were therefore able to observe whether the use of ECM-like fibre structures induced any alterations in the expression or deposition of ECM protein components from the intestinal epithelial cells. Caco-2 monolayers cultured on both the standard Transwell insert and the PLLA fibre insert were probed, using antibody staining techniques, for their relative expression of ECM basement membrane (BM) proteins fibronectin (FN) and collagen type IV (COL4), alongside cytoskeleton protein actin, and imaged using confocal microscopy.

Expression of both BM ECM proteins, COL4 and FN, was observed in models on both cell culture surfaces (**Figure 4.5A and B**), demonstrating the capacity of cultured Caco-2 cells alone to express BM components. The extent of expression was quantified by fluorescence intensity (**Figure 4.5C**), which demonstrated that PLLA fibre monolayers expressed considerably more of both ECM proteins compared to the Transwell monolayer. The cytoskeletal protein actin appeared to be more highly expressed in Transwell fibres, but the confocal imaging demonstrates this is an artefact of the auto fluorescent Transwell membrane at this wavelength. The most significant difference observed from this data was the morphology of the monolayers, in particular the elongation of cells in the fibre cultivated monolayer, which displayed cell heights over 3-fold higher than the Transwell equivalent (38.0 $\pm$1.2 µm and 11.8 $\pm$0.6 µm, respectively for Fibre and TW) (**Figure 4.5D**). This morphological difference was also accompanied by considerably different deposition of ECM proteins between fibre and Transwell monolayers. The Z-stack images (**Figure 4.5A and B**) as well as the Z-Profile plots of fluorescence intensity as a function of sample depth in **Figure 4.6A and B**, highlight that Caco-2 cells grown on PLLA fibres have considerably have broader ECM

distribution than TW monolayers, with deposition of ECM components surrounding the cells, basolaterally, intercellularly and apically.

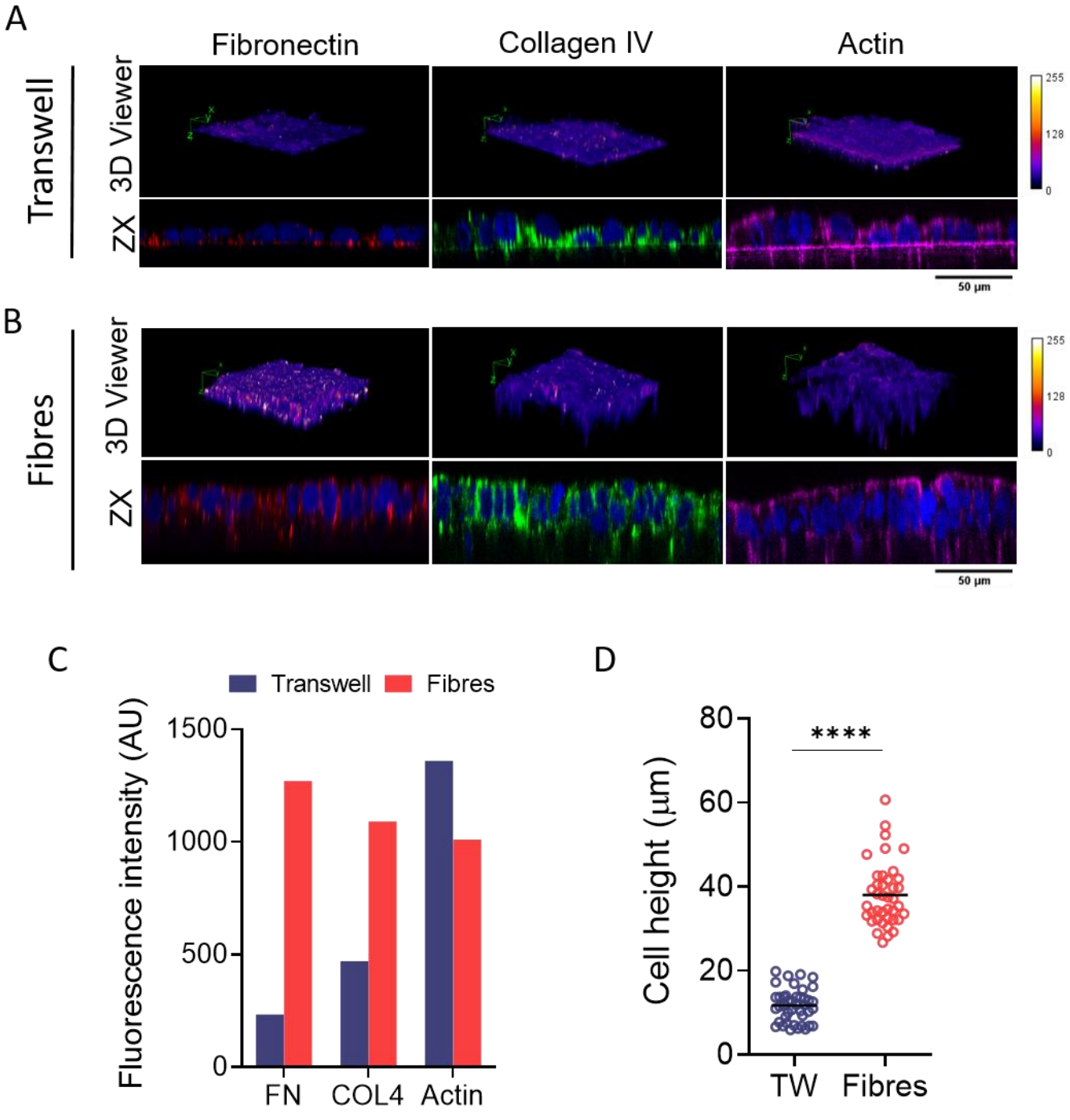

Figure 4.5 Basement Membrane ECM Protein Expression

Comparison of ECM protein expression of Fibronectin, Collagen type IV and Actin in Caco-2 monolayers cultured on Transwell (**A**) and PLLA fibre inserts (**B**) on day 7, quantified using Image J (**C**). Images show a 3D viewer rendering of protein expression as a function of fluorescence intensity (*above*) as well as a ZX orthogonal view. All images shown with DAPI counterstain, scale bar= 50 µm. (**D**) Height of cell monolayer on TW and fibres, n=40, Significance calculated from unpaired t-test P-value <0.0001.

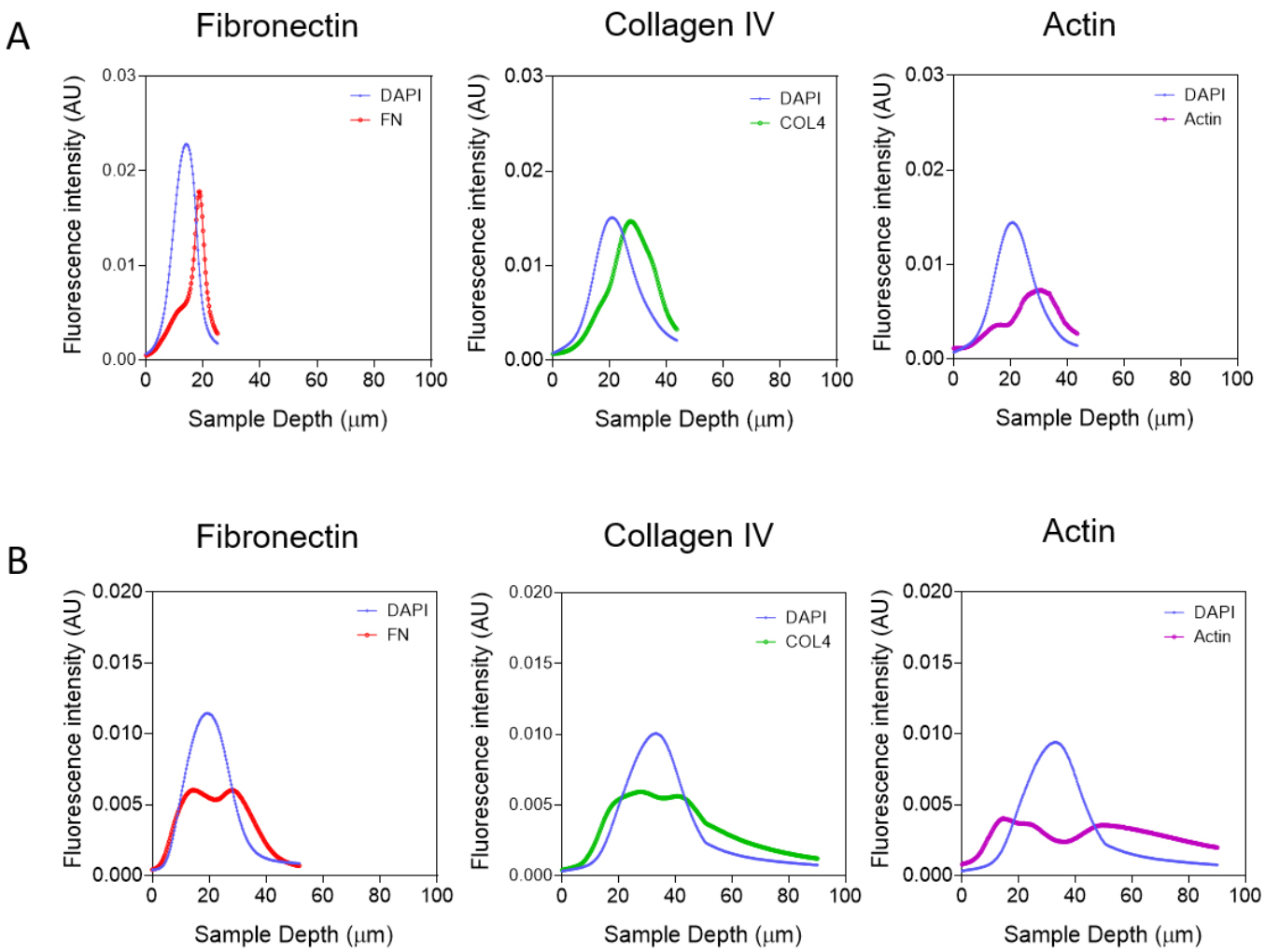

Figure 4.6 Distribution of ECM Protein

Comparison of ECM protein distribution of Fibronectin, Collagen type IV and Actin in Caco-2 monolayers cultured on Transwell (**A**) and PLLA fibre inserts (**B**) plotted as fluorescence intensity relative to sample depth in microns.

To further observe any differences in extracellular matrix components of the monolayer models, relative mRNA expression of genes coding for the BM-specific proteins fibronectin (FN1), collagen type IV (COL4), laminin alpha chains 3 and 5 (LAMA3 and LAMA5), nidogen (NID1) and perlecan (HSPG2) were analysed using RT-qPCR over the course of 21 days (**Figure 4.7A-F**). Across all genes analysed, a trend of increasing expression over time was observed, particularly for LAMA5 and HSPG2, where the gene expression on day 21 was notably higher than in the previous weeks. For all genes analysed, with the exception of LAMA3, PLLA fibre grown monolayers expressed equivalent or higher levels of ECM-related genes by day 21. This correlates with the previous protein expression data for COL4 and FN, but also extends this to the majority of ECM BM components. This would suggest that the ECM-like fibrous structure of PLLA induces Caco-2 cells to increase expression of ECM constituents at both the gene and protein level.

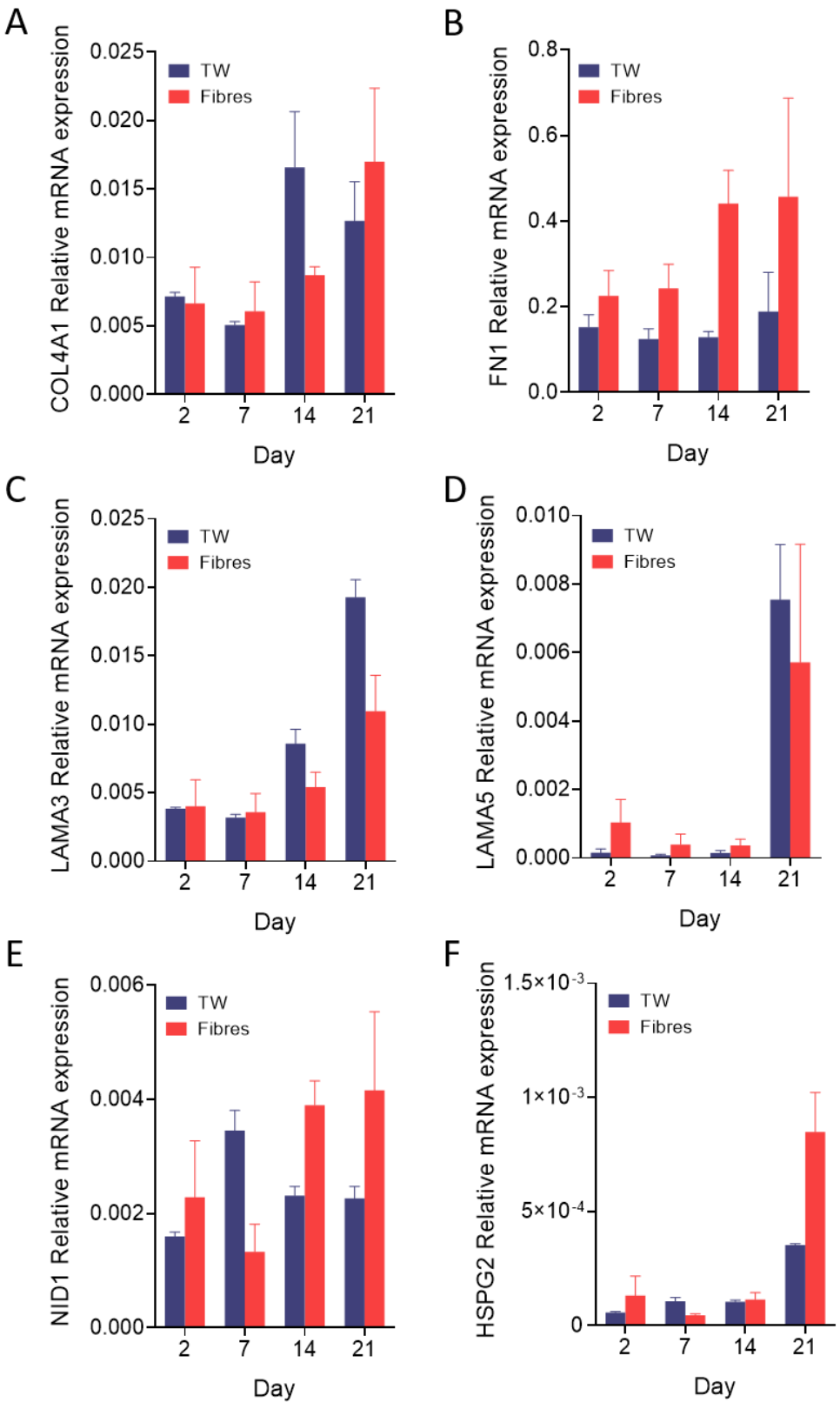

Figure 4.7 Gene Expression Levels of Basement Membrane ECM Proteins

Relative mRNA expression of genes encoding the basement membrane proteins Collagen type IV (**A**) Fibronectin (**B**), Laminin subunit-alpha 3 (**C**), Laminin subunit-alpha 5 (**D**) Nidogen (**E**), and Perlecan (**D**) in Caco-2 monolayers cultured on Transwell and PLLA fibre inserts for 2, 7, 14 and 21 days (Mean ± SEM, n=3).

4.3.4 Evaluation of the Barrier Function of Intestinal Monolayers

The primary function of the intestinal epithelial monolayer is as a barrier; selectively facilitating the transport of solutes and xenobiotic compounds from the external environment of the digestive tract, to the internal environment of the systemic blood network. It is vital therefore that in its most rudimentary capacity, an intestinal model should recapitulate these barrier properties. However, it is commonly cited that the Caco-2 Transwell monolayer model demonstrates heightened Transepithelial electrical resistance (TEER) values and lower permeability than found *in vivo*. Therefore, we evaluated whether Caco-2 monolayers cultured on PLLA fibre membranes demonstrated epithelial barrier integrity and how it compared to the classic Transwell model.

Firstly, TEER values of Caco-2 monolayers were monitored over the full course of the 21 day differentiation period for both Transwell and PLLA fibre membranes. Strikingly, PLLA fibre monolayers demonstrated significantly lower TEER values for the entire time period monitored (**Figure 4.8A**). For both monolayers, the TEER value increased over time, indicating cell growth into a fully confluent barrier layer, however by day 21 the mean TEER value for the Transwell model was almost 10-fold higher at 2290 $\pm$48 Ωcm^2 compared to the fibre model at 268 $\pm$28 Ωcm^2 (**Figure 4.8B**). Although still higher than the published *in vivo* human value of 100 Ωcm^2, the PLLA fibre monolayer demonstrates a much more representative TEER value of native tissues than the Transwell monolayer, indicating that the PLLA culture insert has overcome one of the biggest limitations of the classic Caco-2 Transwell model.

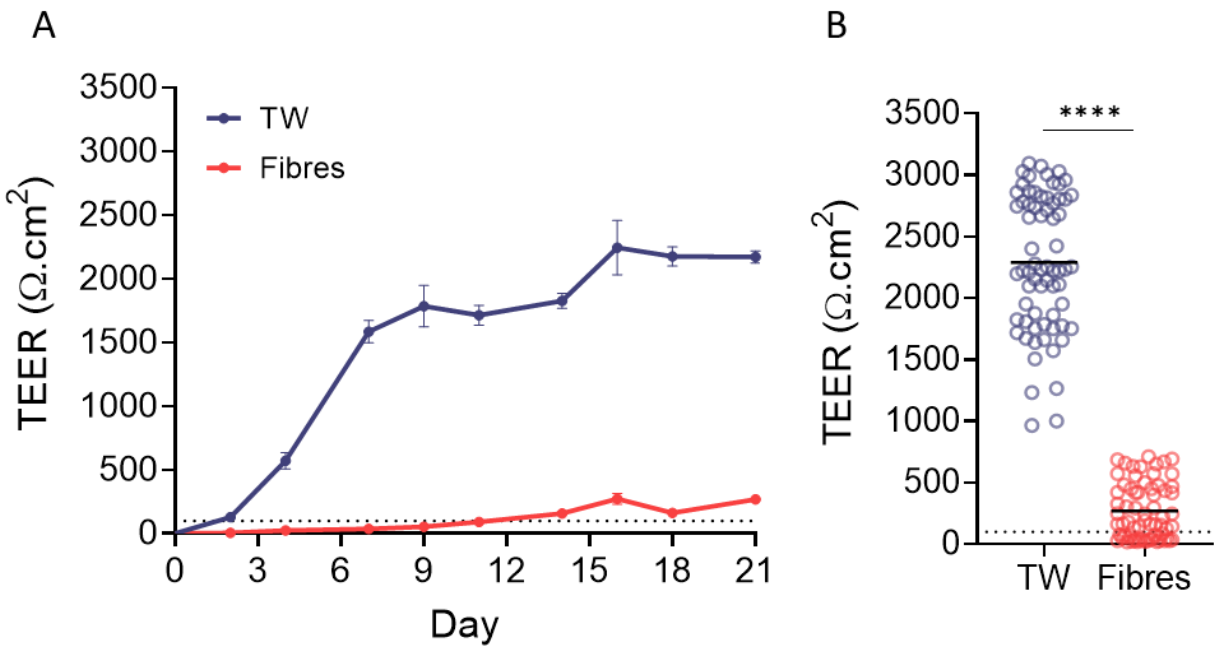

Figure 4.8 Trans-Epithelial Electrical Resistance (TEER) of Caco-2 Monolayers on Cell Culture Inserts

(**A**) TEER values of monolayers on Transwell (TW) and PLLA fibres over the period of 21 days, mean ± SEM, n ≥ 10. (**B**) Distribution of all TEER values for TW and fibre monolayers on Day 21, bar shows mean, n > 60, Significance calculated from Mann-Whitney test P-value <0.0001. Dotted line shows approximate human TEER value 100 Ω.cm^2.

Where TEER values reflect the ion conductance of the paracellular pathway in an epithelium, they do not necessarily correlate with paracellular water flow and consequently the paracellular permeability of small hydrophilic molecules [211]. As such, the paracellular flux of the non-electrolyte, fluorescent compound Lucifer yellow (LY) was compared between both Transwell and PLLA fibre monolayers to determine whether there was any observed differences in the way in which compounds move paracellularly across the different models. Due to the intrinsic differences in material and porosity of the membranes themselves, the apparent permeability coefficient (P_{app}) of LY was first assessed in the apical-basolateral direction for blank inserts with no cultured cells, and on inserts with cultured Caco-2 monolayers (**Figure 4.9A**). As hypothesised, due to its inherently increased porosity, the blank PLLA fibre membrane exhibited a higher level of permeability (mean 2.01 $\pm$0.1 x10^{-5} cm/s) to LY compared to the blank Transwell membrane (mean 1.45 $\pm$0.08 x10^{-5} cm/s). For Caco-2 cells cultured in a monolayer, both surfaces showed a significant decrease ($P<0.0001$) in the mean P_{app} of LY (0.08 $\pm$0.02 x10^{-5} cm/s and 0.16 $\pm$0.06 x10^{-5} cm/s respectively for Transwell and fibres) than their blank equivalents, demonstrating the formation of epithelial barrier on both culture membranes. To observe the way in which paracellular permeability to LY changed over the course of the 21 differentiation period, the same experiment was carried out on day 2, 7, 14 and 21 of culture (**Figure 4.9B**). This data shows that in both instances, the paracellular permeability decreases as the monolayer epithelial barrier is formed. The eventual permeability of LY by day 21 is greater in PLLA fibre monolayers (**Figure 4.9C**), displaying a mean permeability over 2-fold higher than Transwell equivalents, although still below the *in vivo* human value.

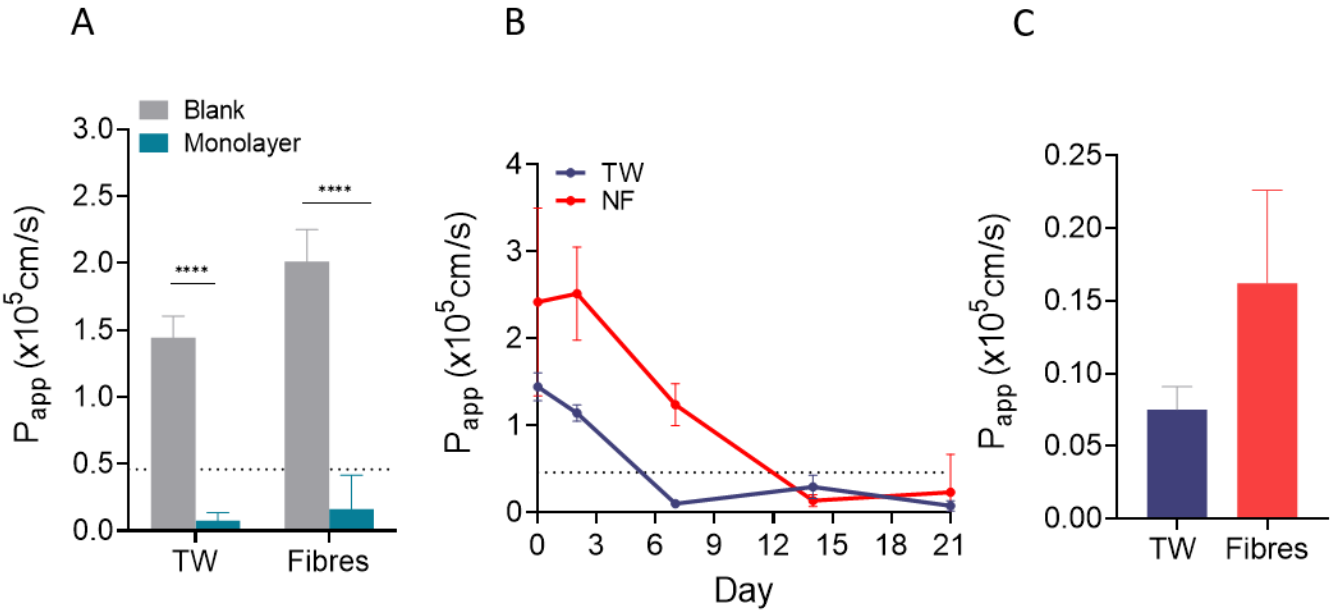

Figure 4.9 Paracellular Permeability of Caco-2 Monolayers on Cell Culture Inserts

Apical-basolateral apparent permeability coefficient (P_{app}) of Lucifer Yellow (LY) for Caco-2 monolayers cultured on Transwell (TW) and PLLA fibre cell surfaces over 21 days. (**A**) LY P_{app} on membranes without cells (Blank) and with Caco-2 Monolayer (Monolayer), mean ± SD, n≥4. Significance calculated from a two-way ANOVA with Tukey's multiple comparisons P-value <0.0001. (**B**) LY P_{app} across Caco-2 monolayers over the period of 21 days, mean ± SD, n≥3. Dotted line shows reported Papp for LY across human intestine 0.46 $x10^5$ cm/s. (**C**) LY P_{app} on Day 21 in TW and fibre inserts.

The main components of the epithelium that contribute to the formation of a selective barrier, are the tight junction proteins; complexes between adjacent cells that draw them together like a zipper to tightly regulate the paracellular movement of molecules. In light of the results presented in **Figures 4.8** and **4.9**, it was important to confirm that the observations of lower TEER values and increased paracellular permeability for PLLA fibre models are not due to a lack of tight junction integrity. The protein Zona Occludens-1 (ZO-1), also known as Tight Junction Protein 1 (TJP1), was probed using immunostaining, alongside a cell nuclei counterstain (DAPI), to observe its expression in both Transwell and PLLA fibre monolayers. **Figure 4.10A and D** confirm that both monolayer models display the typical cobblestone appearance of ZO-1 protein on both day 7 and day 21 of culture. Furthermore, Z-stack images (**Figures 4.10B and E**) displaying the orthogonal view of the monolayer present comparable localisation of ZO-1, as expressed apically in both models. Quantification of ZO-1 expression in each model was carried out by calculating the number of peaks in a Z-profile plot that corresponded to ZO-1 fluorescence (see methods section 2.5.2.3) and divided by the number of cell nuclei (**Figure 4.10C and F**). In this analysis, on both day 7 and day 21 there was no significant difference (unpaired t-test) between the ZO-1 expression on either surface, however the ratio was lower on day 21 than day 7 in both instances. Together with the Z-stack images in **Figure 4.10B and E** this data appears to show that there is no significant change in the localisation, or expression of ZO-1 between all conditions, and that the decrease in the ratio of ZO-1 expression on day 21 is a result of increased cell nuclei in a more compact and confluent monolayer. Overall this suggests that there is no evidence to suggest a lack of ZO-1 tight junction integrity in PLLA fibre monolayers.

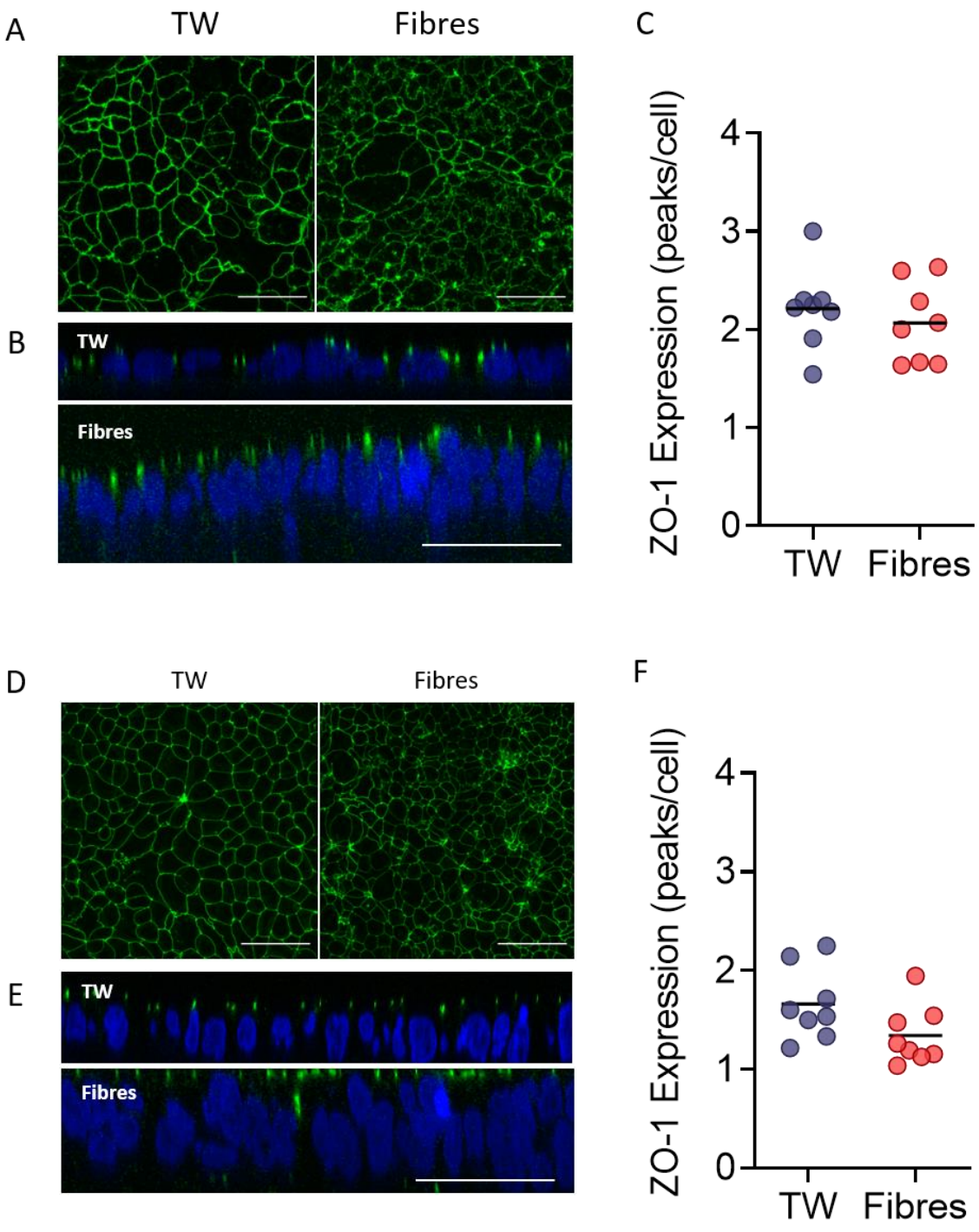

Figure 4.10 Expression of ZO-1 in Caco-2 Monolayers on Cell Culture Inserts

Representative images of Caco-2 monolayers grown on Transwell (TW) and PLLA fibre inserts on Day 7 (***Above***) and Day 21 (***Below***) immunostained for ZO-1 protein (*green*) and cell nuclei (*blue*). Shown from above as the sum projection of the Z-stack (**A**, **D**) and in the XZ orthogonal view (**B**, **E**) Scale bar = 50 µm. ZO-1 expression for each culture insert on Day 7 and Day 21 was quantified using image analysis as the ratio of ZO-1 expression per cell (**C**, **F**).

As the tight junction is formed from a complex of proteins, not just TJP1/ZO-1, the gene expression of all three major tight junction proteins, TJP1, Occludin-1 and Claudin-1 were analysed using RT-qPCR (**Figure 4.11**). The relative mRNA expression of all three proteins was quantified on day 2, 7, 14 and 21 of culture and revealed comparable, if not slightly increased expression in the PLLA fibre monolayers compared to the Transwell model. Together, these findings suggest that the growth of Caco-2 cells on PLLA fibres gives rise to an epithelial monolayer that demonstrates a more physiologically relevant barrier function that is not a result of compromised tight junctions.

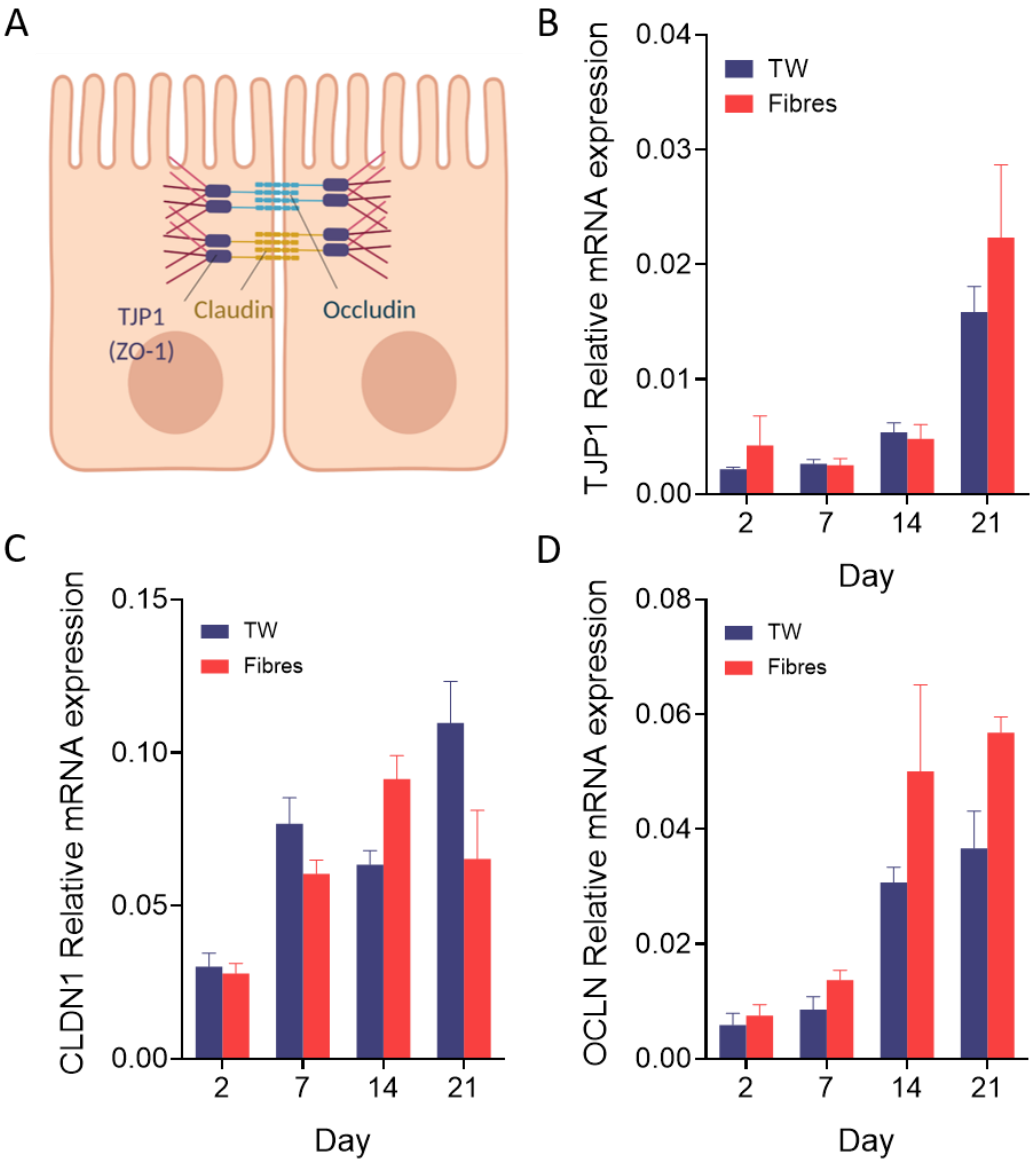

Figure 4.11 Gene Expression of Tight Junction Proteins

(**A**) Tight Junction in an epithelial cell showing the location of Tight Junction Protein 1 (TJP1/ ZO-1), Claudin 1 (CLDN 1) and Occludin (OCLN). Relative mRNA expression of TJP1 (**B**), CLDN1 (**C**), and OCLN (**D**) in Caco-2 monolayers cultured on Transwell and PLLA fibre inserts for 2, 7, 14 and 21 days (Mean ± SEM, n=3).

4.4 Discussion

Having established in Chapter 3 that electrospun PLLA fibrous membranes are a biocompatible material, suitable for cell culture, it was hypothesised that the BM-like, topographical characteristic properties of the PLLA fibres would provide a cell culture surface, on which an improved Caco-2 epithelial model could be developed for investigating intestinal absorption and transport.

4.4.1 PLLA Fibre Inserts Cultivate a Homogenous Caco-2 Monolayer

Using a verified cell safe adhesive, we recreated the bicompartmental well system of the classic Transwell model, yet replaced the PET plastic surface with PLLA fibre membranes adhered to the polystyrene insert. This resulted in a highly comparable cell culture system, with identical volume, cell culture surface area, dimensions, structural material and culture modality as the standard Transwell model. By retaining every element of the simple and accessible Transwell insert, apart from the cell culture surface material, this provided a reliable method of isolating the impact of the PLLA fibres upon the development and behaviour of the Caco-2 monolayer. Additionally, it facilitated the use of industry standard protocols in the validation of the PLLA fibre monolayer model, as well as a robust method to compare its functional performance in parallel to the standard Transwell monolayer model. The only other work to date that has employed the use of fibrous membranes for intestinal monolayer culture was published by Patient et al. 2019 [203], wherein the fibrous PET membranes were affixed using Snapwell® securing clips as opposed to adhesive bonding as presented here. Although our adhesive methodology was reproducible and reliable for small scale study, work by the Kim group [229] in directly spinning fibres onto inserts would provide a scalable method in producing fibre-based culture inserts.

The work presented here also sustained the use of Caco-2 enterocyte cells; on the one hand to maintain continuity in the intrinsic assessment of the performance and influence of PLLA fibres, but also due to their inherent value as an industry-wide, FDA accepted and well-established intestinal epithelial cell line. Although using primary human intestinal epithelial cells may be perceived as more pertinent in the pursuit of a

more physiologically complex model of the human intestine, the practicalities are not justified. The cost-effectiveness and high throughput capacity of the Caco-2 cell line, as well as its ease of use in culture, are what have led to its dominant use in pharmacokinetic studies to date, whereas primary cells are notoriously difficult to culture reproducibly. Results presented in section 4.4.1 demonstrate the ability of Caco-2 cells cultured on PLLA fibres to form a fully confluent, homogenous monolayer of enterocytes after 21 days in culture. Physically creating a contiguous monolayer is of vital importance when assessing transport across the epithelium, so that permeability and transport is not distorted by holes or gaps in the cell layer.

4.4.2 PLLA Fibre Monolayers Show Equivalent Enterocytic Differentiation

The ability of Caco-2 cells to differentiate spontaneously over time to represent an *in vivo*-like epithelium with characteristically polarised cells with apical microvilli [204,230] is another crucial element of the Transwell model that was necessary to verify with the PLLA fibre monolayer model. Over the established differentiation time of 21 days [84], the gene expression levels of apical brush border (BB) proteins in Caco-2 cells were analysed. Villin, a cytoskeletal protein shown to be the most abundantly expressed of all the BB proteins [231], was also the most highly expressed in both the Transwell and PLLA fibre monolayers to a similar magnitude. Additionally, all other BB proteins analysed, including the enzymes ALP and ANPEP, as well as the most highly expressed solute carrier transporter, SLC15A1 (which encodes the PEPT1 transporter), and the ABC efflux transporter, ABCB1, showed significant increases in gene expression. This time dependent increase in all BB genes over the 21 days, clearly demonstrated changes occurring in the PLLA monolayer over time that mirrored the differentiation of the Transwell cultured Caco-2 cells. It must be noted however, that although this data verifies the PLLA fibre model as comparative in its timing of differentiation gene expression levels to the Transwell monolayer model, the overall expression levels of genes in Caco-2 cells have been shown to vary compared to that observed in native intestinal tissues [129]. For example, the over or under expression of protein and efflux transporters in Caco-2 models compared to human intestinal tissues [216,217]. In Chapter 5 of this thesis, the activity of transporters, known to be differentially expressed in Caco-2 cells than human intestine, is studied in more depth.

Furthermore, although mRNA expression is a strong indicator of protein expression, they do not necessarily directly correlate. Therefore, the functional activity of the BB enzyme alkaline phosphatase (ALP) was assessed to confirm the presence and activity of this protein over the same time period. Akin to its observed increase in gene expression, the activity of ALP increased overtime in both models. This data is analogous to other work of Caco-2 monolayers cultured on topographical scaffolds, that showed comparable ALP activity to their flat counter parts [125,223]. One paper suggests that culturing Caco-2 cells on flat coatings of ECM proteins, particularly laminin, increased the ALP activity in Caco-2 cells, however, this data was only recorded over the time period of seven days rather than the established time course of three weeks [222]. Together, the growth imaging data and the satisfactorily comparable differentiation of Caco-2 cells, distinguished the PLLA fibre model as a representative epithelium suitable with which to further probe function and behaviour.

4.4.3 PLLA Fibres Induce Increased Expression and Deposition of ECM

Previous literature comparing the expression of BM protein elements in the native intestine and in intestinal models is scarce and contradictory. The majority of studies utilise transcriptomic and proteomic analysis to focus on a comparison of the quantity of genes expressed or upregulated in either the proliferation or differentiation stage of Caco-2 culture, as opposed to comparing the expression of specific genes themselves [232–234]. Moreover, alternative 3D intestinal models rarely probe or investigate ECM protein expression and deposition, as a result of the artificial ECM coatings on culture surfaces or used within cell culture scaffolds. The ability of this study to use neat PLLA fibres, without artificially deposited ECM proteins, allowed a unique opportunity to investigate whether the expression profile of ECM proteins was altered between the two monolayers on the different culture surfaces.

Using confocal Z-stack imaging, the 3D expression profiles, differences in the spatial distribution and fluorescence intensity of both fibronectin and collagen IV were captured in both Transwell and PLLA fibre monolayers. Although fluorescent imaging is limited as a quantitative technique, as it can induce artefacts due to off-target binding of fluorophores, or as a result of image processing in the analysis phase, when it comes

to observing the distribution and 3D localisation of regions of interest, confocal imaging remains one of the best techniques. Indeed, the most significant finding of this work was the stark contrast in the morphology of Caco-2 cells on each surface. PLLA fibres cultivated Caco-2 monolayers with significantly elongated and polarised enterocytes that had an increased intensity and broader, more 3D distribution of ECM protein expression than the Transwell model, which appears to express or deposit less protein, and is predominantly located basolaterally along the plastic membrane.

To strengthen the interpretation of imaging data, this study also analysed the gene expression levels of a number of key BM proteins. As previously mentioned, although mRNA does not directly correlate with protein expression, it is a strong indication of protein expression levels. RT-qPCR allowed for panel of relevant genes to be analysed quantitatively from within the same samples, facilitating a broader study of ECM protein expression over the entire differentiation period of 21 days. Analogous to the gene expression analysis of differentiation markers earlier in this chapter, data revealed that Caco-2 cells cultivated on both surfaces demonstrated an upregulation in the gene expression of ECM proteins over time, corresponding with enterocytic differentiation. This appears to contradict previous claims that down-regulation of fibronectin and laminin are associated with differentiation [235,236]. However, the gene expression analysis herein is strongly supported by more recent work, carried out using advanced microarray gene expression methods, that also show an increase in gene expression of FN1, COL4A, LAMA3 and NID2 (a variant of nidogen) in Caco-2 cells over the same time period [237]. Moreover, the increased expression of both Laminin alpha 3 and alpha 5 are strongly correlated with the differentiated villus *in vivo* [238,239], linking our data not only to other observations in Caco-2 cells, but also native intestinal tissue. It was further noted, that all ECM protein related genes except LAMA3, were more highly expressed on PLLA fibre surfaces than in Transwell monolayers, indicating that ECM related proteins are increased at both the gene and protein level.

4.4.4 PLLA Fibre Monolayers Show Improved Physiological Barrier Function

Despite its utility in assessing numerous aspects of drug permeability and bioavailability, limitations of poor permeability, accompanied by non-physiological TEER values have persisted in Transwell based Caco-2 models. A variety of innovative methods have been implemented to address these issues, including; ECM coatings [223,240], villus shaped scaffolds [122,123,152,226], decellularised ECM scaffold coatings [126,241] and using primary cells [101,242], however, the majority of these solutions still use a flat plastic Transwell membranes as the main semi-permeable surface, or incorporate aspects that act as a physical barrier and inhibit the study of transport across the epithelia. An exception to this, is similar, recent work by Patient et al.[203] that uses PET nanofibers as a replacement for the Transwell PET membrane, in the development of an epithelial monolayer. Unlike the work presented in this chapter, however, these PET fibres had smaller diameters and required Collagen coating to initiate suitable cell adhesion.

In the present study, uncoated PLLA fibrous membranes, validated to cultivate a contiguous, differentiated epithelium, demonstrated a significant increase in their paracellular permeability and decrease in TEER values. On average fibre grown monolayers had TEER values almost 10-fold lower than standard Transwells, considerably more representative of the *in vivo* intestine [129,211]. This was accompanied by paracellular permeability coefficients of Lucifer Yellow that correlated better with the published values for porcine jejunal samples [203] and more importantly *ex vivo* human tissue samples [243,244]; overcoming a major limitation of the Caco-2 Transwell monolayer in predicting *in vivo* absorption [245]. These findings are in agreement with the other fibre-based epithelial model previous published [203], that demonstrated comparable decreases in their TEER values and increases in LY P_{app} values compared to Transwell models. Further analysis of paracellular permeability with alternative, commonly used paracellular compounds such as inulin, PEG 4000 [246] or [^{14}C]mannitol [84], would provide a robust analysis of the findings of this chapter, however were not chosen due to the necessity for HPLC or radioactivity detection, as opposed to simple fluorescence. More significantly, future work comparing the permeability coefficients

of atenolol and terbutaline in both monolayers would be highly valuable, as the paracellular permeabilities of these compounds have been shown to be 27 and 79 times lower in Transwell Caco-2 models than human jejunum [213].

One rationale for the stark difference in the permeability of the Caco-2 Transwell monolayer model and human *in vivo* absorption has been attributed to distinct differences in their tight junction (TJ) pore sizes; Caco-2 cell pore diameters reported as ~4.5Å [247], nearly half that of human enterocytes at 11-13Å [248]. Moreover, it is known that immune cytokines (such as TNFα) [249], surfactants[250] and pharmaceutical excipients [251,252] can all modulate increases in permeability by disrupting TJs. Although our data did not recognise any substantial differences in the appearance of TJ formation through immunostaining for ZO-1, and only moderately increased TJP1 and OCLN gene expression in fibre models, this analysis was not exhaustive as there are many more protein constituents, including, ZO-2, ZO-3, cingulin, junctional adhesion molecules (JAMs) and 26 other Claudin proteins [253], that contribute to tight junction formation but were not covered by the scope of this study. Indeed, work in which Caco-2 cells were grown on engineered ECM substrates showed a considerable increase in the expression of the TJ protein Claudin-2 (a protein linked to leakier tight junctions), at both the protein and gene expression level, that corresponded to increased paracellular permeability [126]. The study also identified increased polarised morphology and compactness of Caco-2 cells grown on engineered ECM, which reflect that observed in this chapter, and correlate with the work of Darling et al. [128] that observed considerable elongation and lateral membrane morphological differences in their Caco-2 co-culture model that accompanied permeability improvements.

4.5 Conclusions

In summary, this chapter has evidenced that the fabrication of a PLLA fibre membrane-based cell culture insert can support the growth of a Caco-2 intestinal epithelial monolayer that demonstrates equivalent enterocytic differentiation markers. Additionally, the use of a structurally comparable ECM substrate as a cell culture surface prompts Caco-2 cells to alter the expression and deposition of basement membrane specific proteins. Most significantly, the work presented in this chapter

attests to the plasticity of Caco-2 cell function as a result of cell culture surface, by demonstrating that monolayers cultured on PLLA fibrous membranes overcome major limitations of the standard Caco-2 model with regard to TEER values and paracellular permeability.

5. Intestinal Bilayer Models and the Role of Subepithelial Fibroblasts

5.1 Introduction

The increasing capability to recapitulate tissue complexities to whole organ scales has revolutionised the field of regenerative medicine as well as research and development in many therapeutic areas. The ability to culture multiple cell types in 3D geometries with the incorporation of numerous physiological components, have allowed significant scientific and medical advancement. The intestine is no exception to this, with organotypic cultures emerging for use in tissue replacements and medical grafts [254], the study of pathogeneses such as cancer [255], Crohn's disease and inflammatory bowel disease (IBD) [256,257], as well as in the development of pharmaceuticals [129]. Enhanced, tissue engineered models of the intestine for the accurate screening of therapeutic compound bioavailability, and gut interactions *in vitro,* would contribute substantially to improving the efficiency in the development of new drugs; minimising timelines, financial expenditure and the use of animal models. Moreover, it would improve the understanding of the extra-epithelial mechanisms underlying absorption and detoxification, leading to the rational design of more successful compounds from the outset.

The evolution of the complexities of intestinal models range from multicellular monolayer cultures, to human stem cell explant organoids. However, as previously discussed, the success of the current "gold standard" Transwell Caco-2 model in the study of absorption and transport is rooted in its simplicity and assay versatility. It is no surprise then that a large proportion of the literature today still retain the use of the Caco-2 monolayer model as a starting point and main source of enterocytes. Early endeavours to expand the complexity and diversity of the homogenous Caco-2 monolayer included co-cultures with mucus producing goblet cells HT29-MTX. The rationale behind these multicellular monolayers being to induce the production of the mucus layer barrier in the study of epithelial transport. These models were heralded as

an improved model for studying paracellular passive transport, as the lack of tight junction formation between HT29-MTX and Caco-2 cells increased permeability [105,258], as well as the observation of a reduction ABCB1 efflux transporter activity in these multicellular models [259]. However, the improvements these models bring are largely due to a decrease in the density of enterocytes (reducing ABCB1 activity and increasing permeability) and are therefore highly dependent on the seeding protocols and ratios of HT29-MTX cell inclusion into the monolayer.

More recently, the focus has shifted to the value of underlying mesenchyme of the intestine in cellular models. The mesenchyme is the collective term for the milieu of extracellular matrix proteins and stromal cells that make up the general connective tissue underlying the epithelium [260]. In the intestine, the epithelium is supported by a specialised mesenchyme, stratified into distinct layers that include the basement membrane and the lamina propria (Figure 1.7). The most ubiquitous stromal cells of the intestinal mesenchyme are subepithelial fibroblasts; specialist cells that not only fill the extracellular interstitial space, but secrete a plethora of extracellular matrix components, provide structural support for the epithelia as well as the 3D architecture of the villi, and communicate crucial physical and chemical cues, which can influence epithelial function [116,120,121].

The importance of epithelial-mesenchymal interactions are inherently displayed in the necessity for both elements for the correct *in vivo* morphogenesis of the mucosal architecture of the intestinal epithelium, from embryo to adulthood [261]. Further to this, the epithelia-ECM and epithelia-mesenchymal interactions constitutively maintain homeostasis in the intestinal epithelia [116]. As a bioactive scaffold, the ECM proteins provide physical, mechanical and chemical cues to surrounding tissues; yet these cues can be intricately or dramatically altered by the ECM remodelling and secretion from stromal fibroblasts [262], causing alterations in the overall behaviour and function of the epithelium. Primarily, published work with intestinal cell types *in vitro* have shown the role of fibroblasts to be key in epithelial growth, proliferation and differentiation [263], through adjacent crosstalk [264] and by a variety of secreted paracrine chemical factors [263,265,266]. However, how these epithelial-mesenchymal interactions impact intestinal absorption and detoxification functions is yet to be fully elucidated.

Mesenchymal elements have been successfully incorporated in numerous creative ways to elaborate upon the traditional Transwell Caco-2 monolayer for the purpose of creating a more physiologically relevant intestinal model to observe transport in the gut. Caco-2 monolayers cultured above NIH3T3 fibroblasts embedded in Collagen I gels showed considerable enhancement of TEER tightness values and paracellular permeability [127]. Additionally, intestinal CCD18co fibroblasts cultured in a Matrigel® matrix alongside a co-culture of Caco-2 and HT29-MTX goblet cells also showed improved paracellular transport [130]. These trends were also observed in another complex model of Caco-2, HT29-MTX, NIH3T3 mouse fibroblasts and collagen gel [267], that also analysed a number of pharmacokinetic parameters to reveal decreased expression of the efflux transporters ABCB1 and BCRP, and improved correlation between the absorption of a set of model compounds in their 3D model and the *in vivo* human absorption fraction (F_a). In all these models, the common usage of synthetic or artificially fabricated ECM components of Matrigel® or collagen serve to replicate the ECM microenvironment, but hinder the ability for certain transport studies, and the individual observation of fibroblast cell ECM and signalling. Moreover, by comparing multicellular co-cultures that include non-human and non-intestinal fibroblasts to Caco-2 monolayers introduce areas of discrepancies into conclusions drawn. Despite their increased physiologically complexity, many models also preclude the direct dissection of intestinal stromal cell impact on epithelial pharmacokinetic function, as few studies have looked exclusively at the impact of fibroblasts alone. Recent work by Darling et al. [128] has made the most significant steps towards dissecting the role of subepithelial fibroblasts in intestinal epithelia function, by co-culturing dermal and intestinal fibroblasts and their conditioned media with a Caco-2 epithelium, to show enhanced polarisation, decreased TEER and increased paracellular permeability. However, a large focus of this study is on cell morphology rather than pharmacokinetic function.

The need for physiologically relevant intestinal models is evident, not only in determining the best drug candidates faster, but to also understand the mechanisms that dictate the absorption and detoxification pathways in the intestine. The largest additional cell type in intestinal tissue are the subepithelial fibroblasts of the underlying mesenchyme, which have previously been shown to play a role in epithelial

growth, differentiation, but also in aspects of barrier function. However, many of these models incorporate artificial ECM protein layers that hinder a full complement of intestinal barrier function analyses. Therefore, the hypothesis of this chapter, is that the incorporation of human subepithelial fibroblasts into models of the intestine, using a topographic, basement membrane-like, PLLA fibrous membrane (that has already shown Caco-2 adhesion and growth (Chapter 3) to form a contiguous monolayer demonstrating superior barrier function (Chapter 4)), will create a more physiologically relevant model for pharmacokinetic studies of transport, absorption and detoxification.

5.2 Aims

The aim of this chapter is to introduce increased physiological relevance to the previously established PLLA fibre monolayer model of the small intestine, by the incorporation of elements of the mesenchyme, predominantly subepithelial fibroblasts. Moreover, by establishing a series of models with differing spatial arrangements of subepithelial fibroblasts, in both Transwell and PLLA fibre-based cultures, this work aimed to dissect the underlying role of fibroblasts on the functional activity of the intestinal epithelia.

- Analyse the impact of various mesenchymal elements on the key areas of TEER values and paracellular permeability.
- Create a bilayer of Caco-2 epithelial cells and CCD18co subepithelial fibroblasts.
- Dissect the impact of CCD18co fibroblast on Caco-2 function by creating a series of models incorporating both proximal and distal fibroblasts.
- Use models to analyse all major aspects of intestinal activity relevant to pharmacokinetic studies.

5.3 Results

5.3.1 The Impact of ECM Coating and Fibroblast Subtypes on Intestinal Barrier Function

PLLA fibrous membranes have been shown to provide a topographic surface mimicking the intestinal basement membrane that could be used neat and uncoated for the attachment of Caco-2 intestinal cells (Chapter 3). Further to this, the proliferation of Caco-2 enterocytes into a contiguous epithelium produced a monolayer model with superior barrier function in terms of trans-epithelial electrical resistance (TEER) and Lucifer Yellow paracellular permeability, compared to the standard Transwell monolayer (Chapter 4). Following this, the next logical step for this chapter was to incorporate a variety of mesenchymal components (ECM protein and fibroblast cells), to increase the physiological complexity of the intestinal models, and assess their individual impact on the key barrier properties previously investigated.

Although the PLLA fibre monolayer model previously established in this thesis developed an epithelium upon uncoated fibres, a large proportion of 3D intestinal models in literature incorporate Collagen I, either to improve biocompatibility and cell adhesion, or as a mode of mimicking the BM. To this extent, PLLA fibre inserts were coated with Collagen type I to create an ECM coated fibre monolayer model (+Collagen) (**Figure 5.1**). Additionally, the impact of fibroblasts, the main stromal cell subtype underlying the intestinal epithelia, was also assessed on PLLA fibre membranes. Incorporation of two different fibroblast subtypes were analysed in a bilayer model with Caco-2 cells; including a generic, widely available, 3T3 mouse fibroblast immortalised cell line (+3T3), as well as the tissue-specific, human intestinal subepithelial CCD18co fibroblasts (+CCD18co) (**Figure 5.1**).

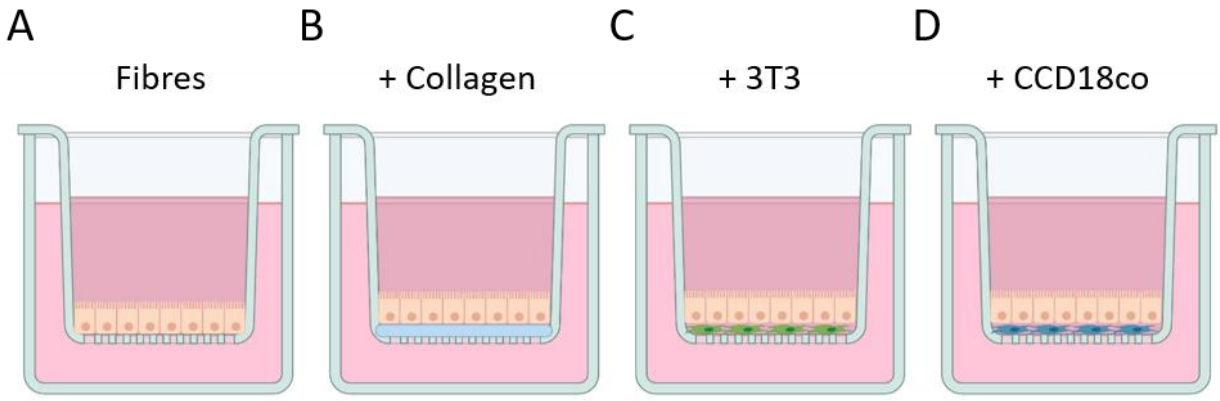

Figure 5.1 Schematic of ECM and Fibroblast Models

Models of the intestinal epithelia, showing the culture of Caco-2 enterocyte monolayers on uncoated (**A**) and collagen coated PLLA fibres (**B**). As well as PLLA fibre insert bilayers with Caco-2 cells cultured adjacent to either 3T3 mouse fibroblasts (**C**) or CCD18co intestinal subepithelial fibroblasts (**D**).

As in Chapter 4, the TEER values of the cell models were monitored throughout their period of growth, up to day 21 (**Figure 5.2A**), when the intrinsic paracellular permeability of the fluorescent test compound Lucifer Yellow (LY) was assessed (**Figure 5.2B**). Each of the three new mesenchyme-based models, collagen coated fibre monolayer (+Collagen), 3T3 bilayer (+3T3) and CCD18co bilayer (+CCD18co) were compared to the uncoated PLLA fibre monolayer already established (Fibres). The TEER values recorded for all models, followed a similar trend of growth, increasing over time as the Caco-2 epithelium became confluent and established a barrier of tight junctions. Similarly all models showed considerably low TEER values by day 21, reaching mean maximum values of 268 $\pm$28 $\Omega.cm^2$ (uncoated fibres), 351 $\pm$64 $\Omega.cm^2$ (+collagen), 336 $\pm$24 $\Omega.cm^2$ (+3T3), and 482 $\pm$37 $\Omega.cm^2$ (+CCD18co) respectively, whereas the standard Transwell monolayer recorded >2000 $\Omega.cm^2$ (data shown in **Figure 4.8**). These results emphasize the observation that Caco-2 cells cultivated on PLLA fibre membrane inserts demonstrate considerably lower TEER than on Transwell plastic inserts, however do not display considerable differences between the four mesenchyme based models tested, despite the inclusion of Collagen or stromal fibroblasts.

Similarly, no statistically significant difference was observed between the models when assessed for their paracellular permeability of LY (**Figure 5.2B**), with the exception of the CCD18co bilayer model (+CCD18co). This incorporation of intestinal specific subepithelial fibroblasts significantly (P=0.0078) increased the mean apparent permeability coefficient of LY from 0.16 $\pm$0.06 $x10^{-5}$ cm/s in the uncoated PLLA fibre monolayer (fibres) to 0.44 $\pm$0.21 $x10^{-5}$ cm/s in the +CCD18co bilayer, very close to the reported human *in vivo* value (0.46 $x10^{-5}$ cm/s [243]) indicated by the dotted line. As a result of both TEER and P_{app} data, it was concluded that in terms of overcoming the major limitations of the standard Transwell model, the most significant addition to the PLLA fibre monolayer model, was the incorporation of tissue-specific fibroblasts. Unlike the +Collagen or +3T3 models which showed no significant difference to the uncoated fibres model, the +CCD18co bilayer retained improved TEER values, yet further increased the paracellular permeability of LY to almost physiological level.

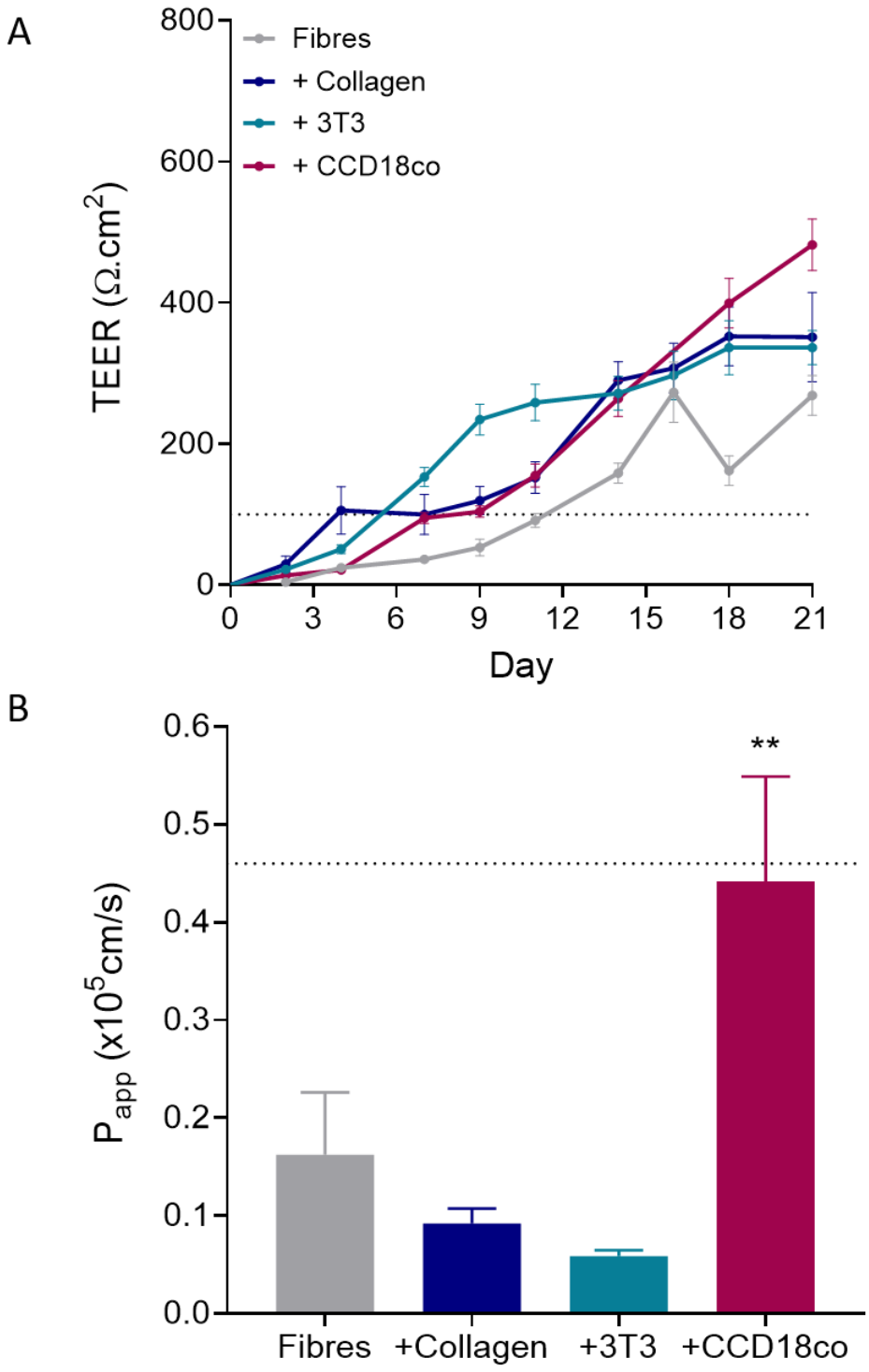

Figure 5.2 Barrier Function of PLLA Fibre Models with ECM and Stromal Cells

(**A**) TEER values of mesenchymal models on PLLA fibres over the period of 21 days, mean ±SEM, n ≥10. (**B**) Apical-basolateral apparent permeability coefficient (P_{app}) of Lucifer Yellow (LY) on day 21 mean ±SEM, n ≥5. Dotted line shows approximate human value. Significance calculated compared to uncoated fibres values from one-way ANOVA with Dunnett's multiple comparisons.

5.3.2 Morphology and Basement Membrane Protein Expression in Bilayer Models

Due to the success of the PLLA fibre Caco-2/CCD18co (+CCD18co) bilayer in improving paracellular permeability of LY, it was selected as the most physiologically relevant model to take forward for further study. As such, PLLA fibre cultured Caco-2/CCD18co bilayers were then directly compared to Transwell cultivated Caco-2/CCD18co bilayers in the evaluation of the impact of subepithelial intestinal fibroblasts on key aspects of enterocyte morphology, and ECM BM protein expression.

Firstly, bilayers cultivated on both Transwell and PLLA fibre inserts were assessed for any morphological differences by immunostaining for the cytoskeletal protein actin. **Figure 5.3A** shows a significant difference between the morphology of the bilayer models, namely, the epithelium architecture, thickness and enterocyte elongation. Despite the same seeding densities and cell types, the PLLA fibre bilayer demonstrates an epithelium with an undulating architecture, outlined clearly by the dense actin staining around the apical microvilli brush border, whereas the Transwell equivalent is relatively planar and flat.

Quantification of the mean cell height (**Figure 5.3B**) in both models, reveals PLLA fibre grown bilayer models to be over double the thickness of Transwell bilayer equivalents (30.1 $\pm$0.5 µm and 69.9 $\pm$0.9 µm respectively for TW and Fibres), showing significantly ($P<0.0001$) more Caco-2 cell elongation. Moreover, when compared to the cell heights measured previously in Chapter 4 for TW and fibre monolayers (see **Figure 4.5**), the data revealed that in inclusion of CCD18co fibroblasts led to a two-fold increase in Caco-2 elongation in both models.

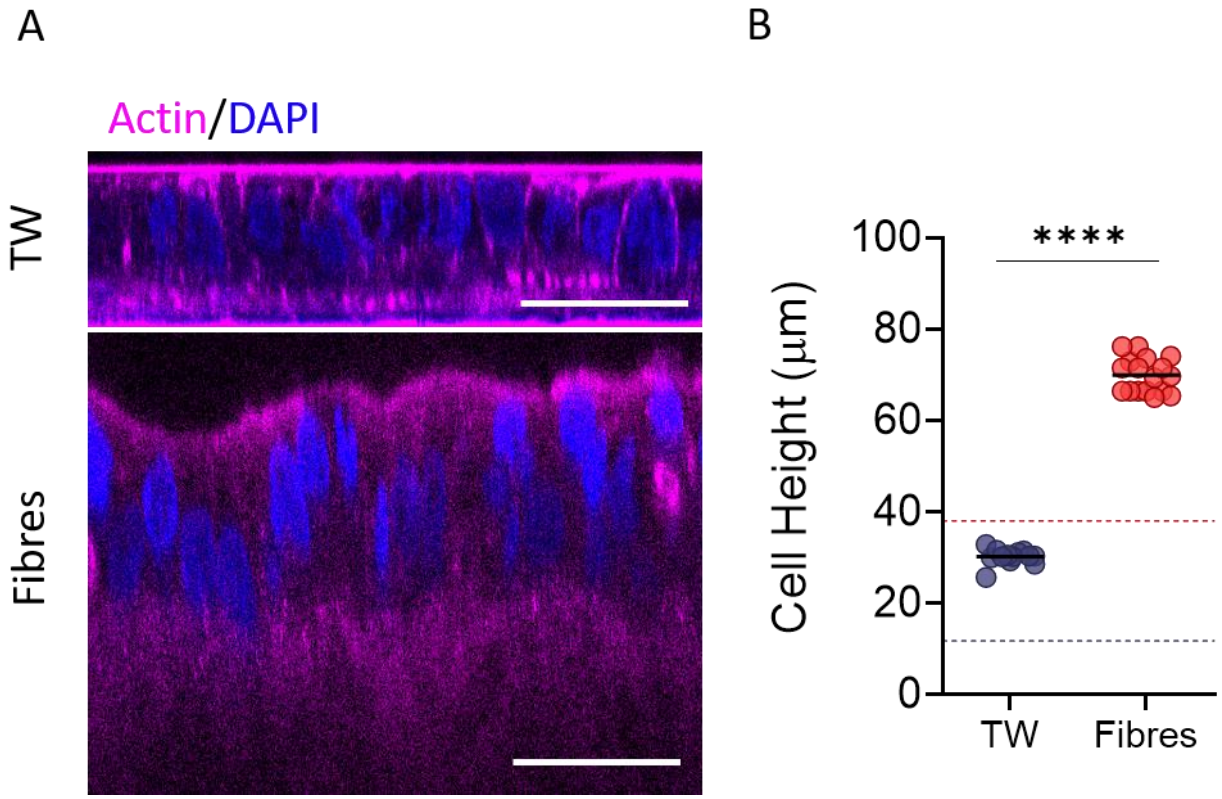

Figure 5.3 Morphology of Epithelial Bilayers

Representative Z-stack orthogonal view images of Caco-2/CCD18co bilayers grown for 21 days on Transwell (TW) and PLLA fibre inserts (**A**) immunostained for Actin cytoskeleton protein (*magenta*) and cell nuclei (*blue*). Scale bar = 50 µm. Elongation was quantified by measuring the height of the epithelial cells (**B**), dotted lines show the height of monolayers calculated in Chapter 4. Significance calculated using unpaired t-test.

Next, both bilayers were probed for the presence of tight junction protein ZO-1, a key controller of barrier permeability. When immunostained and visualised using confocal microscopy Z-stack imaging, the expression of ZO-1 protein can be observed located at the apical membrane of the epithelial layer in both bilayer models (**Figure 5.4A, B**). Sum Z-project images of ZO-1 staining as seen from above (**Figure 5.4C, D**) also show a cobblestone pattern of ZO-1 expression typical of the intestinal epithelium, indicating the connecting boundaries between cells. Interestingly, in both bilayer models there is a large variation in the patterning of theses intercellular connections, showing diversity in the shape and size of cell-cell junctions; unlike the more uniform, circular expression seen in monolayer models (see **Figure 4.10**). One reason for this can be clearly attributed to the undulating 3D epithelium as seen in the fibre bilayer orthogonal view (**Figure 5.4B**). The quantification of ZO-1 expression, relative to cell number is plotted in Figure 5.4E, demonstrating no significant difference in the expression of ZO-1 protein in Caco-2 bilayers cultivated on both Transwell and PLLA fibre inserts. Moreover, this expression shows no marked difference to the ZO-1 quantified from monolayers in Chapter 4, indicating that there is also no observable difference in ZO-1 expression between monolayers and bilayers.

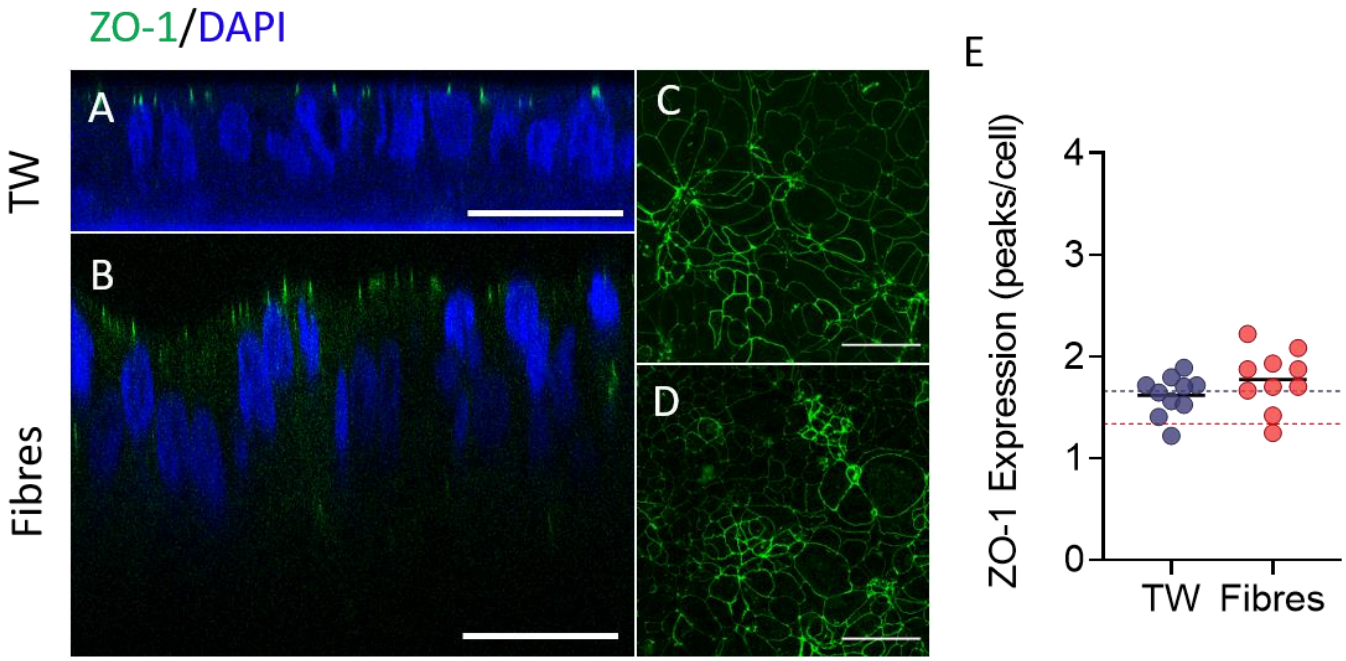

Figure 5.4 Expression of Tight Junction protein ZO-1 in Bilayers

Representative images of Caco-2 monolayers grown for 21 days on Transwell (TW) (**A, C**) and PLLA fibre inserts (**B, D**) immunostained for ZO-1 protein (*green*) and cell nuclei (*blue*). Shown in the XZ orthogonal view (**A**, **B**) and from above as the sum projection of the Z-stack (**C**, **D**). Scale bar = 50 µm. (**E**) ZO-1 expression for each culture insert was quantified using image analysis as the ratio of ZO-1 expression per cell, dotted lines show ZO-1 expression in monolayers calculated in Chapter 4.

Finally, epithelial bilayer models were analysed for the presence of ECM basement membrane proteins fibronectin (FN) and collagen type IV (COL4) using immunostaining and confocal Z-stack microscopy (**Figure 5.5**). In both bilayer models, there was significant staining for both ECM components. Transwell bilayers show a significant deposition of both ECM proteins in thin layer between the epithelial and fibroblast cells as indicated with a white arrow (**Figure 5.5 A, F**), reminiscent of the basal lamina layer of the basement membrane (see **Figure 1.7**). This can also be seen, albeit to a lesser extent in the PLLA fibre bilayer (**Figure 5.5B, F**), however, due to the nature of the fibres, this is not as distinct nor as planar. Additionally, the localisation of fluorescence for both ECM proteins appears more broadly distributed in cells of the PLLA fibre bilayer, showing significant apical and intracellular expression. Sum Z-project images (**Figure 5.5C, D, G, and H**) further highlight the topographic nature of the protein expression in the basal lamina area indicated with the white arrow. The Transwell bilayer illustrates a flat, homogenous sheet of protein, whereas the PLLA bilayer demonstrates the secretion of BM proteins to cover the fibrous structure of the membrane. Quantification of both fibronectin and collagen was calculated from the fluorescence intensity of the Sum Z-project images (**Figure 5.5J**), revealing increased fluorescence intensity for both proteins in Transwell models, however this is likely due to its planar nature.

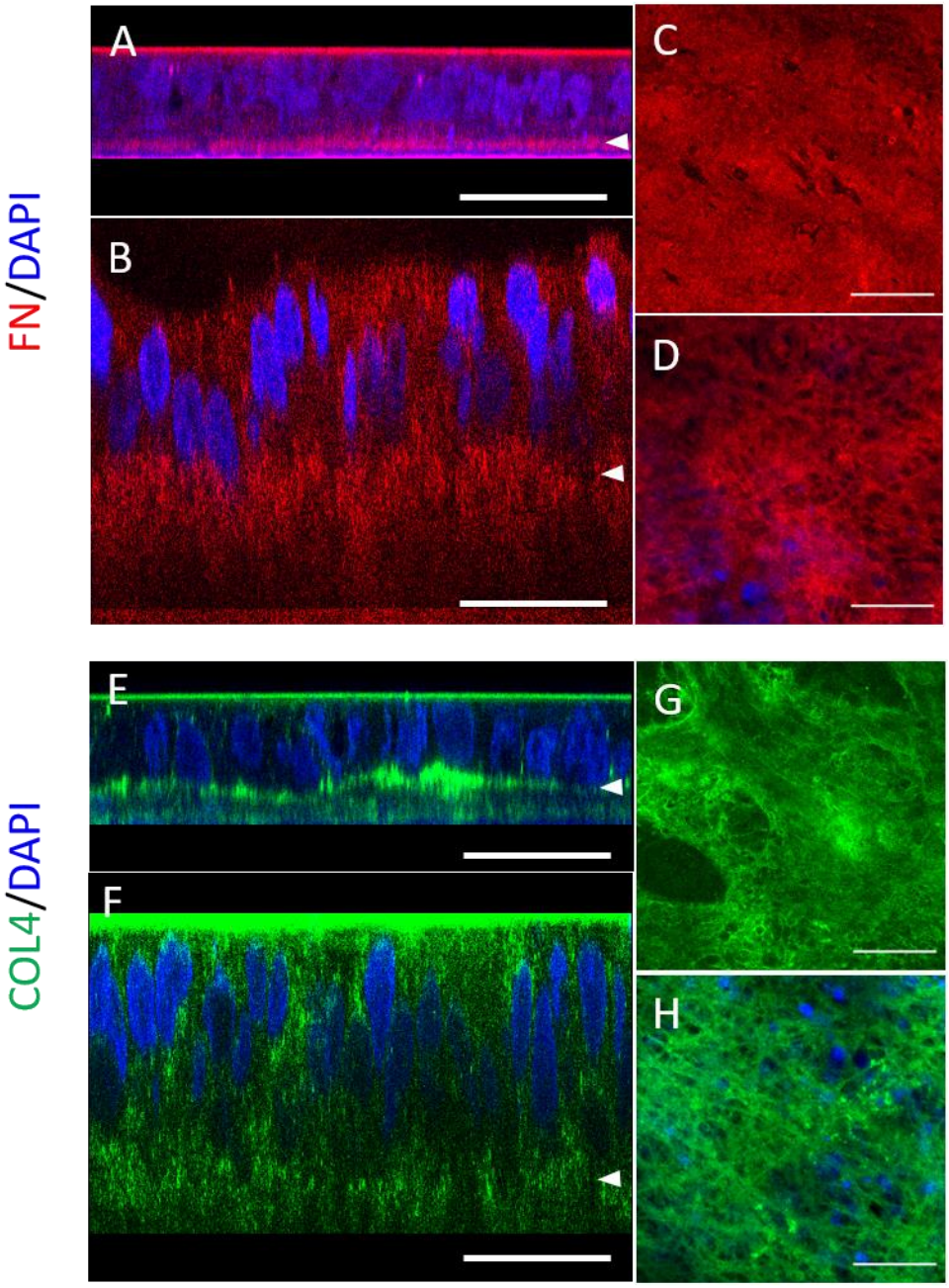
FN/DAPI
A
B
C
D
COL4/DAPI
E
F
G
H
J
Fluorescence intesity (AU)
800
600
400
200
0
TW
Fibres
FN
COL4

Figure 5.5 Basement Membrane ECM Protein Expression in Bilayers

ECM protein expression of Fibronectin (*red*) and Collagen type IV (*green*) in Caco-2 Bilayers cultured on Transwell (**A, C, E, G**) and PLLA fibre inserts (**B, D, F, H**) on day 21, quantified using Image J (**J**). Images show ZX orthogonal view (**A, B, E, F**) as well as a sum projection of the Z-stack at the area shown with the white arrow (**C, D, G, H**). All images shown with DAPI counterstain (*blue*), scale bar= 50 µm.

5.3.3 Proximal and Distal Effects of Subepithelial Fibroblasts on Paracellular Permeability

The physiologically topographic surface of PLLA fibres has exhibited considerable impact on the morphology and function of both Caco-2 monolayers and Caco-2/CCD18co bilayers, compared to PET Transwell equivalents. Equally, the incorporation of CCD18co cells to form a bilayer epithelium has also greatly impacted intestinal architecture and permeability, compared to simple monolayers alone. The next stage in this work was to determine the role of subepithelial fibroblasts in various functional aspects of epithelial function, in order to optimise a physiologically relevant intestinal model with the capacity to study absorption, transport and detoxification. To this end, we created a total of eight intestinal models with which to examine how different cellular, and topographic elements combine to drive intestinal function. A series of cellular models with increasing proximity of fibroblasts included Monolayer (Mono), Conditioned media (CM), Co-culture (Co), and Bilayer (Bi) models, cultivated in both Transwell and PLLA Fibre inserts with Caco-2 and CCD18co cells (**Figure 5.6**). These models allowed both a direct comparison between fibre and Transwell inserts, to determine the impact of culture surface, as well as creating a set of models with increasing epithelial-stromal interactions, enabling the examination of the role of these fibroblasts.

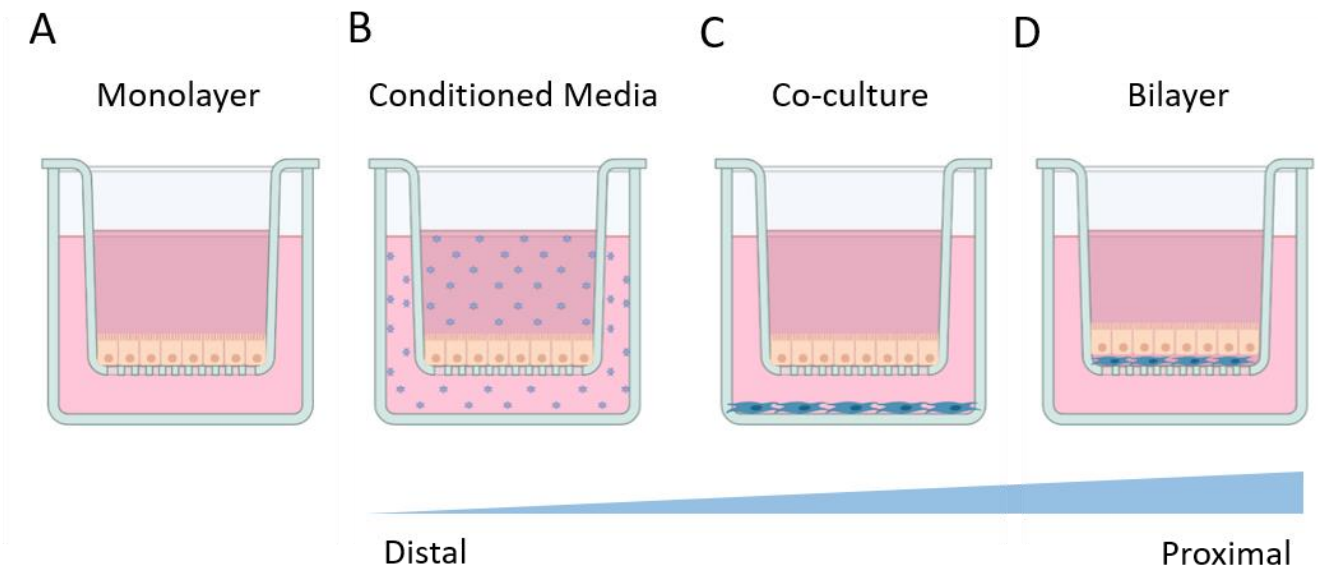

Figure 5.6 Schematic of Subepithelial Fibroblast Models

Models of the intestinal epithelia, showing the culture of Caco-2 enterocytes on cell culture inserts (TW or PLLA fibre) as a Monolayer (mono) (**A**), Conditioned Media (CM) (**B**), Co-culture (Co) (**C**) and with Bilayer (Bi) (**D**). Wedge shows relative proximity of fibroblasts to Caco-2 cells.

Firstly, we compared the TEER values over the course of 21 days to observe both barrier formation and integrity as well as tightness of the epithelia. In all instances, TEER values increased with time, reflecting the formation of an integrated barrier as cells proliferated to confluency. Figures 5.7A and B show that the presence of fibroblasts in Transwell models (CM, Co and Bi), whether proximal or distal, was sufficient to significantly decrease the TEER value in all cases ($P<0.0001$), to values between 800-1300 $\Omega.cm^2$ as opposed to >2000 $\Omega.cm^2$ of the monolayer. Conversely, for PLLA fibre models, which already demonstrated strikingly lower TEER values in monolayers alone, there was no further significant difference with the addition of fibroblasts (**Figure 5.7C, D**), with all PLLA models demonstrating TEER values between 250-510 $\Omega.cm^2$.

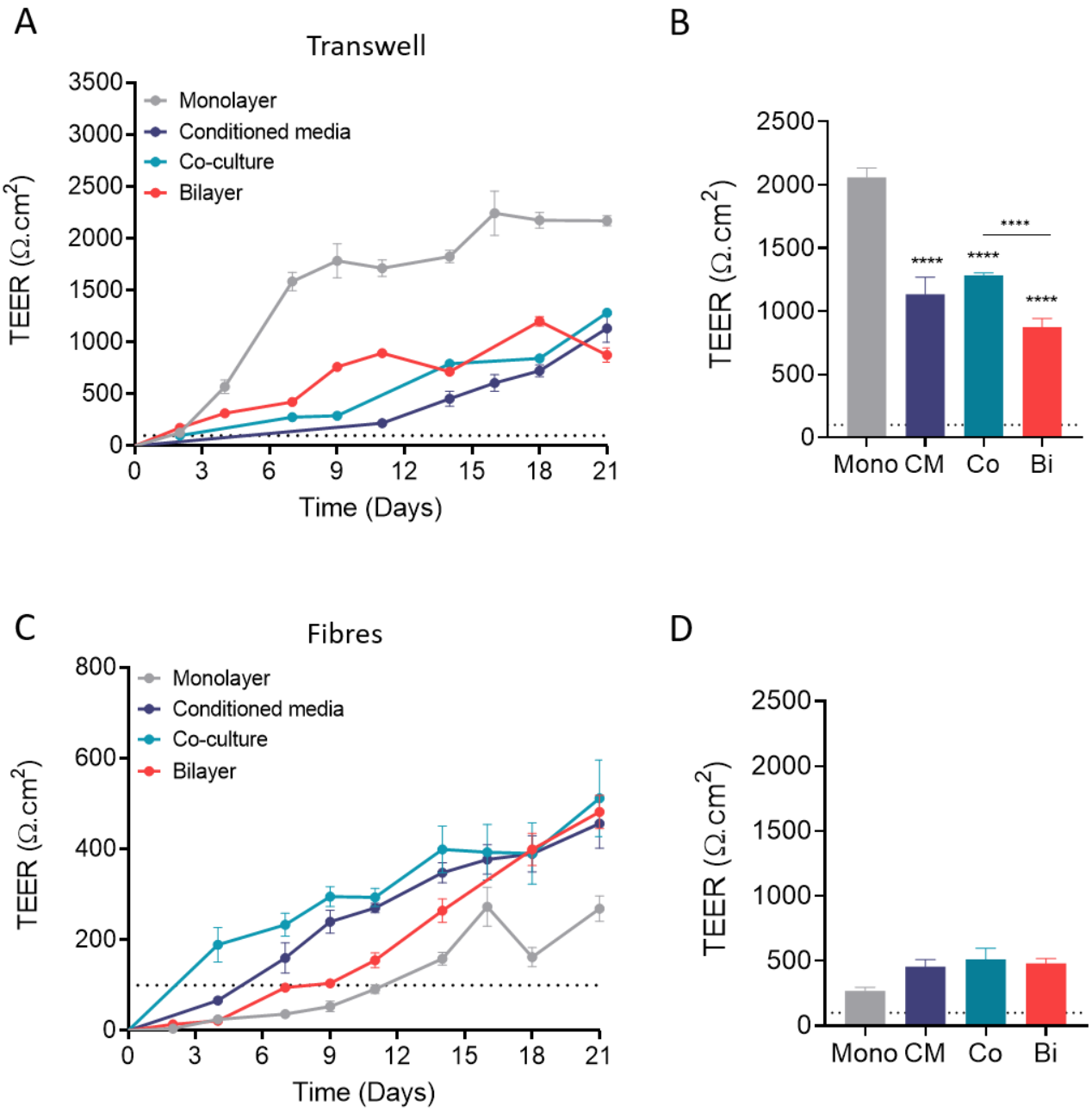

Figure 5.7 Trans-epithelial Electrical Resistance (TEER) of Intestinal Models

(**A**) TEER values of intestinal models over the period of 21 days on Transwell (**A**) and PLLA fibres (**C**), mean ±SEM, n ≥4. Comparison of all TEER values for TW (**B**) and PLLA fibre (**D**) models on Day 21 mean ±SEM, n ≥4. Significance calculated from one-way ANOVA with Tukey's multiple comparisons. Dotted line shows approximate human TEER value 100 Ω.cm^2.

As previously discussed in Chapter 4, the paracellular permeability of standard Transwell monolayers is notoriously poorly correlated with *in vivo* absorption and remains one its biggest limitations as a model of transport in the intestinal epithelia for small hydrophilic compounds. This thesis already established that PLLA fibre monolayers contributed to improved permeability with regard to Lucifer Yellow (see **Figure 4.9**).

Figure 5.8A demonstrates that there is no significant difference in the LY P_{app} between any of the Transwell models, displaying values of 0.08 (Mono), 0.11 (CM), 0.09 (Co), and 0.06 $x10^5$ cm/s (Bi), respectively. On the other hand, **Figure 5.8B** shows that all PLLA fibre models demonstrated higher LY P_{app} values than their Transwell equivalents, displaying values of 0.16 $\pm$0.06 (Mono), 0.14 $\pm$0.02 (CM), 0.15 $\pm$0.03 (Co), 0.44 $\pm$0.02 $x10^5$ cm/s (Bi), respectively. This data also reveals that Caco-2/CCD18co bilayers cultivated on PLLA fibres produce an epithelium with a significantly higher permeability for LY ($P<0.01$), which is remarkably close to the reported human *in vivo* permeability of 0.46 $x10^5$ cm/s [243]. Interestingly, Conditioned media (CM) and Co-culture (Co) PLLA fibre models, which include stromal fibroblasts but not in direct contact with the epithelium, do not induce any significant changes in the permeability of LY compared to the monolayer (Mono). This indicates that PLLA cultivated Caco-2 cells require direct interaction with adjacent fibroblasts for the most physiologically relevant LY permeability.

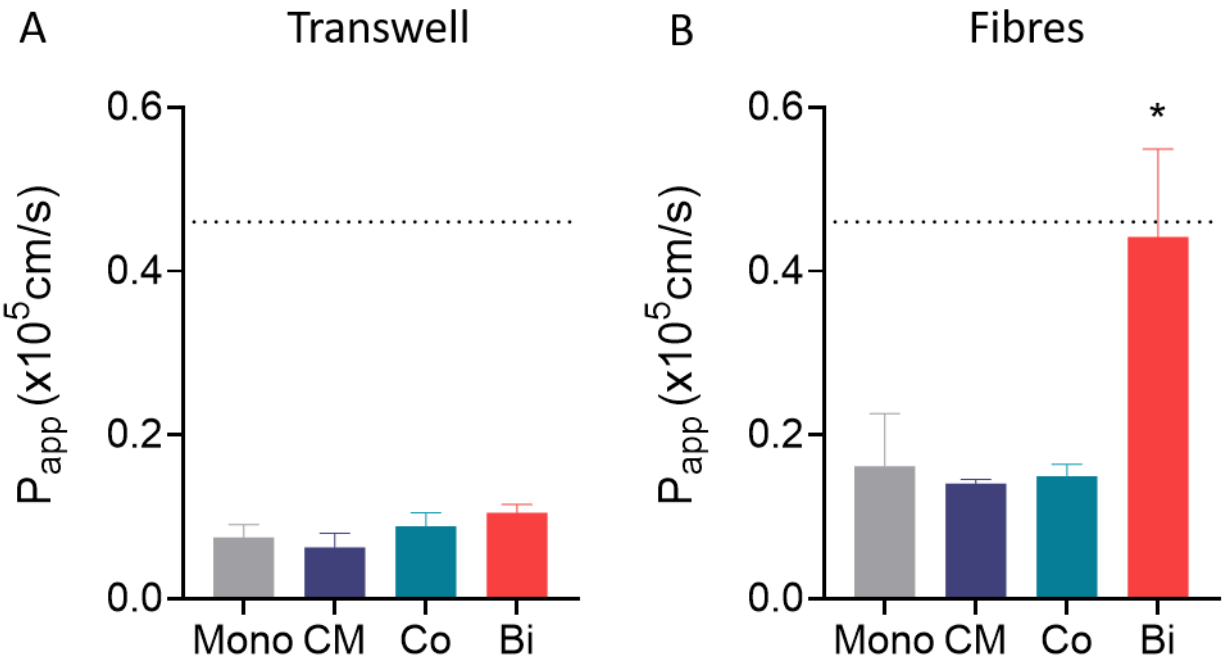

Figure 5.8 Paracellular Permeability of Lucifer Yellow

Apical-basolateral apparent permeability coefficient (P_{app}) of Lucifer Yellow (LY) for Caco-2 models cultured on Transwell (**A**) and PLLA fibres (**B**) for 21 days. Mean ±SEM, n≥4, significance calculated compared to monolayer values from one-way ANOVA with Dunnett's multiple comparisons. Dotted line shows reported Papp for LY across human intestine 0.46 $x10^5$ cm/s.

As paracellular permeability is such a widely reported limitation of the current standard Transwell monolayer model, it was important to further evaluate other paracellularly transported compounds in these eight models. To this end, the apparent paracellular permeability of two fluorescently labelled dextrans (FITC-dextran) of considerably differing molecular weights (4 kDa and 70 kDa) were analysed as an alternative paracellular substrate that would also give insights into size exclusion limits of paracellular routes in the different models.

Initially, the intrinsic permeability of both Transwell and PLLA fibre inserts for FITC-dextran 4 kDa (FD4) and FITC-dextran 70 kDa (FD70) was analysed in blank inserts as a baseline (**Figure 5.9A, B**). Without the presence of any cells, TW and Fibre inserts showed no significant difference between the permeability of the two surfaces for the apical-basolateral transport of both FD4 and FD70. As anticipated, the addition of a Caco-2 monolayer barrier significantly reduced the permeability of both FD4 and FD70. This data also revealed that PLLA Fibre monolayers showed considerably higher permeability (0.99 $\pm$0.27 x10^5 cm/s) to the smaller FD4 compound than the Transwell monolayer (0.02 $\pm$0.001 x10^5 cm/s). Additionally, this PLLA Fibre FD4 P_{app} was also nearly 100 times greater than the permeability of the FD70 compound (0.01 $\pm$0.002 x10^5 cm/s) on the same insert surface.

On comparison of the different fibroblast models, the Transwell models (**Figure 5.9C**) revealed that similar to the results of LY, the addition of fibroblasts do not significantly increase the permeability of FD4 or FD70, with the exception of the Co-culture model, which shows significantly higher permeability for FD4 than the monolayer ($P<0.0001$). However, considering the low n numbers for this experiment, this is likely an anomalous result. For PLLA fibre models (**Figure 5.9D**), distal fibroblast models (CM and Co) showed a slight decrease ($P<0.05$) in the FD4 permeability compared to Mono, however the bilayer maintained the highest FD4 permeability of all eight models tested (1.62 $\pm$0.02 x10^5 cm/s). As with the Transwell models, the permeability of FD70 in all fibroblast models on PLLA fibres showed no significant differences. In all cases, the permeability of the FD4 compound was higher than for FD70, indicating a correlation between size and paracellular transport in these models.

Overall, this FD paracellular permeability data is not as clear cut as the LY data, possibly due to the low number of samples, as well as the use of sink conditions increasing the likelihood for error, especially for such low permeability values. However, both LY and FD data agree that the PLLA fibre bilayer showed the higher permeability out of all the models examined.

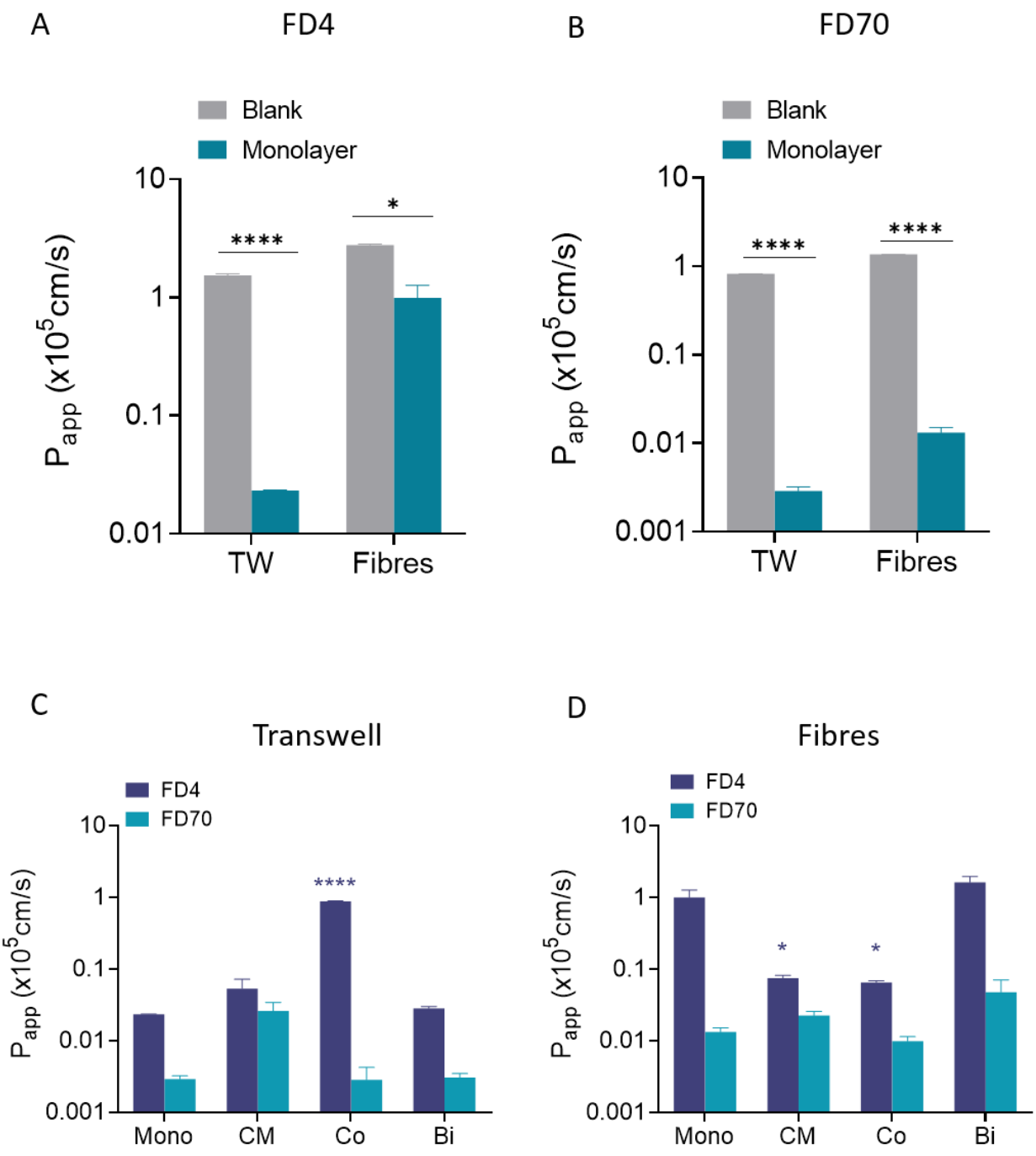

Figure 5.9 Paracellular permeability of FITC-Dextrans

Apical-basolateral apparent permeability coefficient (P_{app}) of FITC-Dextrans MW 4 kDa (FD4) (**A**) MW 70 kDa (FD70) (**B**) on membranes without cells (Blank) and with Caco-2 Monolayer (Monolayer). Mean ±SEM, n=3, significance calculated from a two-way ANOVA with Tukey's multiple comparisons. P_{app} of FITC-Dextrans for Caco-2 models cultured on Transwell (**C**) and PLLA fibres (**D**) for 21 days. Mean ±SEM, n=3, significance calculated compared to monolayer values from one-way ANOVA with Dunnett's multiple comparisons.

5.3.4 Proximal and Distal Effects of Subepithelial Fibroblasts on Enzyme Activity

The enterocyte epithelium of the intestine is a successful barrier in the first line of defence for preventing the absorption of unwanted or toxic compounds into the body. However, there exist numerous additional mechanisms by which the intestinal epithelium regulates compound entry into the circulatory system; one such mechanism is enzymatic biotransformation. The microvilli brush border of the luminal facing, apical side of enterocytes expresses the enzyme alkaline phosphatase (ALP), which *in vivo* functions in to maintain gut homeostasis by modification of various peptides and fatty acids, as well as detoxification against lipopolysaccharides [268]. *In vitro*, however ALP is also used as a key marker of Caco-2 cell differentiation to an enterocytic phenotype.

Here, the activity of ALP was measured in all eight models as an indicator of enterocyte brush border differentiation, as well as detoxification enzymatic capacity. ALP activity in all Transwell and PLLA fibre models showed elevated ALP activity on day 21 compared to day 7 (dotted line), indicating successful differentiation in all cases (**Figure 5.10**). For Transwell models (**Figure 5.10A**), the inclusion of fibroblasts (Co and Bi models) increased the ALP activity (33.0 $\pm$7.4 and 36.9 $\pm$3.9 $\mu Mmin^{-1}$, respectively) compared to the monolayer model (23.6 $\pm$2.8 $\mu Mmin^{-1}$), and highlighted a trend of increasing activity with increasing fibroblast proximity, although this was not statistically significant. The fibre models (**Figure 5.10B**) showed a similar trend with the bilayer model inducing the highest rate of ALP product turnover (38.1 $\pm$1.0 $\mu Mmin^{-1}$). In these models however, the Co-culture and CM models did not improve the enzymatic turnover rate.

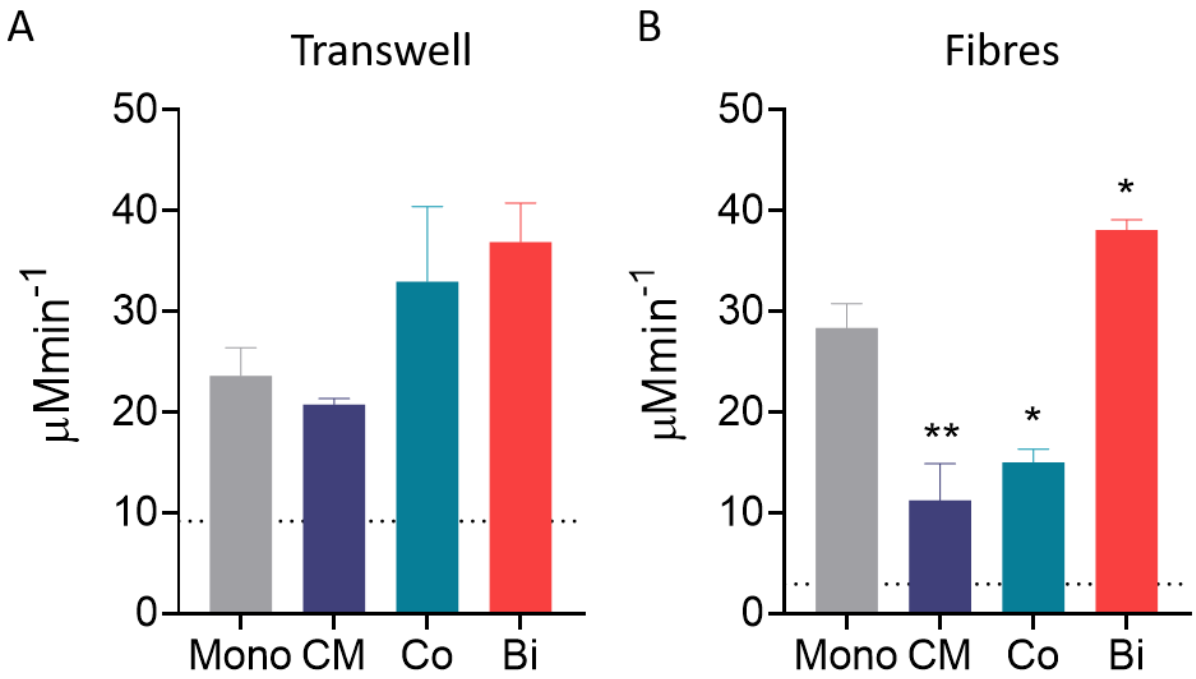

Figure 5.10 Alkaline Phosphatase Activity

ALP brush border enzyme activity of Transwell (**A**) and PLLA fibre (**B**) Caco-2 models on day 21, measured as a rate of product concentration, Mean ± SEM, n≥3. Significance calculated compared to monolayer values from one-way ANOVA with Dunnett's multiple comparisons. Dotted line shows monolayer activity on day 7 of culture.

The next enzyme assessed for its activity across the intestinal models was the drug metabolising enzyme cytochrome P450 3A4 (CYP3A4). CYP3A4 functions to oxidise small organic xenobiotics such as toxins or drugs, inside enterocytes, into products that are either no longer toxic, or substrates for efflux out of the body. Responsible for the metabolism of >50% of oral drugs, the activity of CYP3A4 can significantly lower the plasma concentrations of drugs *in vivo* so is vital to the bioavailability of novel therapeutic compounds. However, Caco-2 enterocytes significantly under express this enzyme in typical Transwell monolayer culture [217]. Consequently, the eight intestinal models developed herein were assessed for their capacity to metabolise CYP3A4 substrate 7-benzyloxymethyloxy-3-cyanocoumarin (BOMCC) to the fluorescent metabolite 3-cyano-hydroxycoumarin (CHC).

On comparison of the Transwell based models (**Figure 5.11A**), all three fibroblasts models (CM, Co and Bi) produced increased mean relative fluorescence (1684 ±101, 1345 ±45 and 1849 ±48 RFU, respectively) compared to the Transwell monolayer (1155 RFU), with the CM and Bi conditions being statistically significant. Conversely, in **Figure 5.11B** no significant difference was observed in the CM and Co, PLLA fibre models (940 ±64, 863 ±52 RFU) compared to the PLLA monolayer (1039 ±42 RFU), however a greater than 6-fold increase in mean relative fluorescence was observed for the PLLA bilayer model (6509 ±431 RFU, $P<0.0001$). Therefore, on both insert surfaces, the most significant increase in CYP3A4 activity was observed in the bilayers with adjacent fibroblasts, however this effect was considerably more profound on PLLA fibre membranes.

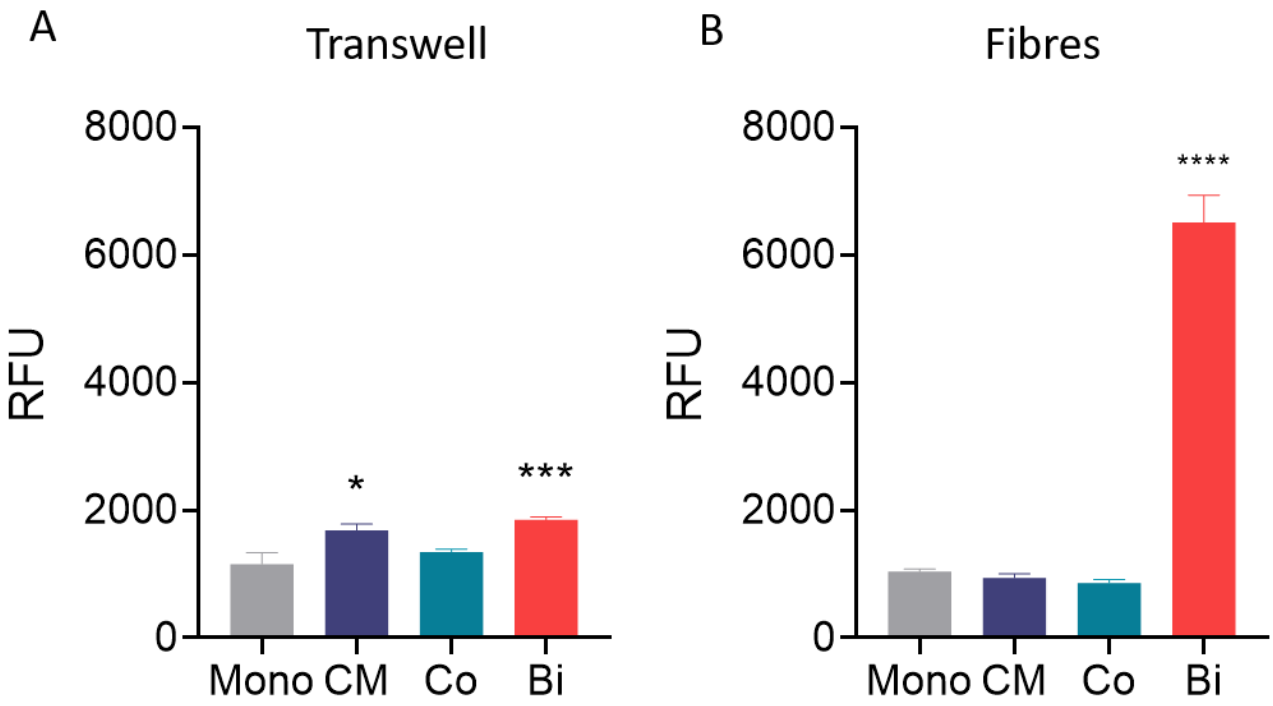

Figure 5.11 CYP3A4 Metabolic Enzyme Activity

CYP3A4 enzyme activity of (**A**) Transwell and (**B**) PLLA fibre Caco-2 models on day 21, measured as the relative fluorescence of product metabolite CHC, Mean ±SEM, n≥3. Significance calculated compared to monolayer values from one-way ANOVA with Dunnett's multiple comparisons.

5.3.5 Proximal and Distal effects of Subepithelial Fibroblasts on Carrier-Mediated Transport

Where passive transport, both paracellularly and transcellularly are more dependent on the physical characteristics of the compounds themselves, the absorption of compounds transported via carrier-mediated transport is heavily influenced by the abundance of that particular transporter. As such, the final aspect of this chapter was to examine the influence of cell culture surface and fibroblast incorporation on the transport of carrier mediated compounds in epithelial models.

PEPT1 is an apically located peptide-based influx transporter that is generally considered overexpressed in the standard Caco-2 monolayer model compared to human *in vivo* [87,269], however it has also been shown to be easily influenced by cell culture conditions [219]. Therefore, the transport of the fluorescently tagged, PEPT1 transporter substrate, D-Ala-Leu-Lys-7-amido-4-methylcoumarin (AMCA), was examined in all models of the intestinal epithelium. In **Figure 5.12A and B** both Transwell and PLLA fibre models show a similar trend in intracellular AMCA accumulation, with the highest fluorescence observed in both monolayer cultures (8986 $\pm$574 and 10302 $\pm$586 RFU for Transwell and fibres, respectively). On both insert types, the mean fluorescence of accumulated AMCA is significantly ($P<0.0001$) lower in all fibroblast based models, compared to monolayers. For Transwell models, the relative fluorescence increased with increasing proximity of fibroblasts with CM, Co and Bi models displaying means of 1164 $\pm$49, 2074 $\pm$27 and 4161 $\pm$115 RFU accordingly. This was similar to PLLA fibres, yet there was no considerable increased between CM and Co models (1169 $\pm$119 and 1062 $\pm$38 RFU), but a big difference between these and the bilayer model (7271 $\pm$99 RFU).

Together, this data suggests that the addition of fibroblasts to cell culture, whether as conditioned media, co-culture or as a bilayer, decreases the epithelial transport of PEPT1 substrate AMCA in both Transwell and fibre based models. Interestingly this is seen most markedly in conditioned media models in all cases.

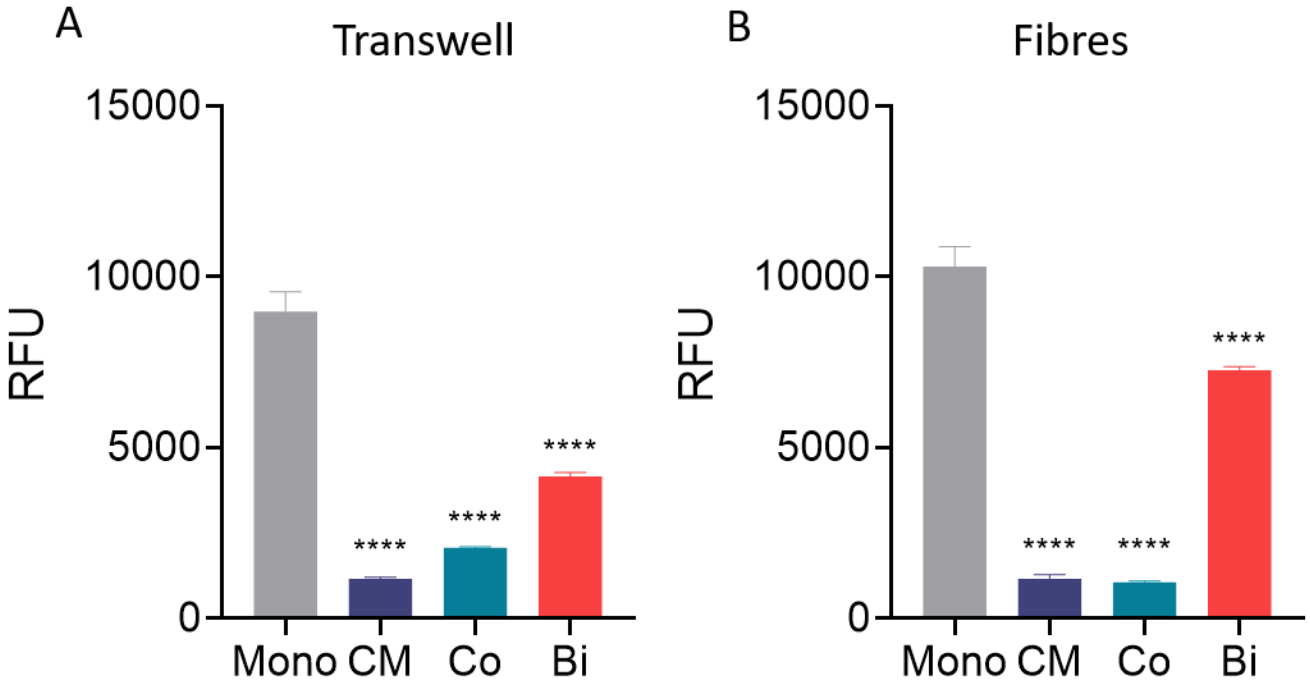

Figure 5.12 PEPT1 Influx Transporter Activity

Relative fluorescence of AMCA, a substrate of PEPT1 for Transwell (**A**) and PLLA fibre (**B**) Caco-2 models on day 21, Mean ± SEM, n≥3. Significance calculated compared to monolayer values from one-way ANOVA with Dunnett's multiple comparisons.

The final transport evaluation in this chapter examined the relative efflux activity of the ABCB1 efflux transporter. A known modulator of a plethora of therapeutic compounds due to its broad substrate specificity, the ABCB1 transporter minimises the plasma concentration by shunting absorbed compounds back to the intestinal lumen for excretion. ABCB1 has been shown to be considerably over expressed in the standard Caco-2 Transwell monolayer model, leading to severe underestimates of the absorbed fraction of compounds compared to *in vivo*. By using the ABCB1 inhibitor verapamil, the efflux activity could be calculated for each model by comparing the intracellular concentration of fluorescent substrate Calcein AM between normal and inhibited cells.

In Transwell models, **Figure 5.13A** shows the relative efflux activity of ABCB1 decreased with increasing proximity of fibroblasts, with the CM model showing similar percentage efflux to the monolayer model (62.3 ±5.9 and 53.9 ±3.8%), yet Co and Bi models both demonstrating significantly (P=0.0057 and 0.0030) lower efflux (20.1 ±4.8 and 15.9 5.9%, respectively). A similar trend was observed with the PLLA fibre models (**Figure 5.13B**), however these results were more variable and so no significance was calculated between the monolayer, bilayer or co-culture models. Yet, of all the PLLA models, the bilayer demonstrated the least efflux activity (15.7 ±2.9%). This data demonstrates that there is lower ABCB1 efflux activity in fibroblast based models, particularly bilayers, showing a potential improvement to the ABCB1 overexpression reported for the standard Caco-2 Transwell model.

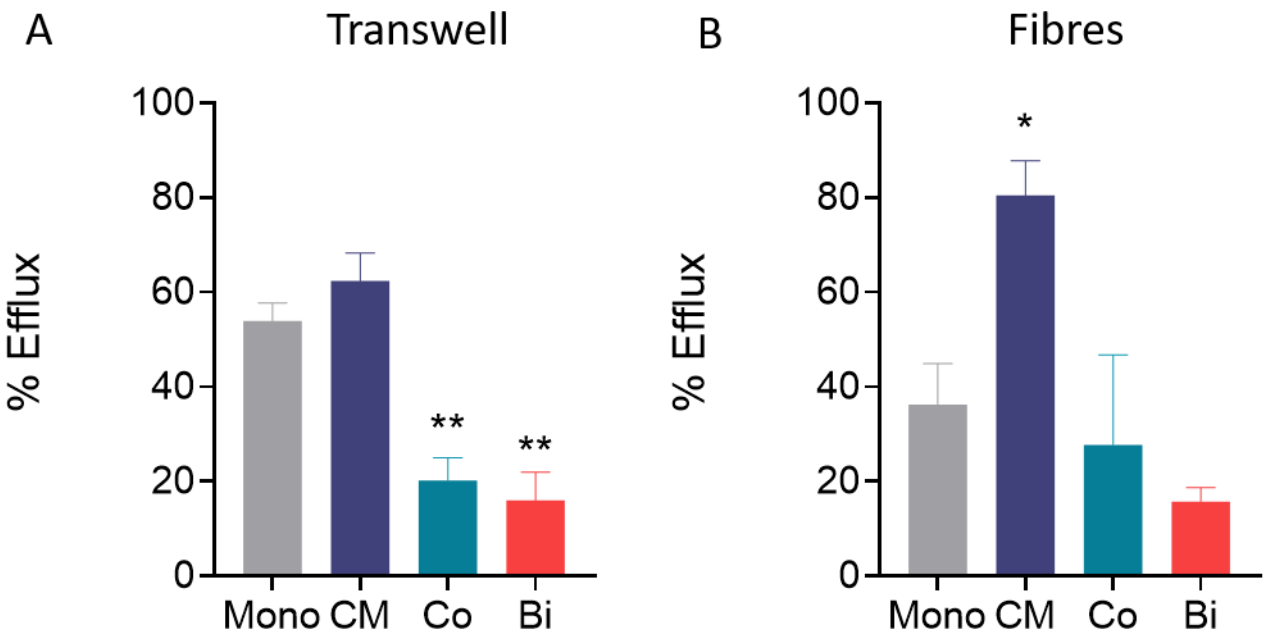

Figure 5.13 Efflux Activity of ABCB1 Transporter

Calcein AM efflux as a percentage of Verapamil inhibited control in Transwell (**A**) and PLLA fibre (**B**) Caco-2 models on day 21, Mean ± SEM, n≥3. Significance calculated compared to monolayer values from one-way ANOVA with Dunnett's multiple comparisons.

5.4 Discussion

The significance of the subepithelial mesenchyme in the function and modulation of intestinal absorption and detoxification is not yet fully understood. As the largest physical and biochemical interface with the intestinal epithelium, it has been the subject of exploration in a number of *in vitro* recreations, ranging from highly complex 3D tissue models [135,136], to simpler co-cultures [125,128,130]. For some, the focus has been on the combination of epithelial cells with ECM proteins [126,223,240], others have introduced stromal fibroblast cells [128,129,264], and many include both [130,267,270]. Earlier chapters of this thesis have concluded that the topographical ECM-like surface of PLLA fibres can considerably improve the relevance of intestinal epithelial barrier properties. Therefore, this chapter focussed on assessing the impact of incorporating additional mesenchymal elements to the novel PLLA fibrous membrane insert.

5.4.1 Barrier Function of PLLA Fibre-Based Epithelial Models Are Improved with the Incorporation of Human Subepithelial Fibroblasts

Initially, a handful of models were created that included additional elements, namely ECM coatings and stromal fibroblast cells, which have previously been utilised in establishing a mesenchymal microenvironment in intestinal models. The rationale behind this first analysis was two-fold; firstly, to not neglect the significant body of literature already published in the area, which could aid in establishing an enhanced intestinal model. But secondly, to be able to carefully dissect the contribution of each element to its functional outcome – an analysis that is widely overlooked in all similar published works. In this work, ECM protein was incorporated through the use of Collagen I coatings on PLLA fibre inserts, similar to the work of Patient et al. [203]. The creation of a bilayer model with non-intestinal, mouse 3T3 fibroblasts followed on from previous work by both Zhang et al. [127] and Li et al. [267], whose use of 3T3 fibroblasts in intestinal models showed a considerable decrease on intestinal permeability. The final model was a bilayer with human intestinal subepithelial CCD18co fibroblasts, as used in a number of other co-culture studies [128,130]. Both Caco-2/3T3 and Caco-2/CCD18co bilayers were included in this comparative analysis, to evaluate not only whether more physiologically relevant epithelium function was

achieved from general fibroblasts incorporation, but also whether the effect differed for fibroblasts from different species, and tissue types. This parallels the work recently published, that compared the impact of skin and intestinal fibroblasts on intestinal behaviour[128].

Comparing the TEER values in these models, highlighted that the use of PLLA fibres as a cell culture surface was sufficient to reduce TEER well below the standard Transwell Caco-2 model, as this was achieved in all models, regardless of additional mesenchymal elements. However, data from the study of Lucifer Yellow (LY) paracellular permeability indicated that this ubiquitous decrease in TEER value did not directly correlate with increased permeability. Instead, it was shown that the incorporation of CCD18co human subepithelial intestinal fibroblasts had the most significant impact on improving paracellular permeability. Moreover, that this paracellular permeability was extraordinarily close to reported *in vivo* human values [243].

Unlike previous work, which reported that non-intestinal skin fibroblasts increased LY permeability (although not to the same extent as CCD18co cells) [128], non-intestinal mouse 3T3 fibroblasts did not demonstrate any further increase in permeability to the PLLA monolayer. Together, this suggests that species-specific (human) fibroblasts cells are more valuable in intestinal bilayer models, with ultimate physiological permeability modelling arising from species- and tissue-specific (intestinal) cell types. Furthermore, despite the previous publication [203] that collagen coated fibrous PET membranes to demonstrate improved LY P_{app} to the Transwell PET insert monolayer, the data presented here suggests that Collagen I coating has no significant improvement to uncoated fibre monolayers, and is an unnecessary addition to this intestinal model.

5.4.2 Fibroblasts Induce Epithelial Elongation and In Vivo-Like Morphology In PLLA Fibre-Based Bilayers

Further analysis was carried out in Caco-2/CCD18co bilayers created on both the standard Transwell surface and the PLLA fibrous membrane surface using confocal microscopy, to observe cytoskeletal, tight junction and ECM proteins.

Expression of ECM components of intestinal bilayer models is not commonly explored in the literature, despite *in vivo* evidence of the interplay between epithelial and mesenchymal cells in the production of the basement membrane[271,272]. Staining for ECM proteins demonstrated a clear planar layer of fibronectin and collagen IV deposited between epithelial and stromal cells in the Transwell bilayer. This was recreated to an extent in the PLLA fibre bilayer, however, this was less obvious, as these proteins were deposited in a way in which coated the fibres of the topographic membrane. Overall, the deposition of both fibronectin and collagen IV showed broader distribution in PLLA bilayers, indicating an increase in 3D nature of the ECM. Further quantification of ECM elements using RT-qPCR, would help to distinguish any differences between monolayer and bilayers, at the gene expression level.

Bilayer models did not show any differences in the relative quantity or localisation of TJ protein ZO-1 when grown on either Transwell or fibre surfaces, and displayed results very similar to that of monolayers examined in Chapter 4. Consequently, it could be concluded that ZO-1 is unaffected by changes in culture surface and the incorporation of fibroblasts, or that any changes are not quantifiable using imaging techniques. This does not however necessarily mean that there are no changes in TJ formation, as ZO-1 is just one protein in this junctional complex.

The imaging presented, predominantly highlights the elongated, undulant, and *in vivo*-like nature of the epithelium produced in a PLLA fibre bilayer. Although the inclusion of fibroblasts induced the elongation of cells in both Transwell and PLLA bilayers compared to monolayer equivalents, the Transwell bilayer did not show as much 3D tissue architecture or morphology, remaining relatively flat and planar. Together with data from monolayer morphology in Chapter 4, this data indicates that the morphology of intestinal epithelial cells can be improved by both topographic PLLA culture surface, and subepithelial fibroblasts, combining to give the most *in vivo*-like morphology in PLLA fibre bilayers. This is in agreement with previous work that has highlighted cell elongation and increased epithelial thickness in bilayers incorporating fibroblasts [128,129].

5.4.3 Epithelial TEER Is Improved By Paracrine Fibroblast Factors, but Is Most Relevant On PLLA Fibres

The overwhelming evidence, from both previously published work [129,130], and the early work in this chapter demonstrates a clear role for intestinal fibroblasts in the modulation of intestinal epithelial barrier function. Numerous studies in Caco-2/CCD18co co-cultures [265,266,273], as well as Caco-2 monolayers cultured with fibroblast secreted growth factors [263] have also highlighted the influential role of intestinal fibroblast-secreted chemokines such as Keratinocyte Growth Factor (KGF) and Hepatocyte Growth Factor (HGF). As small, molecular, signalling molecules, originating from the mesenchyme of tissues, growth factors secreted into the surrounding culture medium, have been shown to enhance and promote epithelial proliferation and differentiation [263–266]. Moreover, the extracellular matrix is a bioactive physical scaffold, with the ability to modulate tissue activity through mechanical and chemical cues, is itself constantly remodelled and regulated by fibroblast cell activity [115,262]. As such, the second half of this chapter was therefore focussed on identifying the impact of these fibroblasts on a wide variety of epithelial cell functions, with particular interest to those closely associated with key pharmacokinetic defining parameters. Further to this, this study also explored to what extent these outcomes were a result of direct physical contact with fibroblasts, or whether a product of paracrine signalling factors secreted from fibroblasts.

Thus, eight intestinal models, on both standard Transwell inserts and PLLA fibrous inserts, ranging in their proximity to CCD18co human fibroblasts, were compared to monolayers with no mesenchymal components. In order of increasing fibroblasts proximity, these included; Caco-2 monolayers incubated with fibroblast conditioned media, Co-cultures of both cell lineages, seeded in separate chambers of the culture inserts, and bilayers of Caco-2 cells cultured directly on top of fibroblasts. Conditioned media models, incorporated fibroblast factors only in the culture medium and allowed no real-time signalling between the mesenchyme and epithelial cells, similar to recent work, using this method in the context of epithelial function, published by Darling et al. [128]. Co-cultures shared the same chemical space and allowed for real-time paracrine

interactions in both directions; akin to previous studies of fibroblast paracrine growth factors [266,273], and also that of similar airway epithelia-mesenchymal models [274]. Bilayers, the most proximal models, were not dissimilar to other direct intestinal bilayer models [129,130] and similar to those that encapsulated fibroblasts directly adjacently to Caco-2 cells within an artificial matrix [128,130].

As the most comprehensively cited shortcoming of the Caco-2 Transwell model, and of considerable importance in pharmacokinetic studies, the tightness of the epithelial barrier and its implications for paracellularly absorbed compounds was the first epithelial function investigated. The TEER values recorded in this study demonstrated that the inclusion of fibroblasts, whether proximally or distally, were sufficient to reduce the excessively high TEER values consistently reported for the Transwell Caco-2 monolayer. Previous work supported these findings by elegantly demonstrating how TEER values in a Transwell monolayer culture could be modulated from high to low by simply switching conditioned media for standard media, and vice versa [273]. Together, this strongly implies a role of fibroblast secreted factors in reducing TEER values. Interestingly, for PLLA fibre models, which already exhibited significantly reduced TEER values in monolayers by means of their surface alone, showed no further reduction in TEER as a result of fibroblasts inclusion. This data clearly highlights a hierarchy of influence in which the PLLA fibrous membrane surface exhibited a greater effect on TEER value reduction than fibroblasts.

5.4.4 Paracellular Permeability Is Most Relevant In PLLA Fibre Bilayers

TEER measurements are a determinant of ionic flux across an epithelium, thought to be closely related to tight junction (TJ) complexes and the paracellular pathway; as TJ complexes form, TEER increases, and paracellular transport decreases. However, TEER values cannot reflect true paracellular permeability, as it does not encompass the charge and size selectivity that regulate the paracellular route [275]. Indeed, our results demonstrate that for both Lucifer Yellow (LY) and FITC-dextran (FD) tracer compounds, Caco-2/CCD18co Transwell models that had demonstrated lower TEER values, did not correlate with any increase in P_{app} value; a phenomenon previously noted in various other co-culture models [128,130,273]. However, PLLA fibre based models showed

increased permeability for all test compounds compared to all Transwell based models. This further highlights how PLLA surface topography has a greater influence on barrier function. These results also support the findings of the only other fibrous scaffold model published, in which a fibrous membrane monolayer increased both FD4 and LY permeability [203] compared to the standard Transwell. Moreover, a dramatic increase LY permeability was observed in PLLA bilayers that was within range of the value recorded for human tissues [243], as well as being the most permeable model to the 4 kDa FD compound. Other work with both scaffold-based bilayers [128], and bioprinted bilayers [129] have both associated adjacently cultured fibroblasts with enhanced LY P_{app}, but did not evaluate FITC dextran transport. The work presented in this chapter has combined two methodologies of improving paracellular permeability; (1) using a topographical fibrous membrane insert, and (2) culturing bilayers with adjacent fibroblast, to create a considerably more physiologically relevant model than either individually.

From the confocal imaging presented earlier in this chapter, it was clear that there was no observable differences in the localisation, or expression levels of TJ protein ZO-1 between Transwell and Fibre bilayers that would explain the significant increase in LY P_{app} seen in PLLA bilayers. Additionally, this was unlikely a result of a change in the size selectivity of the TJs, as in all models, the permeability of the largest compound FD70 (reported to be the upper size limit of hydrophilic TJ transport [276]), was relatively unaltered, showing considerably lower permeabilities than the smaller FD4 compound.

Claudin 2 is a TJ protein highly implicated in "leaky" gut syndromes, proposed to form TJ channels that are selectively permeable to small cations and water [277]. The paracrine signalling of fibroblast-secreted KGF has been proposed to reduce TEER values by increasing the expression of the tight junction protein Claudin 2 [273]. Interestingly, an increase in Claudin 2 was also associated with lower TEER values and increased permeabilities in Caco-2 cells cultured without any fibroblasts, but instead on an engineered ECM coating [126]. In this case, the reduced stiffness of the ECM coating was considered the major driver of increased Claudin 2 expression. As Claudin 2 is upregulated by both fibroblast paracrine factors, and ECM-like surfaces, it is therefore highly likely that the results presented in this chapter, namely decreased

TEER and increased paracellular permeability in PLLA bilayers, may be a result of Claudin 2 upregulation. Additionally, as a small ion channel former, increased Claudin 2 expression would explain the dramatic increase in LY but not FD4 permeability in PLLA bilayers, as LY is a 10-fold smaller ionic molecule compared to FD4. Claudin 2 expression was not explored in the scope of this research, but future work examining both gene and protein expression, through RT-qPCR and immunostaining techniques used already in this thesis, would be highly beneficial to explore whether this is a key mechanism regulating paracellular permeability.

5.4.5 CYP3A4 Activity Is Improved In PLLA Fibre Bilayers

CYP3A4 is a Phase I drug metabolising enzyme known to show very little expression, and therefore activity in Caco-2 cells [92,129,217], with most metabolism experiments, being carried out in genetically modified cells expressing the enzyme [278]. Results in this chapter show that a significant increase in the CYP3A4 activity of Caco-2 enterocytes was achieved when cultured as a model incorporating both topographic and cellular aspects of the mesenchyme (i.e. as a PLLA fibre bilayer). This agrees with previous bioprinted bilayers, which also revealed higher CYP3A4 activity compared to monolayers [129]. Interestingly, work investigating CYP3A4 activity in a gel scaffold-based model, designed to mimic the stiffness of the intestine, demonstrated higher CYP3A4 activity than stiffer conventional Transwells. Moreover, this activity could be reconstituted in Transwell models with inhibition of the yes-associated protein (YAP), a key node in mechano-transduction signalling. This highly implicates the control of CYP3A4 activity to be influenced by mechano-transduction signalling pathways that respond to mechanical cues, such as stiffness of the ECM. It is therefore possible, that the combination of fibroblasts and PLLA fibres led to a Caco-2 culture surface with a more *in vivo*-like stiffness, which improved CYP3A4 activity in PLLA fibre bilayers.

5.4.6 Fibroblasts Improve Relevance of Apical Protein Activity

Unlike morphology, TEER, paracellular permeability and CYP3A4 activity, which demonstrated that the topography of the PLLA fibre surface had the most impact on physiological relevance, other pharmacokinetic parameters evaluated were shown to

be more greatly influenced by the inclusion of fibroblasts. Published observations that alkaline phosphatase activity (ALP) is unaltered in Caco-2 cells when cultured on various ECM-mimicking scaffolds and ECM coatings [152,223,240], was also displayed in our results, in which models on both Transwell and PLLA fibre culture surfaces showed similar trends. Again, bilayer models showed the highest enzymatic turnover, but these were highly similar for both Transwell and fibres, indicating that proximity of fibroblast interactions was of more importance for ALP activity.

This trend was also observed in both carrier-mediated influx and efflux transporter activity. As an influx transporter regulating peptide-based molecules, PEPT1 is widely reported to be over expressed in Caco-2 cells [87,269]. However, PEPT1 expression has been reported to be highly variable, and easily influenced by cell culture conditions and cell line origin [219]. Moreover, minimal research has been published on the effects of mesenchymal elements on its expression and function [279]. Our work appears to show similar trends in the influx of PEPT1 substrate AMCA between Transwell and PLLA fibre models, showing that the inclusion of fibroblasts decreases PEPT1 activity. Interestingly this is seen most markedly in the most distal fibroblast model of conditioned media. These findings demonstrate that the incorporation of fibroblasts help to rectify the heightened PEPT1 activity of standard Caco-2 monolayer, however without a direct human tissue comparison, it is impossible to determine which model is the most physiologically relevant. Further investigation either by gene or protein expression quantification could shed light on the most relevant model regarding this. It is also difficult to hypothesise the reason behind the conditioned media model demonstrating the least activity without further investigation of specific paracrine molecules. However, the results presented here indicate that PEPT1 function is likely modulated by bidirectional signalling between both epithelial and stromal cells.

Caco-2 monolayers typically cultured on Transwell inserts inherently overexpress ABCB1 protein compared to human tissue [87,217]. Although ABCB1 activity can be highly sensitive to culture conditions [280], the results presented in this chapter corroborate the results seen in other fibroblast co-cultures [131,270], that Caco-2/CCD18co bilayers showed the lowest efflux activity. As with PEPT1, the inclusion of fibroblasts helped to resolve the amplified ABCB1 efflux activity typically reported for standard Transwell

Caco-2 models. Conversely, this reduction in activity was most pronounced in bilayer and co culture models, as opposed to conditioned media. Again, the physiological significance and accuracy of each model to native intestinal activity would require further examination of the ABCB1 transporter at both gene and protein levels.

As parameters that all showed a greater degree of variation between fibroblast models than culture surface models, ALP, PEPT1 and ABCB1 also share a common feature of being located at the apical membrane, or within the brush border (BB) of enterocytes. Demonstrating similar trends between Transwell and PLLA fibre culture models, these apical epithelial cell functions appeared less influenced by surface properties, such as stiffness and topography, than the paracellular permeability and intracellular CYP3A4 enzyme functions. Literature dissecting the roles of fibroblast signalling on epithelium function most frequently discuss its influence on enterocyte differentiation [264,265]. Moreover, the differentiation of Caco-2 cells to a more enterocytic phenotype is commonly characterised by columnar polarisation of cell morphology and the appearance and function of an apical BB. It is therefore probable, that as apical BB membrane proteins, changes in ALP, ABCB1 and PEPT1 activity are intrinsically linked to the enterocytic differentiation of Caco-2 cells, which is enhanced in culture with underlying, mesenchymal fibroblast cells.

5.5 Conclusions

In conclusion, the work presented in this chapter has dissected the role underlying mesenchymal elements of the intestinal epithelium, by incorporating both ECM-like topography in PLLA fibre inserts, as well as subepithelial human intestinal fibroblasts, in search of creating a more physiologically relevant model for pharmacokinetic studies. It has shown the importance of species and tissue relevant fibroblasts in key barrier functions, as well as their impacts on cellular architecture and morphology. It can be summarised that inter- and intracellular intestinal features more strongly influenced by PLLA fibre surface topography, such as paracellular permeability and CYP3A4 metabolising enzymes. On the other hand, features that are found on the apical membrane, such as brush border enzymes and protein transporters appear to

be more influenced by fibroblast incorporation and proximity. Together, the most successful model was the PLLA fibre Caco-2/CCD18co bilayer in which both ECM-like structure and tissue cellular diversity has enabled the recapitulation of significant *in vivo*-like properties into the intestinal epithelial model, whilst retaining its simple design and transport amenability.

6. General Discussion and Future Work

Despite progress in understanding the complexities of pathogenic mechanisms, and advancement in chemical engineering and manufacturing technologies, one of the biggest problems facing the pharmaceutical industry remains the extortionate attrition rate of lead therapeutic compounds. The failure of clinical candidates to succeed to Phase II trials, let alone the regulatory approval stage is overwhelming. This creates not only a huge financial burden for pharmaceutical research and development, but a shortfall in the availability of efficacious therapeutics for patients in the healthcare system. Primarily, high attrition rates are associated with discrepancies between the *in vitro* and *in vivo* success of candidates, which can largely be associated with poor pharmacokinetic parameters such as bioavailability [3]. As the foremost barrier tissue in determining oral bioavailability, the intestine is a fundamental organ in determining the *in vivo* fate of new molecular entities. It is therefore of crucial importance to have reliable tools with which to probe the interactions of chemical compounds in the intestine *in vitro*, which correlate accurately to *in vivo* activity.

Although advances in tissue engineering techniques have led to the innovative design of complex, 3D models, including multicellular tissues, synthetic and natural scaffolds, and organoids, these are unsuitable for monitoring transport and adsorption across the epithelium due to the physical barriers of the tissue complexities themselves. Consequently, the industry standard still remains the 2D Transwell model; a monolayer of Caco-2 epithelial cells cultured on a flat, plastic, semi-permeable membrane. Primarily, the 2D Transwell has remained the gold standard due to simlicity, ease of use and high transport amenability, however, it is a very reductionist model and does not account for intestinal tissue complexity. Moreover, this lack of complexities gives rise to uncharacteristic permeability and transport characteristics, unrepresentative of the native intestine [213,281]. It is well established, that the underlying intestinal mesenchyme, comprised of extracellular matrix proteins and stromal fibroblasts, forms a microenvironment that can modulate epithelial growth, differentiation and function

[263,265,266] through both physical and biochemical cues [120,282]. This thesis therefore set out to develop a novel intestinal model, grounded in the simplicity and assayable versatility of the standard Transwell model, yet incorporate key elements of the underlying mesenchyme, to subsequently produce a better predictive model of *in vivo* intestinal bioavailability.

The approach of this thesis was to utilise electrospun poly (l-lactic acid) (PLLA) fibrous membranes as a simple, low cost, biocompatible material, which possess a novel structure able to replicate the fibrous architecture of the extracellular matrix. In particular, the ability of these fibres to mimic the specialised, fibrous, reticular network basement membrane which underlies the intestinal epithelia. Characterisation of this fibrous material in Chapter 3 revealed a mesh of fibres with pore diameters comparable to human intestinal basement membranes [282]. Although the fibre dimensions were slightly larger than the fibrils in the reticular network of the BM, and were larger in diameter than other previous work using nanofibres [203], their unusual porous fibre texture displayed novel nanotopography in addition to their bulk surface microtopography, that was advantageous to cell attachment. Despite the fabrication of these fibres being outside of the scope of this thesis, further work optimising the physical dimensions of these fibres could not only improve upon their intestinal membrane likeness, but could be specifically tuned for other tissues and cell environments. The primary aim of Chapter 3 was to validate these PLLA fibres as a suitable cell culture surface based on their physical characteristics. To this end, the nano-porous fibres were shown to be highly biocompatible and conducive of cell growth and proliferation, despite their hydrophobic surface properties. Moreover, this was confirmed using numerous techniques, including immunofluorescence imaging, metabolic viability assays and protein quantification, solidifying the utility of these fibres in cell culture. Given that further investigation in this thesis identified that epithelial behaviour may be related to culture surface stiffness and mechano-transduction signalling, further characterisation of the mechanical properties of the PLLA fibres using tensile stress-strain curves [157] or Atomic Force Microscopy (AFM) nanoindentation [283], would be useful identifying the most ideal physiological mechanical properties.

Following on from these findings, PLLA fibrous membranes were used in Chapter 4 to fabricate novel cell culture inserts, which were able to cultivate a contiguous monolayer of Caco-2 epithelial cells. Unlike other previous electrospun fibres used in other tissue engineering applications [157,200,203], cell attachment and monolayer formation was successful without the need for artificial ECM coatings. This minimised any preventable physical barriers to the observation of compound transport, as reported in other intestinal basement membrane models [241], and allowed the visualisation of the epithelial-produced ECM components. These fibres were able to support a Caco-2 monolayer displaying equivalent markers of differentiation such as alkaline phosphatase activity, and gene expression of VIL1, ALP and ANPEP, as well as displaying gene expression of proteins of the intestinal basement membrane including COL4, LAMA3, LAMA5 and HSPG2 and the protein expression of fibronectin and collagen type IV. Most significantly, PLLA fibre monolayers overcame TEER and permeability limitations most common to the Transwell monolayer model; significantly reducing TEER values by day 21 and considerably increasing the paracellular permeability of Lucifer Yellow. These results echo the results of other Caco-2 monolayers grown on alternative substrates [126,134,224], and mirror those of the only other known fibre-grown model to date [203], displaying the plasticity of Caco-2 barrier properties as a consequence of the cell culture surface topography.

One potential cause for a change in barrier function was attributed to the morphological changes, such as cell polarisation and elongation, induced by Caco-2 growth on a topographical culture surface. Although this work did not identify any significant gene expression changes in three key tight junction proteins (TJPs) (TJP1, CLDN, OCLN), nor stark differences in ZO-1 immunofluorescence staining, there exists over forty TJPs in total [284], particularly Claudins that were not covered in this work. In addition, this thesis concentrated on gene expression data and fluorescent imaging techniques to observe such changes. Although succeeding in providing a broad oversight into molecular differences, it would be beneficial to add supporting protein expression data acquired from techniques such as western blotting or mass spectrometry; a global unbiased analysis of protein expression, which could provide a wealth of data to highlight differences in expression between the two models, not only for TJPs but also ECM components and transporters. It would also be of interest to this

study to examine whether the culture surface changes in permeability are controlled by alterations in tight junctions (TJs), by using known modulators of TJP complexes, such as tumour necrosis factor alpha (TNFα) (opens TJs) [285] and myosin light chain kinase (MLCK) inhibitors (closes TJs) [286,287]. It would be hypothesised, that a greater reduction in permeability would be seen on inhibition of TJs in monolayers grown on PLLA fibres compared to Transwells, if their enhanced permeability is related to more or larger TJs. This analysis would also demonstrate to what extent alterations in TJs contribute towards the differences in permeability observed, and could be used in combination with a number of paracellular permeable compounds with differing physicochemical properties, such as molecular weight or charge, to gain broader insight.

The final chapter in this thesis evaluated additional elements of tissue complexity in the established PLLA fibre model and their contribution to overall intestinal epithelial function. Initial trials of mesenchymal elements, including Collagen I ECM coatings and mouse and human fibroblast cell lineages, highlighted the need for tissue-specific and species-relevant cell types for significant differences in epithelial barrier behaviour. Only CCD18co human subepithelial fibroblast demonstrated any improvement from the PLLA monolayer model, in terms of TEER and paracellular permeability. As such, bilayers of human intestinal epithelial cells and stromal fibroblasts were constructed on both Transwell surfaces and PLLA fibres. Imaging data showed that bilayers showed considerable morphological differences, with cell elongation and an undulating epithelia, akin to native intestine. Taken together with data from monolayers in Chapter 4, this demonstrated a role for both underlying structure and subepithelial fibroblasts on the morphology of epithelium. A limitation throughout this thesis, was the reliance on fluorescence imaging methods for quantifying changes in protein adsorption or expression. Although in our findings there were some clear and obvious differences between samples (such as protein adsorption in Chapter 3 and protein localisation in Chapters 4 and 5) there are some caveats in the sample preparation and analysis process, making it difficult to highlight more nuanced differences between similar samples or standardise and compare to externally generated data. As such, combinations of quantitative techniques such as gene expression quantification and

specific protein expression analysis such a western blotting, would allow more robust and reliable conclusions to be drawn in these areas.

Additionally, the role of fibroblasts and culture surfaces were evaluated for their independent contribution to the functional behaviour of the intestinal epithelia. All models, including monolayer, bilayers and two co-culture models with varying fibroblasts proximity were assessed for a full complement of activity, including permeability, enzyme activity, and carrier mediated transport. Overall, the PLLA fibre bilayer showed the most physiologically relevant activity in the majority of parameters, and was selected as the most improved model for intestinal pharmacokinetic modelling. However, these findings also revealed a hierarchy of influence modulating individual functions. For example, TEER values were clearly regulated by fibroblast paracrine signalling, as significant decreases were observed in Transwell Conditioned media models compared to monolayers, however, this was surpassed by even lower TEER values recorded from all models on PLLA fibre membranes. Furthermore, PLLA fibre models were also shown to improve paracellular permeability compared to Transwell equivalents, however again, this was surpassed by the bilayer model which included both PLLA fibre surface and fibroblasts. Interestingly, neither fibroblast incorporation nor PLLA fibre surfaces alone, were sufficient to induce any improvement in CYP3A4 activity independently, yet when combined in PLLA bilayer models, showed dramatically improved activity. Conversely, enzyme and protein function associated with the apical membrane, specifically ALP activity, PEPT1 influx and ABCB1 efflux transport, demonstrated the most physiologically relevant activity (increased ALP activity and decreased PEPT1 and ABCB1 transport) in the presence of fibroblasts irrespective of cell culture surface.

Although confident in the implications of our data, the small number of replicates, cell and fibre batch variability and the multistep sample preparation required for the functional assays used in these experiments are all aspects that may give rise to experimental variations. Assays analysing changes in epithelial functional were favoured over gene and protein expression analyses, as they are a much stronger representation of functional output. However, future work incorporating these into a multi-method approach to each aspect of intestinal function would improve the

robustness and reliability of these conclusions. To solidify these findings, further transporter and activity assays could be used to assess functional behaviour across models using alternative substrates such as mannitol (paracellular permeability), Luciferin IPA (CYP3A4), Rhodamine 123 (ABCB1) or Captopril (PEPT1). In addition, activity could be more robustly analysed with the used of specific inhibitors of transporters and enzymes, such as valacyclovir (PEPT1) or ketoconazole (CYP3A4) to compare the relative activity in each intestinal model, as done in the ABCB1 assay carried out in this thesis.

Emerging evidence from a handful of divergent studies, points to a combination of cell-ECM and cell-cell signalling in the modulation of Caco-2 behaviour. ECM-like surfaces[149,288] and fibroblast co-cultures [128,129] have both demonstrated changes in Caco-2 morphology, promoting enhanced polarisation and elongation, as seen in this study. For fibroblast incorporated models, both morphological and functional differences identified in this study support the prominent idea that increased epithelial cell differentiation is induced by fibroblast cell signalling, including keratinocyte growth factor (KGF)[265,273], hepatocyte growth factor (HGF) [266] and transforming growth factor beta (TGFβ) [289]. Moreover, this work demonstrates that cell-cell signalling between stromal and epithelial cells, does not always have to be via direct contact, but can alter TEER values through conditioned media alone, correlating with the evidence that these factors have paracrine effects on the epithelium [128,263]. Elucidation of the exact mechanisms of growth factor signalling could be as simple as incubating with a number of these isolated factors independently and observing epithelial function, or alternatively could involve large scale genomic and proteomic approaches. However, even without understanding the underlying mechanism, it is evident that the inclusion of fibroblasts into tissue models increases *in vivo* relevance. The mechanisms behind the topographical influence of PLLA fibres on functional behaviour also remain unknown. This study has shown that the most significant improvements derived from PLLA fibre culture surface are related to paracellular mechanisms and metabolic enzymes. Although not analysed in this work, there is a strong indication in the literature for the role of mechano-transduction signalling based on substrate stiffness, as both paracellular permeability and CYP3A4 activity have be independently linked to ECM-like substrate mechanical properties[126,224], and the work of this thesis further

confirming increased functional activity on ECM-like fibres. Although no explicit mechanisms were examined in this work, it has shown a clear relationship between tissue culture surface properties, multicellular tissue composition and intestinal epithelial cell function. As hypothesised, the most anatomical and physiologically relevant intestinal model incorporated both PLLA topographical fibres, and subepithelial human intestinal fibroblasts.

This thesis has shown intestinal epithelial function more reminiscent of native tissue in a PLLA bilayer model of Caco-2 cells and CCD18co fibroblasts. Despite assessing key elements of permeability, metabolic enzyme activity and carrier-mediated transport, this was not a comprehensive analysis of the plethora detoxification enzymes and transporters throughout the intestine. Further, broader study of the transport and detoxification capacity of this model would assist in confirming its superiority as a pharmacokinetic tool. Crucially, further work using High Performance Liquid Chromatography (HPLC) to observe the permeabilities of panel known drug compounds would enable a quantifiable correlation of this model to *in vivo* bioavailability, as carried out in previous work [127,267]. In particular, drugs known to be poorly predicted in Caco-2 Transwell models, such as atenolol and terbutaline [213], would be ideal candidate compounds to demonstrate the extent to which PLLA bilayers improve upon the current gold standard model. In addition, the assessment of the activity of other transporters, known to be considerably over expressed in Transwell Caco-2 monolayers, such as GLUT1, OATP2B1 and OATP4A1 [217,231], or under expressed like ABCG2 [87], would further elucidate the benefits of this more physiologically complex model. A large focus of this thesis concentrated on overcoming limitations in the accuracy of paracellular permeability in the standard Transwell monolayer, and as such did not examine the impact on transcellular absorption routes. Assessment of the permeability of propanol, a compound known to be absorbed via the passive transcellular route [203] would further illuminate any differences the PLLA bilayer model has on this absorption mechanism. Further physiological complexity could also be introduced into the PLLA bilayer model established in this thesis, such as a triple-culture including mucus producing goblet cells, as achieved in previous work [130,258]. However, additional complexity may prove less desirable for a larger scale, versatile, *in vitro* tool, without demonstrating significant advantages over the bilayer.

With further refinement and broader study, the improved physiological relevance of the PLLA fibre bilayer model presents an opportunity to reduce the vast gap between *in vitro* and *in vivo* drug performance by providing a more accurate representation of intestinal transport and detoxification functions. Further reaching implications of this application could include a reduction in the number of clinical animals required, as well as significant cost and time savings. More importantly, it could prove a valuable tool for understanding the way in which different drug classes interact with the defensive barrier properties of the intestine, and lead to a more rational approach to drug design reducing the excessively high attrition rates that plague the industry. Furthermore, as an improved topographic culture surface, the PLLA fibre insert fabricated within this thesis could easily be adapted for other tissues, indeed, collaborators on this project have fabricated porous PLLA fibres for bone regeneration[157,290]. However this thesis highlights its possible use in the development of monolayer and bilayer models of other epithelial and endothelial tissues, including the Blood Brain Barrier (BBB), arterial endothelium, skin, or airway epithelial tissues. These are all soft tissue barriers that also contribute to the bioavailability and distribution of drugs *in vivo*, and share a lot of transporters with intestinal tissue [291,292], indicating PLLA fibres may similarly impact the functional behaviour of these models .

This thesis has explored the use of novel fibrous membranes of electrospun PLLA to create an improved *in vitro* intestinal tissue model that is of higher physiological relevance than the current Transwell *in vitro* model. It has incorporated the major elements of the intestinal mesenchyme; ECM topography and stromal fibroblast cells, as well as highlighting the individual role they play in modulating epithelial cell function. This has enabled the improvement of properties enhanced predominantly by cell surface culture as well as those enhanced by interaction with fibroblasts. Unlike the majority of other 3D models in this research area, this model does not contain an artificially curated composition of ECM proteins, which are usually poorly defined, animal derived, highly variable [128], or physically inhibitive of transporter function [293]. Additionally, it retains a simplicity and versatility, highly reminiscent of the current standard Transwell model format, making it scalable and amenable to well-established standardised pharmacokinetic protocols.

7. References

1. Lloyd, I. Pharma RD Annual Review 2020 Whitepaper | Pharma Intelligence. https://pharmaintelligence.informa.com/resources/product-content/pharma-rd-annual-review-2020-whitepaper (2020).
2. Wouters, O. J., McKee, M. & Luyten, J. Estimated Research and Development Investment Needed to Bring a New Medicine to Market, 2009-2018. *JAMA - Journal of the American Medical Association* vol. 323 844–853 (2020).
3. Seyhan, A. A. Lost in translation: the valley of death across preclinical and clinical divide – identification of problems and overcoming obstacles. *Transl. Med. Commun.* **4**, 1–19 (2019).
4. Lipinski, C. A. Drug-like properties and the causes of poor solubility and poor permeability. *J. Pharmacol. Toxicol. Methods* **44**, 235–249 (2000).
5. Novel Drug Approvals for 2019 | FDA. https://www.fda.gov/drugs/new-drugs-fda-cders-new-molecular-entities-and-new-therapeutic-biological-products/novel-drug-approvals-2019.
6. Betts, J. G., Johnson, E., Wise, J. A., Young, K. A. & al., et. Anatomy and Physiology (OpenStax). (2013).
7. Kiela, P. R. & Ghishan, F. K. Physiology of intestinal absorption and secretion. *Best Practice and Research: Clinical Gastroenterology* vol. 30 145–159 (2016).
8. Artursson, P., Neuhoff, S., Matsson, P. & Tavelin, S. Passive permeability and active transport models for the prediction of oral absorption. in *Comprehensive Medicinal Chemistry II* vol. 5 259–284 (Elsevier Ltd., 2006).
9. Xu, Y., Shrestha, N., Préat, V. & Beloqui, A. Overcoming the intestinal barrier: A look into targeting approaches for improved oral drug delivery systems. *Journal of Controlled Release* vol. 322 486–508 (2020).
10. Villi in the small intestine — Science Learning Hub. https://www.sciencelearn.org.nz/images/2259-villi-in-the-small-intestine.
11. Dahlgren, D. & Lennernäs, H. Intestinal permeability and drug absorption: predictive experimental, computational and in vivo approaches. *Pharmaceutics* vol. 11 (2019).
12. Lipinski, C. A., Lombardo, F., Dominy, B. W. & Feeney, P. J. Experimental and

computational approaches to estimate solubility and permeability in drug discovery and development settings. *Adv. Drug Deliv. Rev.* **46**, 3–26 (2001).

13. Grassl, S. M. Mechanisms of Carrier-Mediated Transport. in *Cell Physiology Source Book* 249–259 (Elsevier, 2001). doi:10.1016/b978-012656976-6/50108-6.
14. Sai, Y. & Tsuji, A. Transporter-mediated drug delivery: Recent progress and experimental approaches. *Drug Discovery Today* vol. 9 712–720 (2004).
15. Friedman, D. I. & Amidon, G. L. *Characterization of the intestinal transport parameters for small peptide drugs*. *Journal of Controlled Release* vol. 13 (1990).
16. Ganapathy, M. E., Huang, W., Wang, H., Ganapathy, V. & Leibach, F. H. Valacyclovir: A substrate for the intestinal and renal peptide transporters PEPT1 and PEPT2. *Biochem. Biophys. Res. Commun.* **246**, 470–475 (1998).
17. Sugano, K. *et al.* Coexistence of passive and carrier-mediated processes in drug transport. *Nature Reviews Drug Discovery* vol. 9 597–614 (2010).
18. Dobson, P. D. & Kell, D. B. Carrier-mediated cellular uptake of pharmaceutical drugs: An exception or the rule? *Nat. Rev. Drug Discov.* **7**, 205–220 (2008).
19. Kell, D. B., Dobson, P. D. & Oliver, S. G. Pharmaceutical drug transport: The issues and the implications that it is essentially carrier-mediated only. *Drug Discovery Today* vol. 16 704–714 (2011).
20. Di, L. *et al.* Evidence-based approach to assess passive diffusion and carrier-mediated drug transport. *Drug Discovery Today* vol. 17 905–912 (2012).
21. Smith, D. *et al.* Passive lipoidal diffusion and carrier-mediated cell uptake are both important mechanisms of membrane permeation in drug disposition. *Molecular Pharmaceutics* vol. 11 1727–1738 (2014).
22. Garcia-Castillo, M. D., Chinnapen, D. J. F. & Lencer, W. I. Membrane transport across polarized epithelia. *Cold Spring Harb. Perspect. Biol.* **9**, 9 (2017).
23. Maluykova, I. *et al.* Latrunculin B facilitates Shiga toxin 1 transcellular transcytosis across T84 intestinal epithelial cells. *Biochim. Biophys. Acta - Mol. Basis Dis.* **1782**, 370–377 (2008).
24. Ahsan, C. R., Hajnóczky, G., Maksymowych, A. B. & Simpson, L. L. Visualization of binding and transcytosis of botulinum toxin by human intestinal epithelial cells. *J. Pharmacol. Exp. Ther.* **315**, 1028–1035 (2005).
25. Russell-Jones, G. J. The potential use of receptor-mediated endocytosis for oral drug delivery. *Adv. Drug Deliv. Rev.* **46**, 59–73 (2001).

26. Rojas, R. & Apodaca, G. Immunoglobulin transport across polarized epithelial cells. *Nature Reviews Molecular Cell Biology* vol. 3 944–955 (2002).
27. Yu, M., Yang, Y., Zhu, C., Guo, S. & Gan, Y. Advances in the transepithelial transport of nanoparticles. *Drug Discovery Today* vol. 21 1155–1161 (2016).
28. Garcia-Castillo, M. D. *et al.* Mucosal absorption of therapeutic peptides by harnessing the endogenous sorting of glycosphingolipids. *Elife* **7**, (2018).
29. Laksitorini, M., Prasasty, V. D., Kiptoo, P. K. & Siahaan, T. J. Pathways and progress in improving drug delivery through the intestinal mucosa and blood-brain barriers. *Therapeutic Delivery* vol. 5 1143–1163 (2014).
30. Sha, X., Yan, G., Wu, Y., Li, J. & Fang, X. Effect of self-microemulsifying drug delivery systems containing Labrasol on tight junctions in Caco-2 cells. *Eur. J. Pharm. Sci.* **24**, 477–486 (2005).
31. Chen, X. Y., Butt, A. M. & Mohd Amin, M. C. I. Enhanced paracellular delivery of vaccine by hydrogel microparticles-mediated reversible tight junction opening for effective oral immunization. *J. Control. Release* **311**–**312**, 50–64 (2019).
32. Beaumont, K. The Importance of Gut Wall Metabolism in Determining Drug Bioavailability. in *Methods and Principles in Medicinal Chemistry* (eds. van de Waterbeemd, H., Lennernas, H. & Artersson, P.) 311–328 (John Wiley & Sons, Ltd, 2003). doi:10.1002/3527601473.ch13.
33. Hinderliter, P. & Saghir, S. A. Pharmacokinetics. in *Encyclopedia of Toxicology: Third Edition* 849–855 (Elsevier, 2014). doi:10.1016/B978-0-12-386454-3.00419-X.
34. Le, J. Drug Bioavailability - Clinical Pharmacology - MSD Manual Professional Edition. https://www.msdmanuals.com/professional/clinical-pharmacology/pharmacokinetics/drug-bioavailability (2020).
35. Kaminsky, L. S. & Zhang, Q. Y. The small intestine as a xenobiotic metabolizing organ. *Drug Metab. Dispos.* **31**, 1520–1525 (2003).
36. Xie, F., Ding, X. & Zhang, Q.-Y. An update on the role of intestinal cytochrome P450 enzymes in drug disposition. *Acta Pharm. Sin. B* **6**, 374–383 (2016).
37. Peters, S. A., Jones, C. R., Ungell, A.-L. & Hatley, O. J. D. Predicting Drug Extraction in the Human Gut Wall: Assessing Contributions from Drug Metabolizing Enzymes and Transporter Proteins using Preclinical Models. *Clin. Pharmacokinet.* **55**, 673–96 (2016).

38. Paine, M. F. *et al.* The human intestinal cytochrome P450 'pie'. *Drug Metab. Dispos.* **34**, 880–6 (2006).
39. Doherty, M. M. & Charman, W. N. The Mucosa of the Small Intestine. *Clin. Pharmacokinet.* **41**, 235–253 (2002).
40. Paine, M. F. *et al.* First-pass metabolism of midazolam by the human intestine*. *Clin. Pharmacol. Ther.* **60**, 14–24 (1996).
41. Galetin, A., Gertz, M. & Houston, J. B. Potential role of intestinal first-pass metabolism in the prediction of drug–drug interactions. *Expert Opin. Drug Metab. Toxicol.* **4**, 909–922 (2008).
42. Matsuda, Y. *et al.* Assessment of Intestinal Availability of Various Drugs in the Oral Absorption Process Using Portal Vein-Cannulated Rats. *Drug Metab. Dispos.* **40**,12: 2231-8 (2012).
43. Gertz, M., Davis, J., Harrison, A., Houston, J. & Galetin, A. Grapefruit Juice-Drug Interaction Studies as a Method to Assess the Extent of Intestinal Availability: Utility and Limitations. *Curr. Drug Metab.* **9**, 785–795 (2008).
44. Galetin, A., Gertz, M. & Brian Houston, J. Contribution of Intestinal Cytochrome P450-Mediated Metabolism to Drug-Drug Inhibition and Induction Interactions. *Drug Metab. Pharmacokinet.* **25**, 28–47 (2010).
45. Galetin, A., Hinton, L., Burt, H., Obach, R. & Houston, J. Maximal Inhibition of Intestinal First-Pass Metabolism as a Pragmatic Indicator of Intestinal Contribution to the Drug-Drug Interactions for CYP3A4 Cleared Drugs. *Curr. Drug Metab.* **8**, 685–693 (2007).
46. Chan, L. M. S., Lowes, S. & Hirst, B. H. The ABCs of drug transport in intestine and liver: Efflux proteins limiting drug absorption and bioavailability. *European Journal of Pharmaceutical Sciences* vol. 21 25–51 (2004).
47. Takano, M., Yumoto, R. & Murakami, T. Expression and function of efflux drug transporters in the intestine. *Pharmacology and Therapeutics* vol. 109 137–161 (2006).
48. Wacher, V. J., Wu, C. Y. & Benet, L. Z. Overlapping substrate specificities and tissue distribution of cytochrome P450 3A and P-glycoprotein: implications for drug delivery and activity in cancer chemotherapy. *Mol. Carcinog.* **13**, 129–34 (1995).
49. Thelen, K. & Dressman, J. B. Cytochrome P450-mediated metabolism in the

human gut wall. *J. Pharm. Pharmacol.* **61**, 541–558 (2009).

50. Benet, L. Z. The drug transporter-metabolism alliance: uncovering and defining the interplay. *Mol. Pharm.* **6**, 1631–43 (2009).
51. van Waterschoot, R. A. B. & Schinkel, A. H. A Critical Analysis of the Interplay between Cytochrome P450 3A and P-Glycoprotein: Recent Insights from Knockout and Transgenic Mice. *Pharmacol. Rev.* **63**(2), 90-410 (2011).
52. Cummins, C. L., Jacobsen, W. & Benet, L. Z. Unmasking the dynamic interplay between intestinal P-glycoprotein and CYP3A4. *J. Pharmacol. Exp. Ther.* **300**, 1036–45 (2002).
53. Cummins, C. L., Jacobsen, W., Christians, U. & Benet, L. Z. CYP3A4-Transfected Caco-2 Cells as a Tool for Understanding Biochemical Absorption Barriers: Studies with Sirolimus and Midazolam. *J. Pharmacol. Exp. Ther.* **308**, 143–155 (2003).
54. van Waterschoot, R. A. B. *et al.* Absence of Both Cytochrome P450 3A and P-glycoprotein Dramatically Increases Docetaxel Oral Bioavailability and Risk of Intestinal Toxicity. *Cancer Res.* **69**, 8996-9002(2009).
55. Sjögren, E. *et al.* In vivo methods for drug absorption – Comparative physiologies, model selection, correlations with in vitro methods (IVIVC), and applications for formulation/API/excipient characterization including food effects. *Eur. J. Pharm. Sci.* **57**, 99–151 (2014).
56. Tang, C. & Prueksaritanont, T. Use of in vivo animal models to assess pharmacokinetic drug-drug interactions. *Pharmaceutical Research* vol. 27 1772–1787 (2010).
57. Raoof, A. A., Augustijns, P. R. & Verbeeck, R. K. In Vivo Assessment of Intestinal, Hepatic, and Pulmonary First Pass Metabolism of Propofol in the Rat. *Pharm. Res.* **13**, 891–895 (1996).
58. Wozniak, K. M. *et al.* Gastrointestinal delivery of propofol from fospropofol: its bioavailability and activity in rodents and human volunteers. *J. Transl. Med.* **13**, 170 (2015).
59. Kwan, K. C. Oral Bioavailability and First-Pass Effects. *Drug Metab. Dispos.* **25**, 1329-36 (1997).
60. Shin, B. S. *et al.* Quantitative Determination of Absorption and First-Pass Metabolism of Apicidin, a Potent Histone Deacetylase Inhibitor. *Drug Metab.*

Dispos. **42**, 974-82 (2014).

61. van Herwaarden, A. E. *et al.* Knockout of cytochrome P450 3A yields new mouse models for understanding xenobiotic metabolism. *J. Clin. Invest.* **117**, 3583–3592 (2007).
62. Choo, E. F. *et al.* Use of Transgenic Mouse Models to Understand the Oral Disposition and Drug-Drug Interaction Potential of Cobimetinib, a MEK Inhibitor. *Drug Metab. Dispos.* **43**, 864-9 (2015).
63. Stappaerts, J., Brouwers, J., Annaert, P. & Augustijns, P. In situ perfusion in rodents to explore intestinal drug absorption: Challenges and opportunities. *Int. J. Pharm.* **478**, 665–681 (2015).
64. Vestergaard, B., Agersø, H. & Lykkesfeldt, J. Nephrectomized and Hepatectomized Animal Models as Tools in Preclinical Pharmacokinetics. *Basic Clin. Pharmacol. Toxicol.* **113**, 75–86 (2013).
65. González-Alvarez, I. *et al.* In situ kinetic modelling of intestinal efflux in rats: functional characterization of segmental differences and correlation within vitro results. *Biopharm. Drug Dispos.* **28**, 229–239 (2007).
66. Sababi, M., Borgå, O. & Hultkvist-Bengtsson, U. The role of P-glycoprotein in limiting intestinal regional absorption of digoxin in rats. *Eur. J. Pharm. Sci.* **14**, 21–7 (2001).
67. Li, M., de Graaf, I. A. M. & Groothuis, G. M. M. Precision-cut intestinal slices: alternative model for drug transport, metabolism, and toxicology research. *Expert Opin. Drug Metab. Toxicol.* **12**, 175–190 (2016).
68. Thomson, A. *et al.* The Ussing chamber system for measuring intestinal permeability in health and disease. *BMC Gastroenterol.* **19**, 98 (2019).
69. Lennernäs, H. Animal data: The contributions of the Ussing Chamber and perfusion systems to predicting human oral drug delivery in vivo. *Advanced Drug Delivery Reviews* vol. 59 1103–1120 (2007).
70. Barthe, L., Woodley, J. F., Kenworthy, S. & Houin, G. An improved everted gut sac as a simple and accurate technique to measure paracellular transport across the small intestine. *Eur. J. Drug Metab. Pharmacokinet.* **23**, 313–323 (1998).
71. Nunes, R., Silva, C. & Chaves, L. Tissue-based in vitro and ex vivo models for intestinal permeability studies. in *Concepts and Models for Drug Permeability Studies: Cell and Tissue based In Vitro Culture Models* 203–236 (Elsevier Inc.,

2016). doi:10.1016/B978-0-08-100094-6.00013-4.

72. Perrin, S. Preclinical research: Make mouse studies work. *Nature* **507**, 423–425 (2014).

73. Kim, H.-R. *et al.* Comparative gene expression profiles of intestinal transporters in mice, rats and humans. *Pharmacol. Res.* **56**, 224–236 (2007).

74. Cao, X. *et al.* Why is it Challenging to Predict Intestinal Drug Absorption and Oral Bioavailability in Human Using Rat Model. *Pharm. Res.* **23**, 1675–1686 (2006).

75. Martignoni, M., Groothuis, G. M. M. & de Kanter, R. Species differences between mouse, rat, dog, monkey and human CYP-mediated drug metabolism, inhibition and induction. *Expert Opin. Drug Metab. Toxicol.* **2**, 875–894 (2006).

76. Nishimuta, H., Nakagawa, T., Nomura, N. & Yabuki, M. Species differences in hepatic and intestinal metabolic activities for 43 human cytochrome P450 substrates between humans and rats or dogs. *Xenobiotica* **43**, 948–955 (2013).

77. Chiou, W. L., Jeong, H. Y., Chung, S. M. & Wu, T. C. Evaluation of using dog as an animal model to study the fraction of oral dose absorbed of 43 drugs in humans. *Pharm. Res.* **17**, 135–40 (2000).

78. Cho, S.-M. *et al.* Expression of intestinal transporter genes in beagle dogs. *Exp. Ther. Med.* **5**, 308–314 (2013).

79. Musther, H., Olivares-Morales, A., Hatley, O. J. D., Liu, B. & Rostami Hodjegan, A. Animal versus human oral drug bioavailability: do they correlate? *Eur. J. Pharm. Sci.* **57**, 280–91 (2014).

80. Hidalgo, I. J., Raub, T. J. & Borchardt, R. T. Characterization of the human colon carcinoma cell line (Caco-2) as a model system for intestinal epithelial permeability. *Gastroenterology* **96**, 736–49 (1989).

81. Artursson, P. & Karlsson, J. Correlation between oral drug absorption in humans and apparent drug permeability coefficients in human intestinal epithelial (Caco-2) cells. *Biochem. Biophys. Res. Commun.* **175**, 880–5 (1991).

82. Artursson, P., Palm, K. & Luthman, K. Caco-2 monolayers in experimental and theoretical predictions of drug transport. *Adv. Drug Deliv. Rev.* **46**, 27–43 (2001).

83. Shah, P., Jogani, V., Bagchi, T. & Misra, A. Role of Caco-2 Cell Monolayers in Prediction of Intestinal Drug Absorption. *Biotechnol. Prog.* **22**, 186–198 (2006).

84. Hubatsch I, Ragnarsson EG, Artursson P. Determination of drug permeability and prediction of drug absorption in Caco-2 monolayers. Nat Protoc.

2007;2(9):2111-2119.

85. Anderle, P., Huang, Y. & Sadée, W. Intestinal membrane transport of drugs and nutrients: genomics of membrane transporters using expression microarrays. *Eur. J. Pharm. Sci.* **21**, 17–24 (2004).

86. Hunter, J., Jepson, M. A., Tsuruo, T., Simmons, N. L. & Hirst, B. H. Functional expression of P-glycoprotein in apical membranes of human intestinal Caco-2 cells. Kinetics of vinblastine secretion and interaction with modulators. *J. Biol. Chem.* **268**, 14991–7 (1993).

87. Maubon, N. *et al.* Analysis of drug transporter expression in human intestinal Caco-2 cells by real-time PCR. *Fundam. Clin. Pharmacol.* **21**, 659–663 (2007).

88. Prueksaritanont, T., Gorham, L. M., Hochman, J. H., Tran, L. O. & Vyas, K. P. Comparative studies of drug-metabolizing enzymes in dog, monkey, and human small intestines, and in Caco-2 cells. *Drug Metab. Dispos.* **24**, 634–42 (1996).

89. Hubatsch, I., Lazorova, L., Vahlne, A. & Artursson, P. Orally Active Antiviral Tripeptide Glycyl-Prolyl-Glycinamide Is Activated by CD26 (Dipeptidyl Peptidase IV) before Transport across the Intestinal Epithelium. *Antimicrob. Agents Chemother.* **49**, 1087–1092 (2005).

90. Biganzoli, E., Cavenaghi, L. A., Rossi, R., Brunati, M. C. & Nolli, M. L. Use of a Caco-2 cell culture model for the characterization of intestinal absorption of antibiotics. *Farmaco* **54**, 594–9 (1999).

91. Au, A. P. & Reddy, M. B. Caco-2 cells can be used to assess human iron bioavailability from a semipurified meal. *J. Nutr.* **130**, 1329–34 (2000).

92. Yamaura, Y., Chapron, B. D., Wang, Z., Himmelfarb, J. & Thummel, K. E. Functional Comparison of Human Colonic Carcinoma Cell Lines and Primary Small Intestinal Epithelial Cells for Investigations of Intestinal Drug Permeability and First-Pass Metabolism. *Drug Metab. Dispos.* **44**, 329–335 (2016).

93. Schmiedlin-Ren, P. *et al.* Expression of enzymatically active CYP3A4 by Caco-2 cells grown on extracellular matrix-coated permeable supports in the presence of 1alpha,25-dihydroxyvitamin D3. *Mol. Pharmacol.* **51**, 741–54 (1997).

94. Crespi, C. L., Penman, B. W. & Hu, M. Development of Caco-2 cells expressing high levels of cDNA-derived cytochrome P4503A4. *Pharm. Res.* **13**, 1635–41 (1996).

95. Hu, M. *et al.* Transport and metabolic characterization of Caco-2 cells expressing

CYP3A4 and CYP3A4 plus oxidoreductase. *Pharm. Res.* **16**, 1352–9 (1999).

96. Lenaerts, K. *et al.* Comparative proteomic analysis of cell lines and scrapings of the human intestinal epithelium. *BMC Genomics* **8**, 91 (2007).
97. DeBerardinis, R. J. & Chandel, N. S. Fundamentals of cancer metabolism. *Sci. Adv.* **2**, e1600200 (2016).
98. Sambuy, Y. *et al.* The Caco-2 cell line as a model of the intestinal barrier: influence of cell and culture-related factors on Caco-2 cell functional characteristics. *Cell Biol. Toxicol.* **21**, 1–26 (2005).
99. Kauffman, A. L. *et al.* Alternative functional in vitro models of human intestinal epithelia. *Front. Pharmacol.* **4**, 79 (2013).
100. Takahashi, K. *et al.* Induction of Pluripotent Stem Cells from Adult Human Fibroblasts by Defined Factors. *Cell* **131**, 861–872 (2007).
101. Takenaka, T. *et al.* Human Small Intestinal Epithelial Cells Differentiated from Adult Intestinal Stem Cells as a Novel System for Predicting Oral Drug Absorption in Humans. *Drug Metab. Dispos.* **42**, 1947-54 (2014).
102. Kodama, N. *et al.* Characteristic Analysis of Intestinal Transport in Enterocyte-Like Cells Differentiated from Human Induced Pluripotent Stem Cells. *Drug Metab. Dispos.* **44**,10 (2016).
103. Ozawa, T. *et al.* Generation of enterocyte-like cells from human induced pluripotent stem cells for drug absorption and metabolism studies in human small intestine. *Sci. Rep.* **5**, 16479 (2015).
104. Iwao, T. *et al.* Generation of Enterocyte-Like Cells with Pharmacokinetic Functions from Human Induced Pluripotent Stem Cells Using Small-Molecule Compounds. *Drug Metab. Dispos.* **43**, 603-10 (2015).
105. Pereira, C., Costa, J., Sarmento, B. & Araújo, F. Cell-based in vitro models for intestinal permeability studies. in *Concepts and Models for Drug Permeability Studies: Cell and Tissue based In Vitro Culture Models* 57–81 (Elsevier Inc., 2016).
106. Mahler, G. J., Shuler, M. L. & Glahn, R. P. Characterization of Caco-2 and HT29-MTX cocultures in an in vitro digestion/cell culture model used to predict iron bioavailability. *J. Nutr. Biochem.* **20**, 494–502 (2009).
107. Araújo, F. & Sarmento, B. Towards the characterization of an in vitro triple co-culture intestine cell model for permeability studies. *Int. J. Pharm.* **458**, 128–134 (2013).

108. Gullberg, E. *et al.* Expression of specific markers and particle transport in a new human intestinal M-cell model. *Biochem. Biophys. Res. Commun.* **279**, 808–813 (2000).

109. Lozoya-Agullo, I. *et al.* Usefulness of Caco-2/HT29-MTX and Caco-2/HT29-MTX/Raji B coculture models to predict intestinal and colonic permeability compared to Caco-2 monoculture. *Mol. Pharm.* **14**, 1264–1270 (2017).

110. Frantz, C., Stewart, K. & Weaver, V. The Extracellular Matrix at a glance. *J. Cell Sci.* **123**, 4195–4200 (2010).

111. Wade, R. J. & Burdick, J. A. Engineering ECM signals into biomaterials. *Mater. Today* **15**, 454–459 (2012).

112. Hynes, R. O. & Naba, A. Overview of the matrisome-An inventory of extracellular matrix constituents and functions. *Cold Spring Harb. Perspect. Biol.* **4**, 1 (2012).

113. Lodish H, Berk A, Zipursky SL, et al. Molecular Cell Biology. 4th edition. New York: W. H. Freeman; 2000. Section 22.4, Noncollagen Components of the Extracellular Matrix.

114. Kular, J. K., Basu, S. & Sharma, R. I. The extracellular matrix: Structure, composition, age-related differences, tools for analysis and applications for tissue engineering. *Journal of Tissue Engineering* vol. 5, 2041 (2014).

115. Yue, B. Biology of the extracellular matrix: An overview. *Journal of Glaucoma* vol. 23 S20–S23 (2014).

116. Roulis, M. & Flavell, R. A. Fibroblasts and myofibroblasts of the intestinal lamina propria in physiology and disease. *Differentiation* **92**, 116–131 (2016).

117. Meran, L., Baulies, A. & Li, V. S. W. Intestinal Stem Cell Niche: The Extracellular Matrix and Cellular Components. *Stem Cells International* vol. 2017: 79770358 (2017).

118. Laurie, G. W., Leblond, C. P. & Martin, G. R. Localization of type IV collagen, laminin, heparan sulfate proteoglycan, and fibronectin to the basal lamina of basement membranes. *J. Cell Biol.* **95**, 340–344 (1982).

119. Miner, J. H. & Nguyen, N. M. Extracellular Matrix. in *Encyclopedia of Respiratory Medicine, Four-Volume Set* 157–162 (Elsevier Inc., 2006). doi:10.1016/B0-12-370879-6/00143-5.

120. Bates, R. C. Gastrointestinal Matrix, Organization and Significance. in *Encyclopedia of Gastroenterology* 219–223 (Elsevier, 2004).

121. Boudry, G., Yang, P.-C. & Perdue, M. H. Small Intestine, Anatomy. in *Encyclopedia of Gastroenterology* 404–409 (Elsevier, 2004).
122. Creff, J. *et al.* Fabrication of 3D scaffolds reproducing intestinal epithelium topography by high-resolution 3D stereolithography. *Biomaterials* **221**, 119404 (2019).
123. Yi, B. *et al.* Three-dimensional in vitro gut model on a villi-shaped collagen scaffold. *Biochip J.* **11**, 219–231 (2017).
124. Kim, W. J. & Kim, G. H. An innovative cell-printed microscale collagen model for mimicking intestinal villus epithelium. *Chem. Eng. J.* **334**, 2308–2318 (2018).
125. Costello, C. M. *et al.* Synthetic small intestinal scaffolds for improved studies of intestinal differentiation. *Biotechnol. Bioeng.* **111**, 1222–1232 (2014).
126. DiMarco, R. L., Hunt, D. R., Dewi, R. E. & Heilshorn, S. C. Improvement of paracellular transport in the Caco-2 drug screening model using protein-engineered substrates. *Biomaterials* **129**, 152–162 (2017).
127. Zhang, J., Penny, J. & Lu, J. R. Development of a novel in vitro 3D intestinal model for permeability evaluations. *Int. J. Food Sci. Nutr.* **71**, 549–562 (2020).
128. Darling, N. J., Mobbs, C. L., González-Hau, A. L., Freer, M. & Przyborski, S. Bioengineering Novel in vitro Co-culture Models That Represent the Human Intestinal Mucosa With Improved Caco-2 Structure and Barrier Function. *Front. Bioeng. Biotechnol.* **8**, 992 (2020).
129. Madden, L. R. *et al.* Bioprinted 3D Primary Human Intestinal Tissues Model Aspects of Native Physiology and ADME/Tox Functions. *iScience* **2**, 156–167 (2018).
130. Pereira, C., Araújo, F., Barrias, C. C., Granja, P. L. & Sarmento, B. Dissecting stromal-epithelial interactions in a 3D in vitro cellularized intestinal model for permeability studies. *Biomaterials* **56**, 36–45 (2015).
131. Li, N. *et al.* Development of an Improved Three-Dimensional In Vitro Intestinal Mucosa Model for Drug Absorption Evaluation. *Tissue Eng. Part C. Methods* **19**,9: 708-719 (2013).
132. Costa, J. & Ahluwalia, A. Advances and Current Challenges in Intestinal in vitro Model Engineering: A Digest. *Frontiers in Bioengineering and Biotechnology* vol. 18,7: 144 (2019).
133. Wang, L., Murthy, S. K., Fowle, W. H., Barabino, G. A. & Carrier, R. L. Influence of

micro-well biomimetic topography on intestinal epithelial Caco-2 cell phenotype. *Biomaterials* **30**, 6825–6834 (2009).

134. Yu, J., Peng, S., Luo, D. & March, J. C. In vitro 3D human small intestinal villous model for drug permeability determination. *Biotechnol. Bioeng.* **109**, 2173–2178 (2012).
135. Kim, W. & Kim, G. Intestinal Villi Model with Blood Capillaries Fabricated Using Collagen-Based Bioink and Dual-Cell-Printing Process. *ACS Appl. Mater. Interfaces* **10**, 41185–41196 (2018).
136. Chen, Y. *et al.* Robust bioengineered 3D functional human intestinal epithelium. *Sci. Rep.* **5**, 13708 (2015).
137. Chen, Y., Zhou, W., Roh, T., Estes, M. K. & Kaplan, D. L. In vitro enteroid-derived three-dimensional tissue model of human small intestinal epithelium with innate immune responses. *PLoS One* **12**, e0187880 (2017).
138. Ranganathan, S., Smith, E. M., Foulke-Abel, J. D. & Barry, E. M. Research in a time of enteroids and organoids: how the human gut model has transformed the study of enteric bacterial pathogens. *Gut Microbes* vol. 12,1:175492 (2020).
139. Hewes, S. A. *et al.* In Vitro Models of the Small Intestine: Engineering Challenges and Engineering Solutions. *Tissue Engineering - Part B: Reviews* vol. 26 313–326 (2020).
140. Spence, J. R. *et al.* Directed differentiation of human pluripotent stem cells into intestinal tissue in vitro. *Nature* **470**, 105–109 (2011).
141. Barker, N. *et al.* Identification of stem cells in small intestine and colon by marker gene Lgr5. *Nature* **449**, 1003–1007 (2007).
142. Sato, T. *et al.* Single Lgr5 stem cells build crypt-villus structures in vitro without a mesenchymal niche. *Nature* **459**, 262–265 (2009).
143. Fatehullah, A., Tan, S. H. & Barker, N. Organoids as an in vitro model of human development and disease. *Nature Cell Biology* vol. 18 246–254 (2016).
144. Imura, Y., Asano, Y., Sato, K. & Yoshimura, E. A Microfluidic System to Evaluate Intestinal Absorption. *Anal. Sci.* **25**, 1403–1407 (2009).
145. Kim, H. J. & Ingber, D. E. Gut-on-a-Chip microenvironment induces human intestinal cells to undergo villus differentiation. *Integr. Biol.* **5**, 1130 (2013).
146. Shim, K. Y. *et al.* Microfluidic gut-on-a-chip with three-dimensional villi structure. *Biomed. Microdevices* **19**, 1–10 (2017).

147. Kasendra, M. *et al.* Development of a primary human Small Intestine-on-a-Chip using biopsy-derived organoids. *Sci. Rep.* **8**, 2871 (2018).

148. Verhulsel M, Simon A, Bernheim-Dennery M, et al. Developing an advanced gut on chip model enabling the study of epithelial cell/fibroblast interactions. *Lab Chip*. 2021;21(2):365-377.

149. Pusch, J. *et al.* The physiological performance of a three-dimensional model that mimics the microenvironment of the small intestine. *Biomaterials* **32**, 7469–7478 (2011).

150. Scheller, K. *et al.* Upcyte® microvascular endothelial cells repopulate decellularized scaffold. *Tissue Eng. Part C. Methods* **19**, 57–67 (2013).

151. Shabafrooz, V. *et al.* The effect of hyaluronic acid on biofunctionality of gelatin-collagen intestine tissue engineering scaffolds. *J. Biomed. Mater. Res. Part A* **102**, 3130–3139 (2014).

152. Costello, C. M. *et al.* Synthetic small intestinal scaffolds for improved studies of intestinal differentiation. *Biotechnol. Bioeng.* **111**, 1222–32 (2014).

153. Kim, S. H. *et al.* Three-dimensional intestinal villi epithelium enhances protection of human intestinal cells from bacterial infection by inducing mucin expression. *Integr. Biol.* **6**, 1122–1131 (2014).

154. Murphy, C. M., Matsiko, A., Haugh, M. G. & Gleeson, J. P. Mesenchymal stem cell fate is regulated by the composition and mechanical properties of collagen–glycosaminoglycan scaffolds. *J. Mech. Behav. Biomed. Mater.* **11**, 53–62 (2012).

155. Keogh, M. B., O'Brien, F. J. & Daly, J. S. Substrate stiffness and contractile behaviour modulate the functional maturation of osteoblasts on a collagen–GAG scaffold. *Acta Biomater.* **6**, 4305–4313 (2010).

156. Chandler, E. M. *et al.* Stiffness of photocrosslinked RGD-alginate gels regulates adipose progenitor cell behavior. *Biotechnol. Bioeng.* **108**, 1683–1692 (2011).

157. Lu, Z. *et al.* Electrospun highly porous poly(L-lactic acid)-dopamine-SiO2 fibrous membrane for bone regeneration. *Mater. Sci. Eng. C* **117**, 111359 (2020).

158. Downie, L. E., Choi, J., Lim, J. K. H. & Chinnery, H. R. Longitudinal changes to tight junction expression and endothelial cell integrity in a mouse model of sterile corneal inflammation. *Investig. Ophthalmol. Vis. Sci.* **57**, 3477–3484 (2016).

159. Livak, K. J. & Schmittgen, T. D. Analysis of relative gene expression data using real-time quantitative PCR and the 2-ΔΔCT method. *Methods* **25**, 402–408 (2001).

160. Ferruzza, S., Rossi, C., Scarino, M. L. & Sambuy, Y. A protocol for in situ enzyme assays to assess the differentiation of human intestinal Caco-2 cells. *Toxicol. Vitr.* **26**, 1247–1251 (2012).

161. Janson, I. A. & Putnam, A. J. Extracellular matrix elasticity and topography: Material-based cues that affect cell function via conserved mechanisms. *Journal of Biomedical Materials Research - Part A* vol. 103 1246–1258 (2015).

162. Wang, L. & Carrier, R. L. Biomimetic Topography: Bioinspired Cell Culture Substrates and Scaffolds. in *Advances in Biomimetics* (InTech, 2011). doi:10.5772/14383.

163. Loesberg, W. A. *et al.* The threshold at which substrate nanogroove dimensions may influence fibroblast alignment and adhesion. *Biomaterials* **28**, 3944–3951 (2007).

164. Lamers, E. *et al.* The influence of nanoscale grooved substrates on osteoblast behavior and extracellular matrix deposition. *Biomaterials* **31**, 3307–3316 (2010).

165. Tonazzini, I. *et al.* Neuronal contact guidance and YAP signaling on ultra-small nanogratings. *Sci. Rep.* **10**, 1–18 (2020).

166. Bettinger, C. J., Langer, R. & Borenstein, J. T. Engineering substrate topography at the Micro- and nanoscale to control cell function. *Angewandte Chemie - International Edition* vol. 48 5406–5415 (2009).

167. Chou, L., Firth, J. D., Nathanson, D., Uitto, V. J. & Brunette, D. M. Effects of titanium on transcriptional and post-transcriptional regulation of fibronectin in human fibroblasts. *J. Biomed. Mater. Res.* **31**, 209–217 (1996).

168. Cukierman E, Pankov R, Stevens DR, Yamada KM. Taking cell-matrix adhesions to the third dimension. Science. 2001;294(5547):1708-1712.

169. Charest, J. L., Eliason, M. T., García, A. J. & King, W. P. Combined microscale mechanical topography and chemical patterns on polymer cell culture substrates. *Biomaterials* **27**, 2487–2494 (2006).

170. Fitzgerald, K. A., Malhotra, M., Curtin, C. M., O' Brien, F. J. & O' Driscoll, C. M. Life in 3D is never flat: 3D models to optimise drug delivery. *J. Control. Release*

215, 39–54 (2015).

171. Komuro, T. & Hashimoto, Y. Three-Dimensional Structure of the Rat Intestinal Wall (Mucosa and Submucosa). *Arch. Histol. Cytol.* **53**, 1–21 (1990).
172. Roulis, M. & Flavell, R. A. Fibroblasts and myofibroblasts of the intestinal lamina propria in physiology and disease. *Differentiation* **92**, 116–131 (2016).
173. Stevens, M. M. & George, J. H. Exploring and engineering the cell surface interface. *Science* vol. 310 1135–1138 (2005).
174. Thenmozhi, S., Dharmaraj, N., Kadirvelu, K. & Kim, H. Y. Electrospun nanofibers: New generation materials for advanced applications. *Materials Science and Engineering B: Solid-State Materials for Advanced Technology* vol. 217 36–48 (2017).
175. Nemati, S., Kim, S. jeong, Shin, Y. M. & Shin, H. Current progress in application of polymeric nanofibers to tissue engineering. *Nano Convergence* vol. 6: 36 (2019).
176. Liu, H. *et al.* Electrospinning of nanofibers for tissue engineering applications. *Journal of Nanomaterials* vol. 2013, 495708 (2013).
177. Chahal, S., Kumar, A. & Hussian, F. S. J. Development of biomimetic electrospun polymeric biomaterials for bone tissue engineering. A review. *Journal of Biomaterials Science, Polymer Edition* vol. 30 1308–1355 (2019).
178. Tan, Z. *et al.* Electrospun vein grafts with high cell infiltration for vascular tissue engineering. *Mater. Sci. Eng. C* **81**, 407–415 (2017).
179. Xu, C., Yang, F., Wang, S. & Ramakrishna, S. In vitro study of human vascular endothelial cell function on materials with various surface roughness. *J. Biomed. Mater. Res. - Part A* **71**, 154–161 (2004).
180. Kim, D., Pugno, N. M. & Ryu, S. Wetting theory for small droplets on textured solid surfaces. *Sci. Rep.* **6**, 1–8 (2016).
181. Ferrari, M., Cirisano, F. & Morán, M. C. Mammalian Cell Behavior on Hydrophobic Substrates: Influence of Surface Properties. *Colloids and Interfaces* **3**, 48 (2019).
182. Xu, L. C. & Siedlecki, C. A. Effects of surface wettability and contact time on protein adhesion to biomaterial surfaces. *Biomaterials* **28**, 3273–3283 (2007).
183. Boyan, B. D., Hummert, T. W., Dean, D. D. & Schwartz, Z. Role of material surfaces in regulating bone and cartilage cell response. *Biomaterials* **17**, 137–146 (1996).

184. Hlady, V., Buijs, J. & Jennissen, H. P. Methods for studying protein adsorption. *Methods Enzymol.* **309**, 402–429 (1999).

185. Berridge, M. V. & Tan, A. S. Characterization of the Cellular Reduction of 3-(4,5-dimethylthiazol-2- yl)-2,5-diphenyltetrazolium bromide (MTT): Subcellular Localization, Substrate Dependence, and Involvement of Mitochondrial Electron Transport in MTT Reduction. *Arch. Biochem. Biophys.* **303**, 474–482 (1993).

186. Flemming, R. G., Murphy, C. J., Abrams, G. A., Goodman, S. L. & Nealey, P. F. Effects of synthetic micro- and nano-structured surfaces on cell behavior. *Biomaterials* **20**, 573–588 (1999).

187. Rose, J. B. *et al.* In vitro evaluation of electrospun blends of gelatin and PCL for application as a partial thickness corneal graft. *J. Biomed. Mater. Res. Part A* **107**, 828–838 (2019).

188. Dowling, D. P., Miller, I. S., Ardhaoui, M. & Gallagher, W. M. Effect of Surface Wettability and Topography on the Adhesion of Osteosarcoma Cells on Plasma-modified Polystyrene. *J. Biomater. Appl.* **26**,3: 327-47 (2011).

189. Ferrari, M., Cirisano, F. & Morán, M. C. Mammalian Cell Behavior on Hydrophobic Substrates: Influence of Surface Properties. *Colloids and Interfaces* **3**, 48 (2019).

190. Arima, Y. & Iwata, H. Effect of wettability and surface functional groups on protein adsorption and cell adhesion using well-defined mixed self-assembled monolayers. *Biomaterials* **28**, 3074–3082 (2007).

191. Lee, J. H., Khang, G., Lee, J. W. & Lee, H. B. Interaction of different types of cells on polymer surfaces with wettability gradient. *J. Colloid Interface Sci.* **205**, 323–330 (1998).

192. Wei, J. *et al.* Influence of surface wettability on competitive protein adsorption and initial attachment of osteoblasts. *Biomed. Mater.* **4**, 045002(2009).

193. Tamada, Y. & Ikada, Y. Effect of preadsorbed proteins on cell adhesion to polymer surfaces. *J. Colloid Interface Sci.* **155**, 334–339 (1993).

194. Ying, P., Jin, G. & Tao, Z. Competitive adsorption of collagen and bovine serum albumin-effect of the surface wettability. *Colloids Surfaces B Biointerfaces* **33**, 259–263 (2004).

195. Allen, L. T. *et al.* Surface-induced changes in protein adsorption and implications for cellular phenotypic responses to surface interaction. *Biomaterials* **27**, 3096–

3108 (2006).

196. Jiao, Y., Liu, Z., Shao, X. & Zhou, C. Protein adsorption and cytocompatibility of poly(L-lactic acid) surfaces modified with biomacromolecules. *J. Appl. Polym. Sci.* **125**, E501–E510 (2012).

197. Lourenço, B. N. *et al.* Wettability influences cell behavior on superhydrophobic surfaces with different topographies. *Biointerphases* **7**, 1–11 (2012).

198. Leong, M. F., Chian, K. S., Mhaisalkar, P. S., Ong, W. F. & Ratner, B. D. Effect of electrospun poly(D,L-lactide) fibrous scaffold with nanoporous surface on attachment of porcine esophageal epithelial cells and protein adsorption. *J. Biomed. Mater. Res. - Part A* **89**, 1040–1048 (2009).

199. Woo, K. M., Chen, V. J. & Ma, P. X. Nano-fibrous scaffolding architecture selectively enhances protein adsorption contributing to cell attachment. *J. Biomed. Mater. Res.* **67A**, 531–537 (2003).

200. Song, J. *et al.* Hierarchical porous silk fibroin/poly(L-lactic acid) fibrous membranes towards vascular scaffolds. *Int. J. Biol. Macromol.* **166**, 1111–1120 (2021).

201. Muniyandi, P. *et al.* ECM mimetic electrospun porous poly (l-lactic acid) (PLLA) scaffolds as potential substrates for cardiac tissue engineering. *Polymers (Basel).* **12**, 2:451 (2020).

202. Liu, Q. *et al.* Porous nanofibrous poly(l-lactic acid) scaffolds supporting cardiovascular progenitor cells for cardiac tissue engineering. *Acta Biomater.* **26**, 105–114 (2015).

203. Patient, J. D. *et al.* Nanofibrous Scaffolds Support a 3D in vitro Permeability Model of the Human Intestinal Epithelium. *Front. Pharmacol.* **10**, 456 (2019).

204. Chantret, I., Barbat, A., Dussaulx, E., Brattain, M. G. & Zweibaum, A. Epithelial Polarity, Villin Expression, and Enterocytic Differentiation of Cultured Human Colon Carcinoma Cells: A Survey of Twenty Cell Lines. *Cancer Res.* **48**, 7:1936-42 (1988).

205. Halbleib, J. M., Sääf, A. M., Brown, P. O. & Nelson, W. J. Transcriptional modulation of genes encoding structural characteristics of differentiating enterocytes during development of a polarized epithelium in vitro. *Mol. Biol. Cell* **18**, 4261–78 (2007).

206. Artursson, P. Epithelial transport of drugs in cell culture. I: A model for studying

the passive diffusion of drugs over intestinal absorbtive (Caco-2) cells. *J. Pharm. Sci.* **79**, 476–482 (1990).

207. Rubas, W., Jezyk, N. & Grass, G. M. Comparison of the Permeability Characteristics of a Human Colonic Epithelial (Caco-2) Cell Line to Colon of Rabbit, Monkey, and Dog Intestine and Human Drug Absorption. *Pharm. Res. An Off. J. Am. Assoc. Pharm. Sci.* **10**, 113–118 (1993).
208. Kim, D. C., Burton, P. S. & Borchardt, R. T. A Correlation Between the Permeability Characteristics of a Series of Peptides Using an in Vitro Cell Culture Model (Caco-2) and Those Using an in Situ Perfused Rat Ileum Model of the Intestinal Mucosa. *Pharm. Res. An Off. J. Am. Assoc. Pharm. Sci.* **10**, 1710–1714 (1993).
209. Lennernäs, H. Human jejunal effective permeability and its correlation with preclinical drug absorption models. *Journal of Pharmacy and Pharmacology* vol. 49 627–638 (1997).
210. Larregieu, C. A. & Benet, L. Z. Distinguishing between the permeability relationships with absorption and metabolism to improve BCS and BDDCS predictions in early drug discovery. *Mol. Pharm.* **11**, 1335–1344 (2014).
211. Srinivasan, B. *et al.* TEER Measurement Techniques for In Vitro Barrier Model Systems. *Journal of Laboratory Automation* vol. 20 107–126 (2015).
212. Sambuy, Y. *et al. The Caco-2 cell line as a model of the intestinal barrier: in£uence of cell and culture-related factors on Caco-2 cell functional characteristics*. *Cell Biology and Toxicology* vol. 21 https://link.springer.com/content/pdf/10.1007%2Fs10565-005-0085-6.pdf (2005).
213. Lennernäs, H., Palm, K., Fagerholm, U. & Artursson, P. Comparison between active and passive drug transport in human intestinal epithelial (Caco-2) cells in vitro and human jejunum in vivo. *Int. J. Pharm.* **127**, 103–107 (1996).
214. Kamath AV, Morrison RA, Mathias NR, Dando SA, Marino AM, Chong S. Modulation of tight junctions does not predict oral absorption of hydrophilic compounds: use of Caco-2 and Calu-3 cells. Arch Pharm Res. 2007;30(8):1002-1007
215. Balimane, P. V, Han, Y.-H. & Chong, S. *Current Industrial Practices of Assessing Permeability and P-Glycoprotein Interaction*. *The AAPS Journal* vol. 8, 1:1-

13(2006).

216. Maubon, N. *et al.* Analysis of drug transporter expression in human intestinal Caco-2 cells by real-time PCR. *Fundam. Clin. Pharmacol.* **21**, 659–663 (2007).

217. Vaessen, S. F. C. *et al.* Regional expression levels of drug transporters and metabolizing enzymes along the pig and human intestinal tract and comparison with Caco-2 cells. *Drug Metab. Dispos.* **45**, 353–360 (2017).

218. Lee, J. B. *et al.* Quantitative analysis of lab-to-lab variability in Caco-2 permeability assays. *Eur. J. Pharm. Biopharm.* **114**, 38–42 (2017).

219. Behrens, I. & Kissel, T. Do cell culture conditions influence the carrier-mediated transport of peptides in Caco-2 cell monolayers? *Eur. J. Pharm. Sci.* **19**, 433–442 (2003).

220. Delie, F. & Rubas, W. A human colonic cell line sharing similarities with enterocytes as a model to examine oral absorption: Advantages and limitations of the Caco-2 model. *Critical Reviews in Therapeutic Drug Carrier Systems* vol. 14 221–286 (1997).

221. Basson, M. D., Modlin, I. M. & Madri, J. A. Human enterocyte (Caco-2) migration is modulated in vitro by extracellular matrix composition and epidermal growth factor. *J. Clin. Invest.* **90**, 15–23 (1992).

222. Basson, M. D., Turowski, G. & Emenaker, N. J. Regulation of human (Caco-2) intestinal epithelial cell differentiation by extracellular matrix proteins. *Exp. Cell Res.* **225**, 301–305 (1996).

223. Wang, L., Murthy, S. K., Barabino, G. A. & Carrier, R. L. Synergic effects of crypt-like topography and ECM proteins on intestinal cell behavior in collagen based membranes. *Biomaterials* **31**, 7586–7598 (2010).

224. Speer, J. E. *et al.* Molecular transport through primary human small intestinal monolayers by culture on a collagen scaffold with a gradient of chemical cross-linking. *J. Biol. Eng.* **13**, 36 (2019).

225. Snyder, J. *et al.* Materials and Microenvironments for Engineering the Intestinal Epithelium. *Ann. Biomed. Eng.* **48**, 1916–1940 (2020).

226. Yu, J., Peng, S., Luo, D. & March, J. C. In vitro 3D human small intestinal villous model for drug permeability determination. *Biotechnol. Bioeng.* **109**, 2173–2178 (2012).

227. Vllasaliu, D., Falcone, F. H., Stolnik, S. & Garnett, M. Basement membrane

influences intestinal epithelial cell growth and presents a barrier to the movement of macromolecules. *Exp. Cell Res.* **323**, 218–231 (2014).

228. Ferruzza, S., Rossi, C., Scarino, M. L. & Sambuy, Y. A protocol for differentiation of human intestinal Caco-2 cells in asymmetric serum-containing medium. *Toxicol. Vitr.* **26**, 1252–1255 (2012).
229. Eom, S., Park, S. M., Han, S. J., Kim, J. W. & Kim, D. S. One-step fabrication of a tunable nanofibrous well insert: Via electrolyte-assisted electrospinning. *RSC Adv.* **7**, 38300–38306 (2017).
230. Peterson, M. D. & Mooseker, M. S. Characterization of the enterocyte-like brush border cytoskeleton of the C2BBe clones of the human intestinal cell line, Caco-2. *J. Cell Sci.* **102**, (1992).
231. Ölander, M., Wiśniewski, J. R., Matsson, P., Lundquist, P. & Artursson, P. The Proteome of Filter-Grown Caco-2 Cells with a Focus on Proteins Involved in Drug Disposition. *J. Pharm. Sci.* **105**, 817–827 (2016).
232. Tadjali, M., Seidelin, J. B., Olsen, J. & Troelsen, J. T. Transcriptome changes during intestinal cell differentiation. *Biochim. Biophys. Acta - Mol. Cell Res.* **1589**, 160–167 (2002).
233. Tremblay, E. *et al.* Gene expression profiles of normal proliferating and differentiating human intestinal epithelial cells: A comparison with the Caco-2 cell model. *J. Cell. Biochem.* **99**, 1175–1186 (2006).
234. Buhrke, T., Lengler, I. & Lampen, A. Analysis of proteomic changes induced upon cellular differentiation of the human intestinal cell line Caco-2. *Dev. Growth Differ.* **53**, 411–426 (2011).
235. Levy, P. *et al.* Enterocytic differentiation of the human Caco-2 cell line is correlated with down-regulation of fibronectin and laminin. *FEBS Lett.* **338**, 272–276 (1994).
236. Vachon, P. H., Simoneau, A., Herring-Gillam, F. E. & Beaulieu, J. F. Cellular fibronectin expression is down-regulated at the mRNA level in differentiating human intestinal epithelial cells. *Exp. Cell Res.* **216**, 30–34 (1995).
237. Halbleib, J. M., Sääf, A. M., Brown, P. O. & Nelson, W. J. Transcriptional modulation of genes encoding structural characteristics of differentiating enterocytes during development of a polarized epithelium in vitro. *Mol. Biol. Cell* **18**, 4261–78 (2007).

238. Teller, I. C. *et al.* Laminins in the developing and adult human small intestine: Relation with the functional absorptive unit. *Dev. Dyn.* **236**, 1980–1990 (2007).

239. Benoit, Y. D., Groulx, J.-F., Gagné, D. & Beaulieu, J.-F. RGD-Dependent Epithelial Cell-Matrix Interactions in the Human Intestinal Crypt. *J. Signal Transduct.* **2012**, 1–10 (2012).

240. Speer, J. E., Wang, Y., Fallon, J. K., Smith, P. C. & Allbritton, N. L. Evaluation of human primary intestinal monolayers for drug metabolizing capabilities. *J. Biol. Eng.* **13**, (2019).

241. Vllasaliu, D., Falcone, F. H., Stolnik, S. & Garnett, M. Basement membrane influences intestinal epithelial cell growth and presents a barrier to the movement of macromolecules. *Exp. Cell Res.* **323**, 218–231 (2014).

242. Schweinlin, M. *et al.* Development of an advanced primary human in vitro model of the small intestine. *Tissue Eng. - Part C Methods* **22**, 873–883 (2016).

243. Rozehnal, V. *et al.* Human small intestinal and colonic tissue mounted in the Ussing chamber as a tool for characterizing the intestinal absorption of drugs. *Eur. J. Pharm. Sci.* **46**, 367–373 (2012).

244. Michiba, K. *et al.* Characterization of the human intestinal drug transport with ussing chamber system incorporating freshly isolated human jejunum. *Drug Metab. Dispos.* **49**, 84–93 (2021).

245. Haslam, I. S. *et al.* Pancreatoduodenectomy as a source of human small intestine for Ussing chamber investigations and comparative studies with rat tissue. *Biopharm. Drug Dispos.* **32**, 210–221 (2011).

246. Sun, H., Chow, E. C. Y., Liu, S., Du, Y. & Pang, K. S. The Caco-2 cell monolayer: Usefulness and limitations. *Expert Opinion on Drug Metabolism and Toxicology* vol. 4 395–411 (2008).

247. Watson, C. J., Rowland, M. & Warhurst, G. Functional modeling of tight junctions in intestinal cell monolayers using polyethylene glycol oligomers. *Am. J. Physiol. Physiol.* **281**, C388–C397 (2001).

248. Fine, K. D., Ana, C. A. S., Porter, J. L. & Fordtran, J. S. *Effect of Changing Intestinal Flow Rate on a Measurement of Intestinal Permeability*. *GASTROENTEROLOGY* vol. 108 (1995).

249. Andrews, C., McLean, M. H. & Durum, S. K. Cytokine tuning of intestinal epithelial function. *Front. Immunol.* **9**, 1270 (2018).

250. Anderberg, E. K. & Artursson, P. Epithelial transport of drugs in cell culture. VIII: Effects of sodium dodecyl sulfate on cell membrane and tight junction permeability in human intestinal epithelial (Caco-2) cells. *J. Pharm. Sci.* **82**, 392–398 (1993).

251. Lindmark, T., Kimura, Y. & Artursson, P. Absorption Enhancement through Intracellular Regulation of Tight Junction Permeability by Medium Chain Fatty Acids in Caco-2 Cells. *J. Pharmacol. Exp. Ther.* **284**,1: 362-9 (1998).

252. Deli, M. A. Potential use of tight junction modulators to reversibly open membranous barriers and improve drug delivery. *Biochimica et Biophysica Acta - Biomembranes* vol. 1788 892–910 (2009).

253. Bhat, A. A. *et al.* Tight junction proteins and signaling pathways in cancer and inflammation: A functional crosstalk. *Frontiers in Physiology* vol. 10 1942 (2019).

254. Grant, C. N. *et al.* Human and mouse tissue-engineered small intestine both demonstrate digestive and absorptive function. *Am. J. Physiol. Liver Physiol.* **308**, G664–G677 (2015).

255. Nyga, A., Loizidou, M., Emberton, M. & Cheema, U. A novel tissue engineered three-dimensional in vitro colorectal cancer model. *Acta Biomater.* **9**, 7917–7926 (2013).

256. Dosh, R. H., Jordan-Mahy, N., Sammon, C. & Le Maitre, C. L. Long-term in vitro 3D hydrogel co-culture model of inflammatory bowel disease. *Sci. Rep.* **9**, 1–15 (2019).

257. Roh, T. T., Chen, Y., Paul, H. T., Guo, C. & Kaplan, D. L. 3D bioengineered tissue model of the large intestine to study inflammatory bowel disease. *Biomaterials* **225**, 119517 (2019).

258. Antunes, F., Andrade, F., Araújo, F., Ferreira, D. & Sarmento, B. Establishment of a triple co-culture in vitro cell models to study intestinal absorption of peptide drugs. *Eur. J. Pharm. Biopharm.* **83**, 427–435 (2013).

259. Béduneau, A. *et al.* A tunable Caco-2/HT29-MTX co-culture model mimicking variable permeabilities of the human intestine obtained by an original seeding procedure. *Eur. J. Pharm. Biopharm.* **87**, 290–298 (2014).

260. Simon-Assmann, P., Kedinger, M., De Arcangelis, A. et al. Extracellular matrix components in intestinal development. Experientia 51, 883–900 (1995).

261. Powell, D. W., Pinchuk, I. V., Saada, J. I., Chen, X. & Mifflin, R. C. Mesenchymal

cells of the intestinal lamina propria. *Annu. Rev. Physiol.* **73**, 213–237 (2011).

262. Kim, Y., Ko, H., Kwon, I. K. & Shin, K. Extracellular matrix revisited: Roles in tissue engineering. *International Neurourology Journal* vol. 20 S23–S29 (2016).
263. Dignass, A. U., Tsunekawa, S. & Podolsky, D. K. Fibroblast growth factors modulate intestinal epithelial cell growth and migration. *Gastroenterology* **106**, 1254–1262 (1994).
264. Lahar, N. *et al.* Intestinal subepithelial myofibroblasts support in vitro and in vivo growth of human small intestinal epithelium. *PLoS One* **6**, e26898 (2011).
265. Visco, V. *et al.* Human colon fibroblasts induce differentiation and proliferation of intestinal epithelial cells through the direct paracrine action of keratinocyte growth factor. *J. Cell. Physiol.* **220**, 204–213 (2009).
266. Göke, M., Kanai, M. & Podolsky, D. K. Intestinal fibroblasts regulate intestinal epithelial cell proliferation via hepatocyte growth factor. *Am. J. Physiol. - Gastrointest. Liver Physiol.* **274**, (1998).
267. Li, N. *et al.* Development of an improved three-dimensional in vitro intestinal mucosa model for drug absorption evaluation. *Tissue Eng. - Part C Methods* **19**, 708–719 (2013).
268. Singh, S. B., Carroll-Portillo, A., Coffman, C., Ritz, N. L. & Lin, H. C. Intestinal Alkaline Phosphatase Exerts Anti-Inflammatory Effects Against Lipopolysaccharide by Inducing Autophagy. *Sci. Rep.* **10**, 1–15 (2020).
269. Herrera-Ruiz, D. *et al.* Spatial expression patterns of peptide transporters in the human and rat gastrointestinal tracts, Caco-2 in vitro cell culture model, and multiple human tissues. *AAPS PharmSci* vol. 3 100 (2001).
270. Zhang, J., Penny, J. & Lu, J. R. Development of a novel in vitro 3D intestinal model for permeability evaluations. Int. J. Food Sci. Nutr. 71, 549–562 (2020).
271. Hahn, U., Schuppan, D., Hahn, E. G., Merker, H.-J. & Riecken, E.-O. Intestinal cells produce basement membrane proteins in vitro. *Gut* **28**, 143–151 (1987).
272. Stallmach, A., Hahn, U., Merker, H. J., Hahn, E. G. & Riecken, E. O. Differentiation of rat intestinal epithelial cells is induced by organotypic mesenchymal cells in vitro. *Gut* **30**, 959–70 (1989).
273. Kim, T. Il *et al.* Myofibroblast keratinocyte growth factor reduces tight junctional integrity and increases claudin-2 levels in polarized Caco-2 cells. *Growth Factors* **30**, 320–332 (2012).

274. Osei, E. T., Booth, S. & Hackett, T. L. What Have In Vitro Co-Culture Models Taught Us about the Contribution of Epithelial-Mesenchymal Interactions to Airway Inflammation and Remodeling in Asthma? *Cells* vol. 9, 7: 1694 (2020).

275. Hu, Y. J., Wang, Y. D., Tan, F. Q. & Yang, W. X. Regulation of paracellular permeability: Factors and mechanisms. *Mol. Biol. Rep.* **40**, 6123–6142 (2013).

276. Leonard, M., Creed, E., Brayden, D. & Baird, A. W. Evaluation of the Caco-2 monolayer as a model epithelium for iontophoretic transport. *Pharm. Res.* **17**, 1181–1188 (2000).

277. Luettig, J., Rosenthal, R., Barmeyer, C. & Schulzke, J. D. Claudin-2 as a mediator of leaky gut barrier during intestinal inflammation. *Tissue Barriers* vol. 3:1-2 (2015).

278. Takenaka, T. *et al.* Development of Caco-2 cells co-expressing CYP3A4 and NADPH-cytochrome P450 reductase using a human artificial chromosome for the prediction of intestinal extraction ratio of CYP3A4 substrates. *Drug Metab. Pharmacokinet.* **32**, 61–68 (2017).

279. Jochems, P. G. M., Garssen, J., Van Keulen, A. M., Masereeuw, R. & Jeurink, P. V. Evaluating human intestinal cell lines for studying dietary protein absorption. *Nutrients* vol. 10 (2018).

280. Anderle, P. *et al.* P-glycoprotein (P-gp) mediated efflux in Caco-2 cell monolayers: The influence of culturing conditions and drug exposure on P-gp expression levels. *J. Pharm. Sci.* **87**, 757–762 (1998).

281. Chong, S., Dando, S. A., Soucek, K. M. & Morrison, R. A. In vitro permeability through caco-2 cells is not quantitatively predictive of in vivo absorption for peptide-like drugs absorbed via the dipeptide transporter system. *Pharm. Res.* **13**, 120–123 (1996).

282. Roulis, M. & Flavell, R. A. Fibroblasts and myofibroblasts of the intestinal lamina propria in physiology and disease. *Differentiation* **92**, 116–131 (2016).

283. Kennedy, K. M., Bhaw-Luximon, A. & Jhurry, D. Cell-matrix mechanical interaction in electrospun polymeric scaffolds for tissue engineering: Implications for scaffold design and performance. *Acta Biomater.* **50**, 41–55 (2017).

284. Anderson, J. M. & Van Itallie, C. M. Physiology and function of the tight junction. *Cold Spring Harbor perspectives in biology* vol. 1 2584–2585 (2009).

285. Al-Sadi, R., Guo, S., Ye, D. & Ma, T. Y. TNF-α modulation of intestinal epithelial tight junction barrier is regulated by ERK1/2 activation of Elk-1. *Am. J. Pathol.* **183**, 1871–1884 (2013).

286. Feighery, L. M. *et al.* Myosin light chain kinase inhibition: Correction of increased intestinal epithelial permeability in vitro. *Pharm. Res.* **25**, 1377–1386 (2008).

287. Yu, D. *et al.* MLCK-dependent exchange and actin binding region-dependent anchoring of ZO-1 regulate tight junction barrier function. *Proc. Natl. Acad. Sci. U. S. A.* **107**, 8237–8241 (2010).

288. Schreider, C., Peignon, G., Thenet, S., Chambaz, J. & Pinçon-Raymond, M. Integrin-mediated functional polarization of Caco-2 cells through E-cadherin—actin complexes. *J. Cell Sci.* **115**,3: 543-552 (2002).

289. Halttunen, T., Marttinen, A., Rantala, I., Kainulainen, H. & Mäki, M. Fibroblasts and transforming growth factor beta induce organization and differentiation of T84 human epithelial cells. *Gastroenterology* **111**, 1252–62 (1996).

290. Zhu, J. *et al.* Ultrafast bone-like apatite formation on highly porous poly(l-lactic acid)-hydroxyapatite fibres. *Mater. Sci. Eng. C* **116**, 111168 (2020).

291. Ingoglia, F. *et al.* Functional characterization of the organic cation transporters (OCTs) in human airway pulmonary epithelial cells. *Biochim. Biophys. Acta - Biomembr.* **1848**, 1563–1572 (2015).

292. Hagenbuch, B., Gao, B. & Meier, P. J. Transport of Xenobiotics Across the Blood-Brain Barrier. *Physiology* **17**, 231–234 (2002).

293. Vllasaliu, D., Falcone, F. H., Stolnik, S. & Garnett, M. Basement membrane influences intestinal epithelial cell growth and presents a barrier to the movement of macromolecules. *Exp. Cell Res.* **323**, 218–231 (2014).